2008-01-01

Investigation of the Electronic Properties of Organic Systems Using Electroabsorption Spectroscopy

Garrett F. Farrell
Technological University Dublin

Investigation of the electronic properties of organic systems using electroabsorption spectroscopy

By

Garrett F. Farrell

A THESIS SUBMITTED TO THE DUBLIN INSTITUTE OF TECHNOLOGY, FOR THE AWARD OF PHD

Focas Institute / School of Physics,
Dublin Institute of Technology,
Kevin Street, Dublin 8

SUPERVISORS:
Dr. H.J. Byrne
Dr. G. Chambers

January 2008

Declaration

I certify that this thesis which I now submit for examination for the award of Ph.D. is entirely my own work and has not been taken from the work of others save and to the extent that such work has been cited and acknowledged within the text of my work.

This thesis was prepared according to the regulations for postgraduate study by research of the Dublin Institute of Technology and has not been submitted in whole or in part for an award in any other Institute or University.

The work reported on in this thesis conforms to the principles and requirements of the Institute's guidelines for ethics in research. The Institute has permission to keep, to lend or to copy this thesis in whole or in part, on condition that any such use of the material of the thesis be duly acknowledged.

Signature

Garrett F. Farrell

Abstract

The aim of the project is to investigate the effect of bulk structural modification on the electronic properties of fullerene systems as measured using electronic and Electroabsorption (EA) spectroscopy. The existence of a unique solid state feature in C_{60} is the first indication that the material's electronic properties may be influenced by its crystalline environment and as such merits investigation. The nature and extent of these interactions in the solid state is still unclear, in particular whether the molecular electrons remain located on the individual molecules or whether they are delocalised across the solid. The extent of these interactions has major repercussions for any proposed electronic or optical applications for fullerenes e.g. in optical switches or luminescent displays. This work presents the effect of structurally altering fullerene films using systematic thermal treatments. A dramatic irreversible effect is observed in the absorption spectrum of C_{60} as the sample is annealed, indicating a reduction in the charge transfer(CT) processes associated with these transitions. This reduction can be attributed to a closer packing of the molecules in the solid state phase. Data obtained from EA spectroscopy confirms the reduction oscillator strength of the mode at 2.43eV normally associated with the off diagonal CT state again supporting the notion of a closer packed lattice. Analysis of C_{70} fullerene films also shows an associated increase in oscillator strength of the CT integrals as a result of the thermal treatment process, highlighting the importance of the material's crystalline environment in determining the material's electronic properties.

Acknowledgements

Firstly I would sincerely like to thank Dr. Hugh Byrne for allowing me to undertake this course of study and for all his help and guidance in the preparation and correction of this document. I fully acknowledge that as a result of Hugh's remarkable inspiration for all things scientific, my own scientific awareness has been rekindled, a gift for which I will be always grateful. I would also like to thank my co-supervisor, Dr. Gordon Chambers for his valuable experimental and theoretical input into the project over the last number of years and in particular his ability to halt fruitless avenues of investigation by merely saying, "No". I would also like to acknowledge the input of Dr. Alan Dalton during the initial stages of the project. Alan's terrible sense of humour far out weighed his misguided notion that I would have the electroabsorption spectrometer "built in six weeks". I would like to thank Dr. Fran Pedreschi, for proof reading this document also for the occasional lending of various bits and bobs over the years, in particular a Xenon arc lamp, a lockin amplifier and a size 13 spanner. Thanks also must go to Johnny Moghal, for keeping an eye on the EA while I've been away and Alan Casey for all the laughs over the years. I would also like to thank all the members of POMM and the FOCAS technicians down through the years, their help on various issues has been greatly appreciated. Finally on a more personnel note I would like to thank my wife Nicola, and the boys, for allowing me to finish this, sorry it took so long,

TABLE OF CONTENTS

List of Acronyms

ADC	Analogue to Digital Converter
AFM	Atomic Force Microscopy
amu	Atomic Mass Units
ATR	Attenuated Total Reflectance
$\alpha(0)$	Absorption spectra without electric field perturbation
$\alpha(F)$	Absorption spectra with electric field perturbation
$\Delta\alpha$	Electric field induced change of absorption spectra, or electroabsorption spectra
ΔE	Electric field induced energy shift of molecular eigenstates
AC	Alternating Current
Δf	Electric field induced change of oscillator strength
λ	Wavelength of the incident light
ω	Circular frequency of applied electric field
σ	Conductivity of vapour deposited organic thin film
CT	Charge Transfer
d	Thickness of organic thin film
DC	Direct Current
DTGS	Deuterated Triglycine Sulphate detector
E(F)	Energy of the molecular eigenstates with electric-field perturbation
E(0)	Energy of the molecular eigenstates without electric-field perturbation
F(x)	Electric Field inside sample
$f(\nu)$	Gaussian line shape function
EA(x)	Electroabsorption signal
EA1f	Electroabsorption spectrum measured at first harmonic frequency of applied electric field
EA2f	Electroabsorption spectrum measured at second harmonic frequency of applied electric field
Fcc	Face centred cubic
FE	Frenkel Excitons
FTIR	Fourier Transform Infra Red spectroscopy
Hcp	Hexagonal cubic packing
HMO	Hückel Molecular Orbital
HOMO	Highest Occupied Molecular Orbital
HVAC	High Voltage Alternating Current
LI Amp	Lockin Amplifier
LUMO	Lowest Unoccupied Molecular Orbital
ITO	Indium Tin Oxide
IR	Infra Red

I_o	Incident light intensity on sample
I_t	Transmitted light intensity through sample
I_r	Reflected light intensity
K	Kelvin
$\Delta\mu$	Electric-field-induced change of the static dipole moment
Δp	Electric-field-induced change of the polarisability
MNR	Nuclear Magnetic Resonance
MOMO	Monochromator
O.D.	Optical Density
PMT	Photomultiplier tube
PSD	Phase Sensitive Detector
R	Reflectance from surface
RT	Room Temperature
SPM	Scanning Probe Microscopy
SQUID	Superconducting Quantum Interference Devices
$\Delta T/T$	Measured electric-field-induced change of transmission, electroabsorption signal
UV/VIS	Ultraviolet visible spectroscopy
UV/VIS/NIR	Ultraviolet visible spectroscopy Near Infra Red spectrometer
V_{ac}	Applied AC voltage
V_{dc}	Applied DC bias
V_{bi}	Built-in potential
WL	White Light source
XRD	X-ray diffraction measurements

CHAPTER 1

Introduction

and thesis outline

1.1 Introduction

Over the last thirty years there has been a massive increase in the amount of electronic devices used in everyday life. Indeed these devices have uses ranging from the home to the work place, so much so that the world has not only become reliant on these devices but is demanding that they become even faster and smaller. It is this desire for smaller and faster devices that has led scientists to search for and examine new materials. Thus when historians look back on the twentieth century, the discovery of the Buckminsterfullerene will certainly be regarded as one of the most important events to have occurred in modern science, not only because it is a previously unknown allotrope of carbon but also because it brought together scientists from a variety of different fields

who were all working towards a common goal and creating, arguably for the first time, a truly universal branch of science.

1.2 Historical background of fullerenes

While Kroto and Smalley are credited with the discovery of C_{60} in 1985 [1], a number of people had speculated about the possible existence of such structures at least two decades prior to its discovery[2,3]. The actual discovery of fullerenes was purely accidental. Kroto and Smalley made the finding while vaporising a graphite target under a high density helium flow using an Nd:YAG laser[1]. Although their aim had been to recreate the way in which cyanopolyenes (HC_nN) are formed in red giant carbon stars, analysis of the resulting vapour by mass spectroscopy revealed a number of unidentifiable peaks, the most notable at 720 amu and 840 amu. They proposed, proved later by IR and NMR[4,5] spectroscopy in 1990, that the peak at 720 amu was due to a closed carbon cluster made up of sixty carbon atoms arranged at the vertices of a truncated icosahedron as shown in figure 1.1

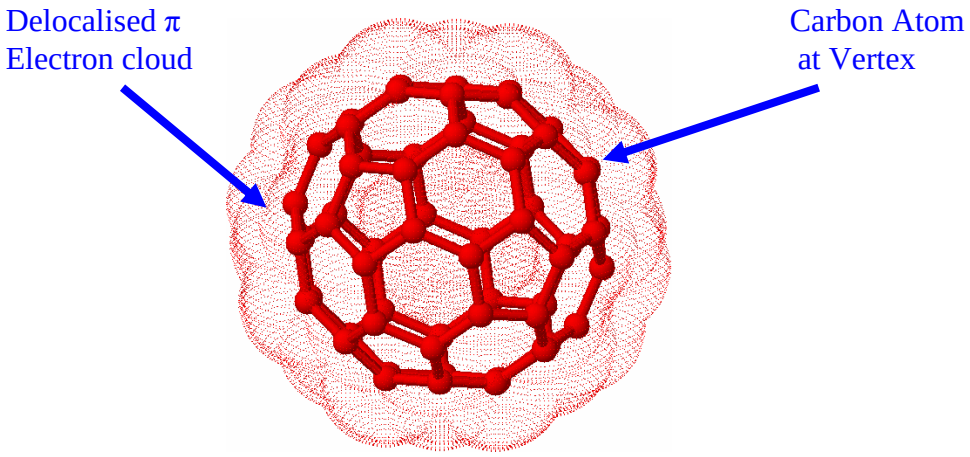

Figure 1.1 Kroto and Smalley's proposed structure of the Buckminsterfullerene (C_{60}). The truncated icosahedral structure resemblances that of a soccer ball surrounded by its electron cloud

The new molecule was christened Buckminsterfullerene by its discoverers, because of the structure's likeness to the geodesic domes designed by Richard Buckminster-Fuller in the early 1930's. In a C_{60} molecule the carbon nuclei take up positions on a sphere approximately 7Å in diameter, with a π electron cloud of approximately 1.5Å distributed both inside and outside of the structure. It is this π electron cloud which is primarily responsible for the intense interest in these types of molecules. If each vertex of the icosahedral structure is replaced with a carbon atom, the individual valences of each atom can be fulfilled by forming two single bonds and one double bond, i.e. each carbon has a hybridised sp^2 bonding configuration, which results in the delocalisation of the sixty electrons unevenly around the carbon cage, as shown in figure 1.1.

After the initial discovery, which led to the award of the Nobel Prize in chemistry in 1996, there was an enormous amount of curiosity right through the scientific community regarding the physical and chemical properties of the new material, and in particular the sixty delocalised electrons. However at the outset the scarcity of material for study largely restricted these investigations to structural based theoretical calculations of the molecule[6,7]. However in 1990, the development of a synthetic method for fullerene production by Hoffman and Krätschmer [4] produced the first macroscopic quantities (100 mg/day) of the material. The availability of large quantities of isolated material for study opened up the area of fullerene research to the wider scientific community. Extensive research revealed that C_{60} was only one member of a family of similar molecules including carbon nanotubes, carbon onions, C_{70} and various other large carbon cluster molecules (figure 1.2), of which C_{60} is the archetype. [1]

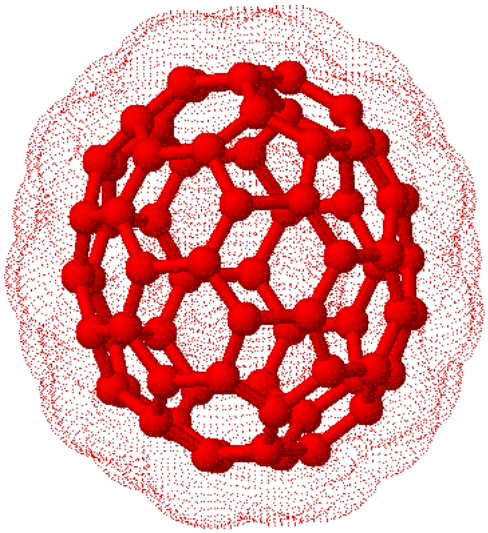

(a)

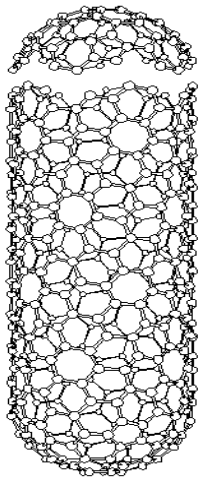

(b)

Figure 1.2 Other carbon clusters in the Fullerene family (a) C_{70} and (b) a single wall nanotube.

1.3 Applications

In light of the unique properties of these materials, scientists were quick to put fullerenes forward as potential candidates for solutions in fields ranging in diversity from viral inhibitors [8] to superconductors[9,10,11]. However, even with the intense amount of research being invested into fullerenes and other members of the family, to date only a few commercial applications of fullerenes have emerged, primarily involving surface coatings [12]. While the commercialisation potential of C_{60}, may not be as glamorous as initially imagined, the optical and electronic properties of fullerenes as governed by the delocalised electrons, still offer huge promise for utilisation in other areas e.g. superconductors. In the solid state, fullerenes crystallise in hexagonal close packed structures. Critical to both optical and electronic applications is the behaviour of the molecule in the solid state environment and specifically the degree of electronic communication between the molecules. The interaction of the delocalised electrons

between adjacent molecules as one moves from the isolated molecule to the bulk solid state and the consequential effects on the material's properties is a theme which will predominate throughout this thesis.

Much of the intense interest in these types of molecules stems from the demonstration that fullerite (C_{60}) can posses the ability to go from an insulator to conductor, to a superconductor and back again to an insulator[9,11]. The implications from a commercial point of view of such material properties are immense, with numerous possible applications such as high speed computer chips based on Josephson junctions and other electronic devices based on SQUIDS (Superconducting Quantum Interference Devices)[13]. The generation of these conductive states generally involves doping the crystal lattice of the fullerite, which is itself an insulator, with alkali metals in different stoichiometric ratios. For example a metallic like state can be obtained by doping the fullerene lattice with a 1:1 ratio of alkali metals such as Potassium or Rubidium i.e. A_1C_{60}[9]. Likewise by altering the ratio of alkali to fullerene to 3:1 (i.e. A_3C_{60}) then a superconducting state is accessible. These highly conductive states arise because of the transfer of an electron from the doping material to the lowest unoccupied molecular orbital (LUMO) of the fullerene molecules.[14] Going to a 6:1 ratio of alkali to fullerene produces an insulating state. Harald Weber [15] postulated that the superconducting nature of C_{60} is one of a confined bulk superconductivity, since although it exhibits zero resistance to electrical current and expels magnetic flux at low temperatures, the recorded current densities are much lower than in other superconductors.

The implications of Weber's results are that within the fullerene lattice, Josephson coupling between individual molecules allows supercurrents to flow through the material. Consequently fullerenes can be described as molecular superconductors, in which the superconducting properties of the material are not restricted by the sample size, but by the cracks within the crystal structure itself, i.e. the grain boundaries. These cracks hinder coupling between the molecules and as a result reduce the current densities. As such ways of reducing or controlling the formation of these grain boundaries is of immense importance in the development of any future devices based on these materials. Unfortunately until the superconducting transition temperature reaches at least 77K practical applications of this superconductivity will not be forthcoming. Transition temperatures as high as 43K have been reported for the intercalation of rubidium (Rb_3C_{60}), and although this is promising it is still someway short of liquid nitrogen temperatures[16]. While the inclusion of alkali metals into a fullerene lattice allows for the generation of highly conductive behaviour it is not the only means of generating these states. Studies have shown that it is possible to generate these metallic like states by either electron injection or optical excitation of the material[9]. The resulting metastable metallic state brought about by the injection of electrons into the lattice gives rise to an intense luminescence which is also accompanied by non linear current characteristics[17]. Likewise the optically excited state exhibits highly luminescent and non-linear characteristics[9].

Of critical importance is understanding the communication between the molecules in the solid state. The indications are that in ground state, molecules which are bound by van der Waals forces, communicate little. An isolated excited state gives rise to a charge transfer (CT) [18] and even polymerisation [19] between adjacent molecules. The

degree of CT depends on the crystal packing and manipulation of CT can lead to enhanced intermolecular electronic communication and therefore potentially lower superconducting transition temperatures.

1.4: Thesis outline

The aim of this study was to characterise the optical and electronic properties of C_{60} and C_{70} thus leading to a better understanding of the communication between the molecules in the solid state. Since the degree of charge transfer between molecules depends on the crystal packing, this work looks to explore these charge transfer states and examine how they can be characterised spectroscopically and manipulated by structural modification.

Initially, in chapter 2, the structure of C_{60} and C_{70} is discussed and the first comparison between the properties of the isolated molecule and the solid state is drawn, a theme which is continued throughout the thesis. In general the chapter raises a number of questions concerning the electronic configuration of the solid state, specifically whether the sixty delocalised electrons of the fullerene molecules become delocalised across the solid or remain located on the individual molecules. Consequently this chapter in effect sets up the arguments for undertaking the research.

Chapter 3 establishes the underlying methodology used throughout the study. It depicts how the thin films of C_{60} and C_{70} were fabricated, and goes on further to describe the more traditional spectroscopic techniques and instruments used throughout the study. It also describes the instrumentation used throughout the structural analysis of the fullerene films.

Chapter 4 describes the design and construction of the electroabsorption spectrometer. The chapter provides information on the performance characteristics of the individual spectrometer components. It also details the two types of sample geometries available as substrates and following on from this, the chapter explains the need for development of a second EA spectrometer. It goes on to furnish data on the performance characteristics of the finalised EA spectrometer as obtained using a standard fullerene film.

Chapter 5 begins by providing some background theory on electronic spectroscopy and its importance in detailing the excitonic processes in fullerenes. It goes onto further to provide a review of electroabsorption spectroscopy. It introduces the concept of the Stark effect and follows on to explain the differences between the linear and quadratic Stark effect. Finally it provides an explanation for the interpretation of EA spectra of fullerenes with particular emphasis being placed on identification of the CT modes.

Chapter 6 starts by examining the reversible effects of temperature on the absorption and electroabsorption spectra of both C_{60} and C_{70}. It then highlights the large irreversible effects of temperature on the absorption and electroabsorption spectra of C_{60} and the much less pronounced effects associated with the C_{70} molecules. Particular emphasis is placed on the exhibited irreversibility associated with the temperature dependent spectra, which is indicative of structural changes within the lattice.

Chapter 7 examines absorption and electroabsorption data obtained from the annealed fullerene films. It goes on further to explore and correlate the changes in CT contributions as the fullerene films are annealed. Also highlighted is the noticeable difference between C_{60} and C_{70} in this regard, and the possible causes of such effects. The possibility of changes in the surface morphology are then explored using AFM, which reveals larger grain boundaries in the annealed films. Interpretation of supportive XRD data backs up the argument that the films have undergone structural changes during the annealing process.

The final chapter of the thesis provides a summary of the work conducted and a general discussion of the work presented. It highlights the continuing need for fundamental research into the properties of C_{60} and C_{70} and the possible implications of this thesis on future C_{60} research.

CHAPTER 2

Introduction to Fullerenes

2.1 Introduction

This chapter gives an insight into the unique structural properties of fullerenes C_{60} and C_{70}. Particular attention is given to the effect of structure on the electronic properties of each material. Since their discovery in 1985 a large amount of work has been aimed at understanding the unique properties of these materials and a wealth of information is available on the molecular structures of these molecules in both the isolated and solid state form[21,21]. Nevertheless there are still some unanswered questions regarding the electronic properties of these materials, particularly those involving the bulk state structure of the materials and their dependence on crystalline structure.

2.2 Defining the structure of C_{60} and C_{70}

In general a fullerene molecule can be defined as a closed cage molecule in which the atoms are arranged at the vertices of hexagonal and pentagonal rings. The name fullerene is given to the entire class of closed caged polyhedral carbon molecules. The relationship between the number of vertices v, faces f, and edges e, for any polyhedron is given by Euler's theorem [22],

- $v + f = e + 2$ *Eqn. 2.2.1*

where f, v and e are respectively the number of faces, vertices and edges of a polyhedral. If a structure contains only pentagons (p) and hexagons (h), then the number of faces should equal the sum of all the pentagons (p) and hexagons (h) i.e.

- $f = p + h$ *Eqn. 2.2.2*

Consequently the number of bonds within such a molecule will be identical to the number of edges and is equal to 3v/2 since each edge joins two faces it can be written.

- $e = \left(\frac{5p + 6h}{2} \right) = \frac{3v}{2}$ *Eqn. 2.2.3*

Combining the above equations yields *Eqn 2.2.4.*

- $6(f + v - e) = p = 12$ *Eqn. 2.2.4.*

Thus the minimum number of pentagons required to close the cage under Euler's law is 12, whereas an arbitrary number of hexagonal faces is allowed, as is the case in higher fullerenes. Based on this assertion the smallest possible carbon based fullerene, is C_{20}, which forms a dodecahedron consisting of 12 pentagonal faces and no hexagonal faces. (figure 2.1) However, the formation of C_{20} is energetically unfavourable since the existence of only pentagonal faces increases the curvature of the molecule and consequently increases the strain within the molecule [23].

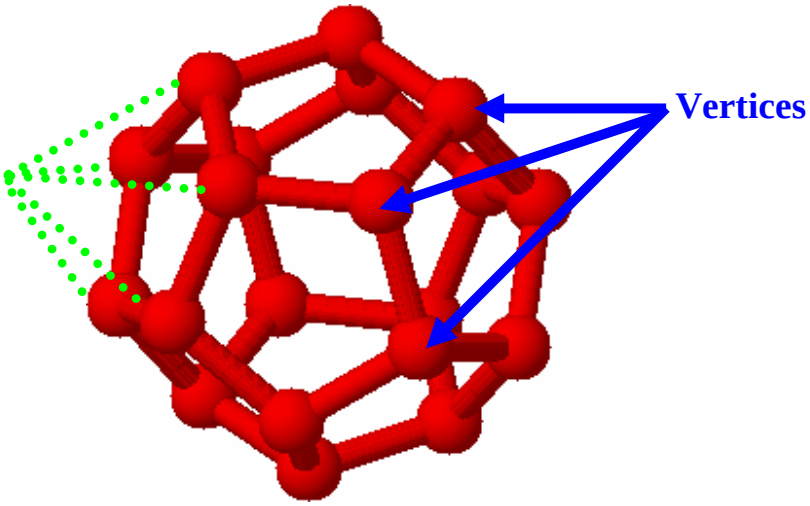

Figure 2.1 Shows the energetically unstable dodecahedron structure of C_{20} made up from 12 pentagons and no hexagons. Also indicated are the structural vertices and the projection of these to a point

The addition of hexagonal faces isolates the pentagonal faces from each other and thus reduces the intramolecular strain on the molecule. The induced strain in the molecule results from the highly pyramidalized sp^2 carbon atoms. Within any fullerene, each carbon atom is bonded to three other carbon atoms in a sp^2 hybridised bonding arrangement. They are usually referred to as "sp^2 carbons" because the orbitals used to sigma-bond the three adjacent carbons are hybrids of the 2s orbital and the two 2p orbitals ($2p_x$ and $2p_y$). The remaining 2p orbital ($2p_z$) is responsible for the π-bond on the hexagonal faces thus making the hexagons electron rich, and the pentagons electron deficient. The pyramidalisation angle between the sp^2 and sp^3 orbitals of the carbon atom is 11.6^o[25]. Of critical importance to this work is the configuration of these sp^2 hybridised bonding arrangements, which gives rise to the delocalised electrons located around the fullerene sphere. These electrons are of particular interest when considering the electronic and optical properties of both C_{60} and C_{70}.

The tendency for pentagons not to be adjacent is known as the isolated pentagon rule. The smallest carbon based fullerene to satisfy this isolated pentagon rule is C_{60}. Hence C_{60} is the smallest stable fullerene and is regarded as the epitome fullerene. C_{60} is made up of 12 pentagons and 20 hexagons [25]. The next most stable fullerene satisfying this condition is C_{70} which contains 12 pentagons and 25 hexagons [25]. Fullerene C_{70} can be formed by taking a C_{60} molecule and splitting it in two, rotating one of the hemispheres by 36^{o}, adding a ring of five hexagons around the equatorial plane of the C_{60} molecule and recombining all the sections to form a spheroid. Many of the properties of the C_{60} and C_{70} molecules are directly related to the molecular shape and consequently understanding each molecules symmetry is crucial in elucidating the structural aspects of the molecule. Through the use of molecular symmetry it is possible to classify both molecules as being in a particular point group.

2.3 Isolated C_{60}

With regard to C_{60}, the symmetry operations of icosahedral group are provided by the relevant point group I_h. The symmetry operations or rotational operations for the icosahedral consist of fifty nine rotations plus an identity element where the vertices remain fixed. These elements can be defined in terms of an identity operation, 12 five-folds axes through the centres of the pentagonal faces, 20 three-fold axes through the centres of the hexagonal faces and 15 two-fold axes through the centres of the edges joining the two hexagons. Additionally the group also contains an inversion operation resulting in 120 symmetry operations [26].

$$I_h = \{E, 12C_5, 12C_5^2, 20C_3, 15C_2\} \times i$$

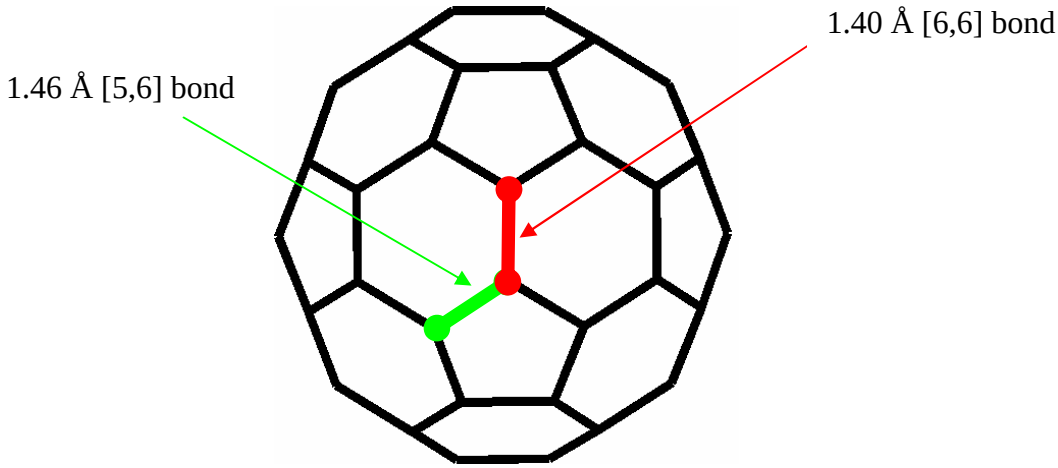

Figure 2.2 Upper diagram shows various bond lengths associated with C_{60}.

Molecules like C_{60} with I_h symmetry display the highest degree of symmetry of any molecule. As a result of the icosahedral symmetry of C_{60} the bond lengths between the carbon atoms varies. Hedberg et al. reported that within C_{60}, the carbon atoms located between a pentagon and a hexagon have a bond length of 1.46Å and the carbon atoms between two hexagons have a bond length of 1.40Å as measured by electron diffraction [27], Figure 2.2. These two different C-C bond lengths in C_{60} indicate that the π electron cloud is not evenly distributed around the molecule.

2.4 Isolated C_{70}

Moving onto C_{70}, there is lowering of the symmetry which results from an elongation of the molecule to a rugby ball shape, described by the point group D_5h [28]. The molecule is composed of 12 pentagons and 25 hexagons and obeys the isolated pentagonal rule. The D_5h point group unlike the I_h point group does not contain a centre of inversion but it does posses a mirror plane which is perpendicular to the elongated axis of the molecule. The group also contains 5 two-fold axes, and thus in the D_5h point

group there are 20 symmetry operations corresponding to a C_5 (z) axis, a C_2 axis and a mirror plane (xy) [25].

$$D_5h = \{E, 2C_5, 2C_5^2, 5C_2', \sigma_h, 2S_5, 2S_5^3, 5\sigma\}$$

The resulting structure has two pentagons at the poles and a belt of hexagons around the equator of the molecule. This elongated 5 fold axis is about 1Å longer than the short axis of the molecule [29], while around the poles of the molecule the bond lengths are similar to those found in C_{60}.

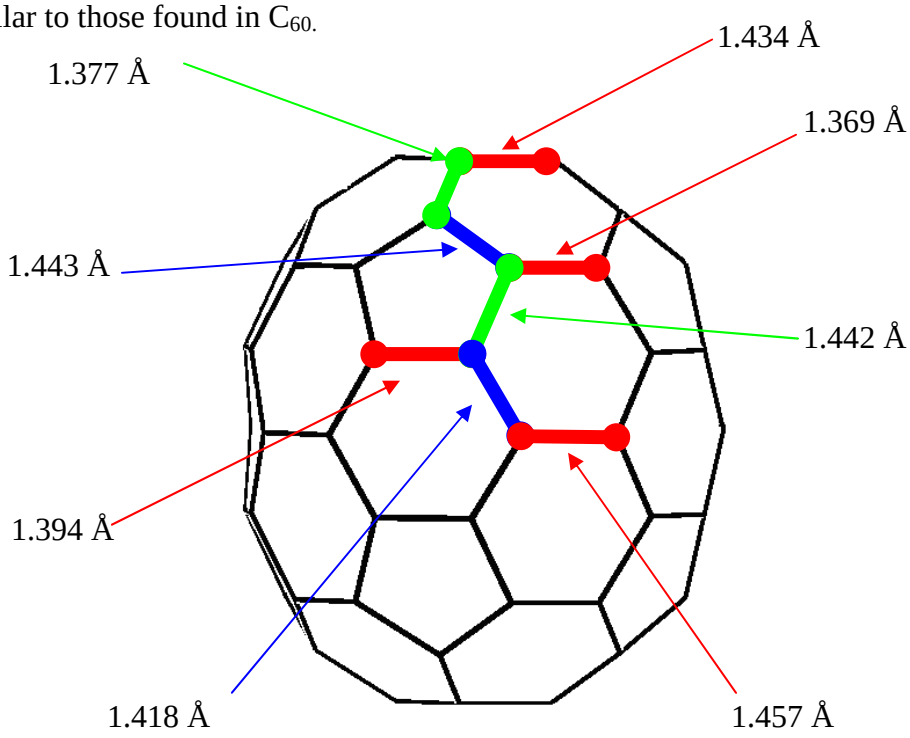

Figure 2.3 Shows the various bond lengths associated with C_{70}

The equatorial region consists of irregular hexagons whose sides are significantly different to those found in graphite. The chemical environment within C_{70}, due to its lower symmetry, has 5 non-equivalent carbon atoms, which is confirmed by NMR [30]. These variations in bond lengths reflect a certain degree of strain in the equatorial region

of the molecule. It has been reported by Smaalen et al. that C_{70} contains 8 different bond lengths ranging from 1.369 Å to 1.457 Å, Figure 2.3 [31]. The manipulation of the electronic properties using alkali metals has led to many proposed applications as discussed in chapter 1. In spite of these proposed applications there are however many questions remaining concerning the exact nature of these electronic configurations, particularly in the solid state environment, which still need to be addressed.

2.4 Electronic structure of fullerenes

In order to understand the electronic structure of fullerenes and their crystalline forms it is important to review the symmetry considerations associated with a particular point group. Examination of the electronic properties of fullerenes is complex since there are 240 and 280 electrons associated with C_{60} and C_{70} respectively. Each C_{60} molecule with an icosahedral symmetry can be considered to have 60x3=180 σ electrons which are involved in forming bonds along the surface of the icosahedral. Although the arrangement of the σ electrons of the single bonds determine the structural and symmetrical properties of both C_{60} and C_{70}, it is their π electrons which determines their electronic properties since the energy of bonding σ levels lie well below the Fermi level and as such are not as important in determining the molecular electronic properties. Consequently only the molecule's π-orbitals need to be considered in models of the electronic structure. It should be noted that as a general rule fullerenes with n_c carbon atoms have n_c π electrons [25]. Examining C_{60} first, Leach et al [32] reported the closed shell electronic configuration for C_{60} in the ground state due to the π orbitals as; $3a_g^{(2)}$ $4t_{1u}^{(6)}$ $4h_g^{(10)}$ $4t_{2u}^{(6)}$ $4g_u^{(8)}$ $4g_g^{(8)}$ $7h_g^{(10)}$ $4h_u^{(10)}$

In a one electron electronic structure model as shown in figure 2.3, a C_{60} molecule in the ground state has two spins for each of the five degenerate filled h_u symmetry orbitals of the Highest Occupied Molecular Orbital (HOMO) orbital [33]. The Lowest Unoccupied Molecular Orbitals (LUMO) comprises of a three fold degenerate t_{1u} one electron states and each orbital t_{1u} state can hold a spin paired electrons. Consequently an electronic transition between these two states, i.e. the $h_u - t_{1u}$ is forbidden since both states have ungerade (u) parity. Nevertheless Leech et al assigned the feature of the solution optical absorption spectrum of C_{60} at 1.89eV to the lowest excitation from the HOMO to the LUMO i.e. $h_u \rightarrow t_{1u}$ [32]. Although this electronic transition is forbidden as a result of parity considerations, the icosahedral symmetry of C_{60} allows for a slight relaxation of the selection rules via Hertzberg-Teller vibrational coupling and Jahn-Teller distortions [34]. Other transitions from either filled ungerade/gerade to empty gerade/ungerade molecular orbitals are allowed provided they satisfy the selection rules for these states. The next highest unoccupied molecular orbital, t_{1g}, is interesting as it is the first optical transition which occurs from, h_u to t_{1g} (HOMO→LUMO+1), with an energy value of 2.5eV. There are five more possible optical excitations: $h_g \rightarrow t_{1u}$, $h_u \rightarrow h_g$, $g_g \rightarrow t_{2u}$, $h_g \rightarrow t_{2u}$, and $h_u \rightarrow g_g$ the first four of which have been indicated on the Hückel Molecular Orbital (HMO) diagram with their respective energies, figure 2.3 [32].

With the lowering of symmetry to a D_{5h} point group which occurs in C_{70}, having a mirror plane along the five fold axis but no inversion symmetry, one must use the lower symmetry group I for relating the icosahedral irreducible representations to those in D_5 [25]. The closed shell electronic configuration for C_{70} in the D_{5h} symmetry is $16a'_1\ 7a'_2\ 23e'_1\ 23e'_2\ 5a''_1\ 14a''_2\ 19e''_1$ and $19e''_2$ [35]. The HOMO is of a''_2 symmetry but it should

also be noted that there is also an e''_1 MO which is very close in energy. The LUMO is of e''_1 symmetry, but similar to the HOMO there exists another MO of a''_1 symmetry with a similar energy [36]. The a"1 LUMO is nonbonding and the lowest dipole allowed transitions are the perpendicular excitations of the HOMO and LUMO-1 to the LUMO+1 levels. The low energies of these orbitals offer a rationalisation of its UV/visible spectrum which extends to longer wavelengths than C_{60} [35].

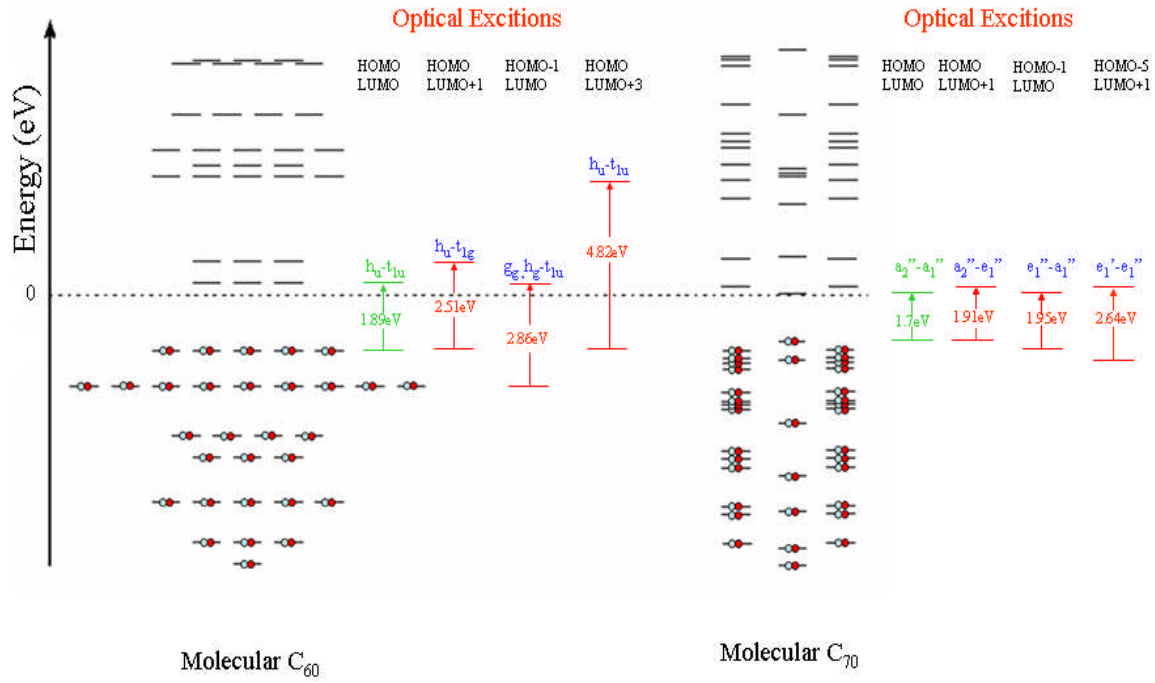

Figure 2.4 The molecular orbital energies for C_{60} and C_{70}. Also indicated are the various electronic transitions associated with the isolated molecules. The symmetry forbidden HOMO –LUMO transitions are indicated by the green text caption

Finally, in the solid, the electronic structure is still largely unknown. The HOMO–LUMO energies have been calculated for both C_{60} and C_{70} in the solid state and are reported to be approximately 1.85eV [38] for C_{60} and 1.7eV for C_{70} [25]. Such a deviation from the molecular band gap implies a significant interaction between electronic states in the solid state of fullerene. However the question regarding the exact

nature of the electronic interactions has never been answered, particularly whether the electrons remain localised on the individual molecule or if they become delocalised across the solid.

2.4 The solid state structure of C_{60}

Both solid state C_{60} and C_{70} and can exist as a number of phases depending on the temperature and pressure of the system. It is known that the room temperature structure of a polycrystalline C_{60} film is represented by a face centred cubic (fcc) phase, with a lattice parameter of 14.17Å, in addition to a number of other distortions [39]. The structure can be envisaged as containing four molecules located at the origin and at the midpoints of three faces of a cubic cell all with the same orientations.

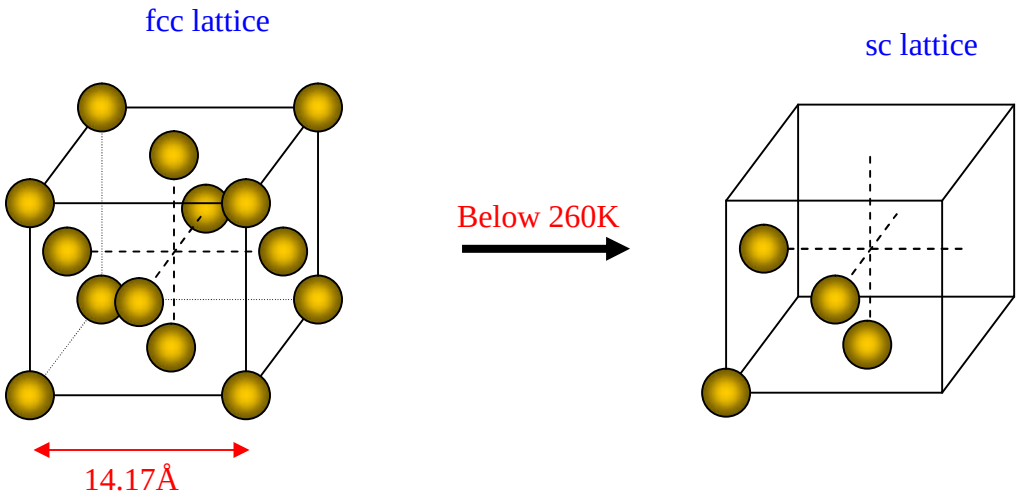

Figure 2.5: Solid state structure of room temperature C_{60} (fcc). The rapid rotation the molecules within a C_{60} lattice means that the individual molecules are crystallographically equivalent resulting in a lattice constants of 14.17Å. Above 249K, the molecules are spinning rapidly, giving rise to a fcc type lattice arrangement. However below 260K the spinning motion is frozen out and a simple cubic type lattice results.

Assignment of individual molecules to one of the two standard orientations raises the lattice symmetry from $Fm\bar{3}$ to $Fm\bar{3}m$ [25]. In the room temperature fcc phase the rapid rotation of the molecules within a C_{60} lattice results in the molecules being crystallographically equivalent resulting in a lattice constants of 14.17Å (see figure 2.4). This fcc phase is sensitive to changes in temperature and below 260K the four molecules in a conventional unit cell of an fcc lattice become orientationally inequivalent and the system experiences a first order transition to a simple cubic (sc) structure with a $Pa\bar{3}$ symmetry, Figure 2.5 [25]. In this low temperature phase, rotation of the molecules is hindered which results in the alignment of an electron rich double bond fusing two hexagons to an electron deficient pentagonal face on an adjacent molecule [40]. Consequently the C_{60} molecules in the fcc lattice positions are no longer equivalent and the lattice constant decreases by 0.13 Å [19]. This low temperature phase of C_{60} exhibits a simple cubic lattice structure and is commonly referred to as the Rachet phase, figure 2.5 [41]. Placing the molecules in an fcc lattice lowers of the symmetry of the icosahedral molecules as a result of crystal field effects on the molecule. However, as shown by Raman spectroscopy these crystal field effects are only weakly evident in the experimental measurements [42] and it demonstrates that in the solid state the molecules retain their I_h character.

2.5 Solid State Structure of C_{70}

Like C_{60} the molecules in C_{70} are bound together by weak van der Waals forces, thus allowing the molecules to spin freely around their lattice positions. However, since C_{70} is slightly elongated along its fivefold axis, the molecules are randomly spinning around their major axes which are aligned parallel to each other [41]. In comparison to C_{60}, the

phase transition behaviour of C_{70} is more complicated. At high temperatures (above 337K) the C_{70} molecules possess complete free rotation and the equilibrium structure is fcc mixed with some hcp structure [41]. At high temperature the closed packed fcc phase with lattice constant of 15.01Å is the most stable although a hcp phase is almost as stable and consequently fcc crystals tend to consist of a mixture of fcc and hcp [25]. The nearest neighbour intraplanar distance between C_{70} molecules on a triangular lattice is 10.12 Å with an inter planar separation of approximately 9.2 Å (see figure 2.5) [44].

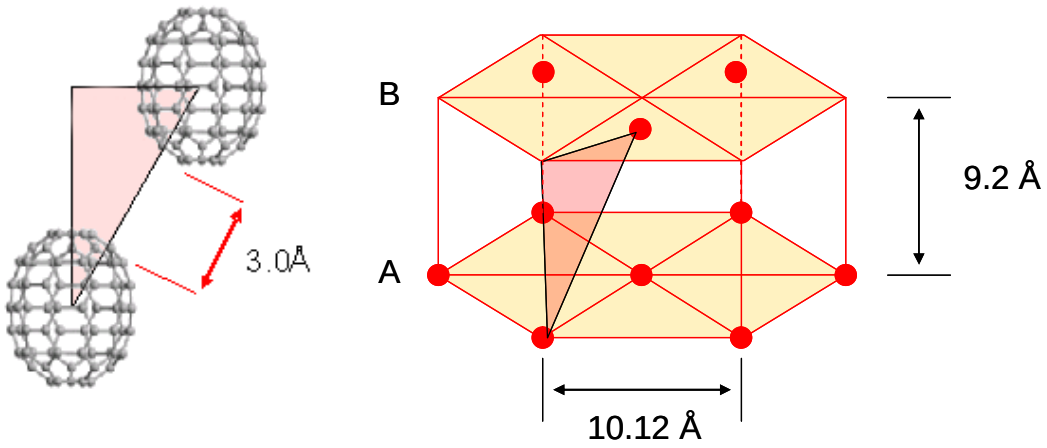

Figure 2.6 Solid state structure of C_{70}.(hcp) The nearest neighbour intraplanar distance between C_{70} molecules on a triangular lattice is 10.12 Å with an intraplanar separation of approximately 9.2 Å. The interstitial distance between adjacent molecules is shown as 3.0 Å

As the temperature of the lattice is lowered below 337K an intermediate hcp phase develops in which the major axes of the C_{70} molecules are aligned parallel to each other with a=b=10.11Å and a c/a ratio of 1.82 [45]. In this phase the free molecular rotations associated with the high temperature phase freeze into rotations only around the five-fold axis. The ratcheting motion around the long axis of the C_{70} molecule exhibits a certain degree of anisotropy which increases with decreasing temperature. As the

temperature is lowered below 276K, the system exists as a fully ordered monoclinic phase similar to the simple cubic phase exhibited by C_{60} at 249K. In this phase with a monoclinic angle β of about 120^{o}, the free rotation around the c-axis also becomes frozen [25]. Identification of the of the space group for the low temperature phase is somewhat contentious with the most likely candidate being C_2 or P_2. Consequently as the temperature is lowered there are less equivalent molecules per unit cell. Hence by controlling the temperature, the communication between the molecules can be altered and as such the electronic properties of the material can potentially be tuned.

While many of the structural properties of fullerenes have been determined, there still remain a number of unanswered questions regarding the molecular interaction in the solid, specifically with respect to the delocalised electrons. It is known that in the absence of oxygen, interaction between the π-electrons in both fullerene C_{60} and C_{70} gives rise to a photoinduced polymerisation in both solid and in solution [33, 46]. The nature and extent of these interactions in the solid state is still unclear, in particular whether the molecular electrons remain located on the individual molecules or whether they are delocalised across the solid. The extent of these interactions has major repercussions for any proposed electronic or optical applications for fullerenes e.g. in optical switches or luminescent displays. These issues among others will be addressed in this thesis. UV visible absorption spectroscopy will be employed to illustrate the differences between the electronic properties of the isolated molecules, as represented by dilute solutions, and the solid state in polycrystalline thin films. The differences have been suggested to be a result of excited state charge transfer excitons and the properties of these will be probed using Electroabsorption spectroscopy. The temperature

dependence of the properties of these states will demonstrate the sensitivity of the electronic communication to crystal packing. At elevated temperature irreversible or annealing effects are manifest and the electronic changes will be correlated to changes in crystalline structure as characterised using X-ray diffraction.

CHAPTER 3

Experimental Methodology

3.1 Introduction

This chapter gives account of the general instrumentation used during the course of the project. Throughout the course of this work a broad range of instruments and techniques has been used and adapted to study the optical and electronic properties of C_{60} and C_{70}, and where necessary further details about specific experimental set ups will be given in the relevant chapters, in particular those pertaining to the electroabsorption measurements will be covered in chapter 4. The techniques discussed in this chapter can be divided up into device fabrication, temperature controlled instrumentation, structural analysis (IR, AFM, XRD) and analysis of electronic properties using UV/Vis spectroscopy.

3.2 C_{60} and C_{70} film sublimation

The two types of fullerene films examined during this study were fabricated by vacuum sublimation. Fullerene films were fabricated onto various substrates including quartz, silicon, sodium chloride plates and indium tin oxide (ITO)/glass coated substrates, depending on their intended use. All the substrates with the exception of the sodium chloride windows were cleaned by refluxing in propan-2-ol for 1 hour prior to deposition. The sodium chloride substrates were cleaned by refluxing in hexane followed by an acetone immersion and subsequent drying in a nitrogen glovebox.

The preparation of the films involved depositing C_{60} or C_{70} onto a particular substrate, which was achieved using an Edwards Auto 306 vacuum deposition system. The substrates were mounted upside down onto a metal template located inside the vacuum chamber. The substrate holder was custom made for supporting the substrates and allowed for easy mounting and removal of samples. In addition to supporting the samples the holder also incorporated an adjustable shadow mask, which allowed for a greater degree of flexibility during device fabrication. The instrument consists of a shutter located between the source and the sample, which was preferentially opened or closed to expose or protect the sample (film) from exposure to the evaporated material. A small quantity (20mg approximately) of pristine "99.9+%" C_{60} soot obtained from SES Research was then placed in an "Edwards c3" molybdenum evaporating boat. The edges of the boat were connected to the positive and negative terminals of the high-tension power supply, see figure 3.1. The chamber was then sealed and pumped down using a rotary backed diffusion pump. The evaporation chamber was evacuated to 10^{-6} mbar with the shutter closed. The molybdenum boat was then heated by gently passing a current approximately 20 Amps, which was controlled from an in built power supply.

After the initial outgassing of the material of any residual solvent for a period of 60 minutes, the current was increased until it reached approximately 40 Amps, at which point the shutter was opened and the current was then gradually increased to approximately 50 amps.

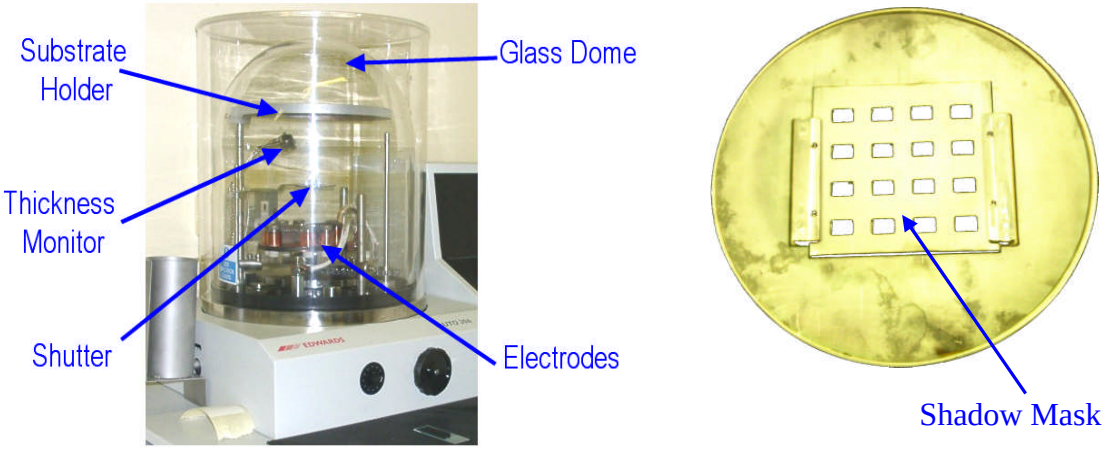

Figure 3.1 Shown in (a) is a labelled picture of the Edwards Auto 306. As the picture indicates both the thickness monitor and substrate holder are located above the sample. Shown in (b) is the substrate holder and shadow mask.

The deposition continued until the desired amount of material had been deposited, which was measured using a quartz thickness monitor and subsequently checked using a Dektak 3 surface profilometer. Once the evaporation was complete the high-tension power supply was turned off and the sample was allowed to cool for approximately 1 hour before the chamber was vented to an external nitrogen atmosphere. This cooling period prevented oxides or other contaminants forming on the surface of the film. The films were then stored in the dark under nitrogen at room temperature.

3.3 Determination of film thickness

Growth of the film thickness during evaporation was monitored using a quartz crystal monitor, which was located inside the Edwards vacuum chamber. The resulting film thicknesses were also checked, after removal from the evaporation chamber using a Detktak3 surface profilometer.

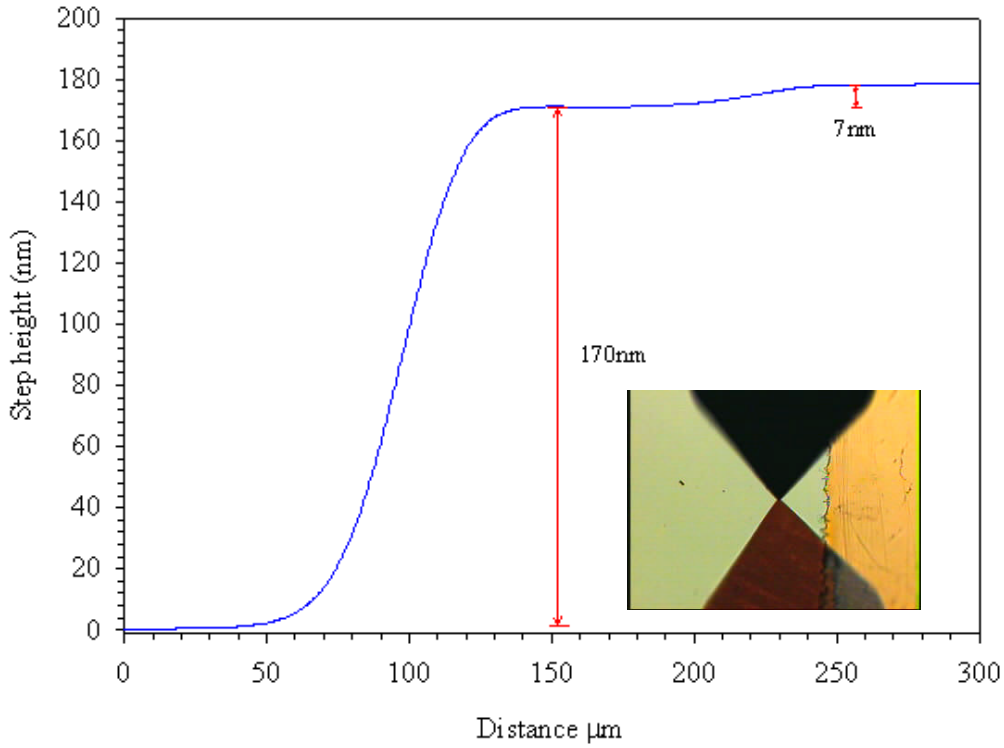

Figure 3.2 Shown in (a) is the recorded surface profile of a fullerene film. Most notable is the step in height of the film,(~170nm) and of the aluminium top electrode(~7nm). The inset shows the image acquired using the Dektak3 video microscope while the stylus is in contact with the sample.

The Dektak instrument is a surface texture measuring system which can analyse the vertical surface profile of a sample, i.e. its roughness, waviness and step height. Measurements are made electromechanically by moving the sample beneath a diamond-tipped stylus 12.5 µm in diameter. It provides accurate height measurements with a reliable measurement accuracy of 10 Å for the step height repeatability, enabling precise

measurements of thin films below 100 Å, figure 3.2. The machine is supplied with a colour video camera and provides both the real time viewing of the scan in progress and also allows saving of the video image of the analyzed surface for further reference, figure 3.2(inset).

3.4 Temperature controlled instrumentation

Throughout the course of this work, the need for low or high temperature measurements necessitated the utilisation of a number of different temperature controlled instruments. For low temperature work (approximately 11K to 330K) a closed cycle helium refrigerator was used. For higher temperature work (77K to 450K) a heating/ cooling stage was employed, with liquid Nitrogen as the coolant.

3.4.1 Closed cycle helium refrigerator

Low temperature measurements, approximately 11K, were preformed using an Oxford Instruments CCC1204 closed cycle Helium fridge. The instrument includes a compressor unit, a cold head and a cryostat shroud suitable for the intended application. Helium gas is compressed to 16 bar in the compressor unit which is connected to the cryostat unit by two flexible lines. The gas expands in the cryostat unit to provide refrigeration, and then returns to the compressor unit. The cold head is in thermal contact with the cold tip which is fitted with a rhodium-iron resistor and a heater for temperature measurement and control. A variable speed motor in the cold head provides adjustable cooling power. At faster speeds, cool down times are reduced and higher heat loads from the sample may be absorbed. When less cooling power is required the compressor may be run at slower speeds, which is achieved by lowering the

gas flow rate on the ITC502 temperature controller. The cryostat is fitted with two radial windows thus providing access for optical measurements. The sample holder is located in an exchange gas sample tube which fits above the cold tip. This allows top loading of samples into the system and samples can be changed while the system remains cold. The CCC1204 was used for recording low temperature Electroabsorption spectra where it was necessary to electrically contact the sample inside the cryostat. To this end a sample holder was designed which would facilitate these measurements. As shown in figure 3.3, the sample holder was fabricated from a SIMM card holder mounted onto a precision made aluminium finger.

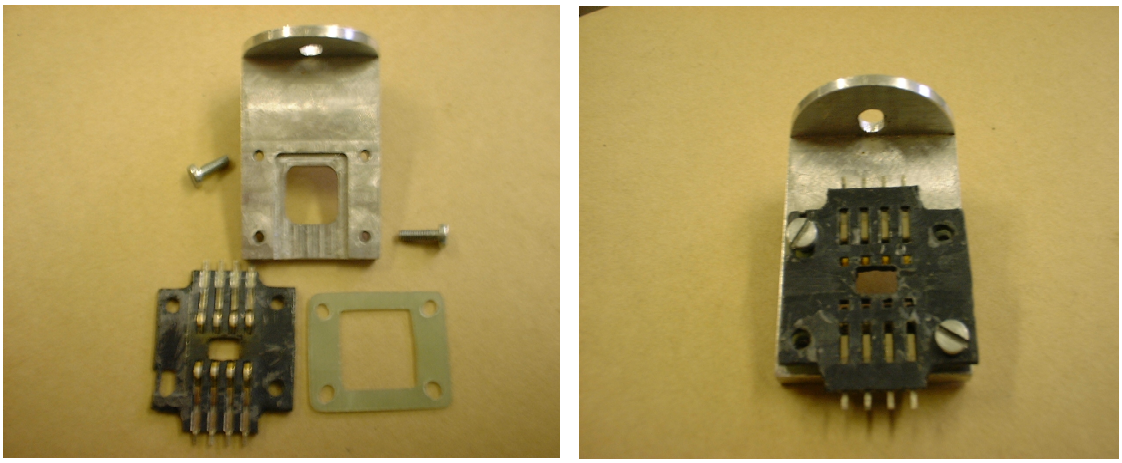

Figure 3.3 Shown in the above left image (a), is the disassembled sample holder unit, which consists of a aluminium base unit, spacer and SIMM card. The image on the right shows the right shows the assembled sample holder ready for mounting and electrical contacting inside the cryostat.

The sample holder is primarily designed to allow transmission of light through the sample under investigation. One constraint associated with this type of sample holder is the need to employ a sandwich type film structure, a consideration which will be dealt with in greater detail in Chapter 4.

3.4.2 Linkam heating/cooling stage

The Linkam THMS600 heating and liquid nitrogen cooling stage allowed for the application different of heating/cooling rates with an accuracy and stability of 0.1K. In general samples were mounted on a 0.17mm cover slip on a highly polished silver heating element to ensure good heat transfer and sensitive temperature measurement. Temperatures were recorded using a 100 Ohm platinum resistor sensor, accurate to 0.01K. The operating temperature range of the instrument is from 77K to 873K with the necessity for water cooling for temperatures above 573K. The unit is gas tight and thus provides an inert atmosphere for all spectroscopic and thermal measurements. The heating/cooling stage also features direct injection of the coolant into the silver block thus allowing rapid cooling of samples. The stage is controlled by a TMS94 temperature controller which can allow for up to 32 different temperature profile ramps to be entered. The stage was used mainly for annealing of samples and in-situ spectroscopic measurement of the annealing process.

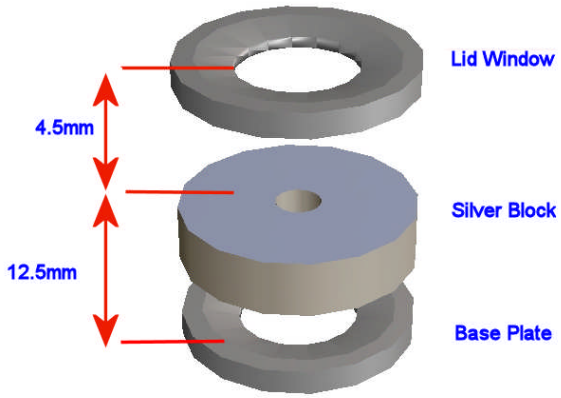

Figure 3.4 Shown above is the Linkam stage schematic depicting the relevant distances between surfaces of the Linkam stage.

The Linkam stage was also used to perform high temperature Electroabsorption measurements. As a result a second sample holder was designed and fabricated to fit inside the heating freezing stage. The design of the holder was hampered by a number of factors. The main constraint was imposed by the small sample space inside the Linkam stage, with a maximum lateral working dimension of 4.5 mm from the silver block to the outer casing, (Figure 3.4). These height restrictions meant that the sample holder had to be thin enough to be mounted on the silver block whilst not touching the outer casing of the stage, (Figure 3.5). To achieve this a block of Teflon, 3mm thick, 15mm in length and 8mm wide was tooled to incorporate a sample substrate, 1.2 mm in thickness, and also an electrical SIMM card, 1mm thick.

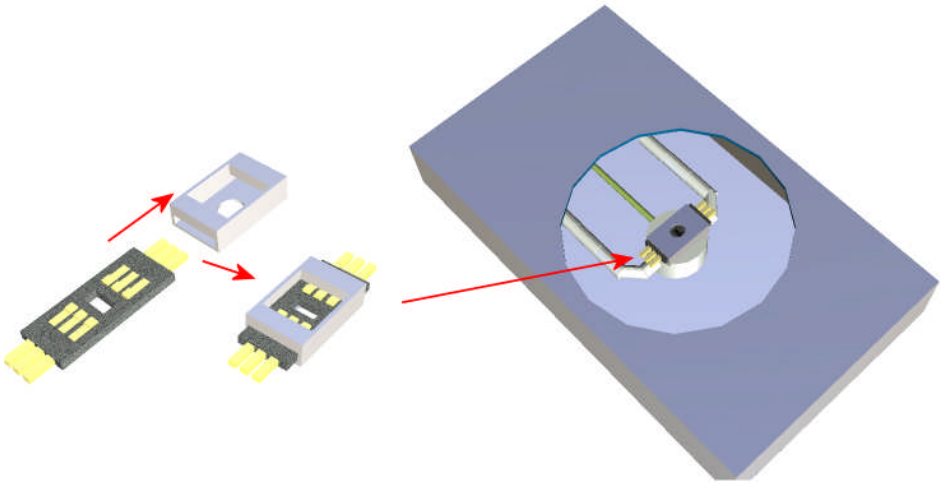

Figure 3.5 Shown above is the diagrammatic representation of the sample holder construction and mounting inside the Linkam heating freezing stage. The sample holder is held in placed with a metal spring clip, (not shown)

The whole holder and sample were affixed to the silver block using a stainless steel spring clip, 0.3 mm in thickness. When assembled the whole unit was 3.3mm in thickness, and provided a clearance of 1.2mm from the outer casing of the Linkam

stage. The use of the sample holder allowed for high temperature (~450K) measurements of samples to be recorded.

3.5 Spectroscopic methods

A number of spectroscopic methods where employed during the characterisation of both C_{60} and C_{70} in solution and the solid form. The spectroscopic methods used allowed the exploration of the phases of C_{60} and C_{70} in their ground states using (IR), in their excited and their transitions to and from excited states using (UV/Vis,).

3.5.1 Infra-Red spectroscopy

Infra-Red (IR) measurements were taken using a Perkin Elmer Spectrum GX, a single-beam Michelson interferometer based Fourier transform Infra Red (FTIR) spectrometer. It has a dual level optical module that is sealed and desiccated. The system is configured with a mid-Infra Red (MIR) single source. MIR and FIR beamsplitters and DTGS detector kits allow the range 7000cm^{-1} to 50cm^{-1} to be covered with a maximum resolution of 0.3cm^{-1}. The spectrometer is configured with the AutoIMAGE microscope system which can operate in transmission or reflectance modes. All microscope operations including adjustments to aperture, focus and illumination are fully automated and controlled from the PC. It includes a built-in 35W tungsten halogen illuminator, a motorised stage and a CCD video camera. An ATR attachment with a micro germanium crystal with a range from 5500cm^{-1} to 600cm^{-1} can be used for micro samples and ATR mapping for surface studies. Film measurements were carried out by sublimation of C_{60} and C_{70} powder onto NaCl windows using an Edwards Auto 306 evaporator. The FTIR microscope was primarily used to characterise the fullerene

samples and in particular for the examination of any polymer formation in the samples during fabrication and annealing.

3.5.2 Electronic (UV/ Visible) spectroscopy

UV/ Visible measurements were taken using a Perkin Elmer Lambda 900 UV/VIS/NIR spectrometer. This is a double-beam, double monochromator ratio recording system with pre-aligned tungsten-halogen and deuterium lamps as sources. The wavelength range is from 175nm to 3300nm with an accuracy of 0.08nm in the UV-visible region and 0.3nm in the near IR region. Accessories available included a 60mm Spectralon coated integrating sphere with a range from 200nm to 2500nm for measurement of samples of high optical density. Solution spectra were taken in a 1cm quartz cell with the solvent system as reference whereas solid samples were mounted in the cell compartment and run against a blank substrate as reference.

.

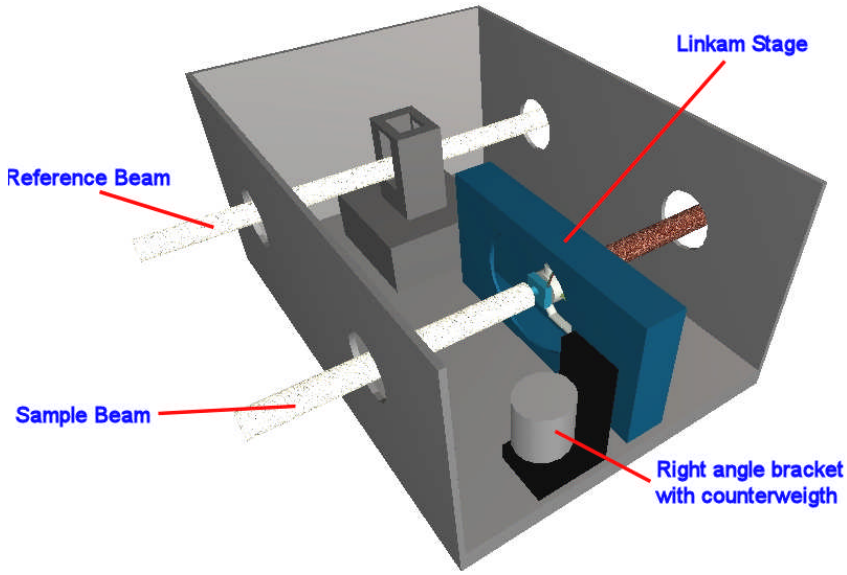

Figure 3.6 Shown is the incorporation of the Linkam stage into the sample compartment of the UV/Vis spectrometer. The whole unit was covered with a black cloth to reduce stray light effects

A common beam mask allowed for the examination of samples with a small surface area and this was generally set to a value of 5 for all temperature dependence measurements. Temperature dependence spectra were recorded using the Linkam heating cooling stage. In order to facilitate these measurements adaptations to the spectrometer sample compartment were necessary (figure 3.6). This involved removing the front panel of the instrument and also the sample cuvette holder assembly. Once removed, the Linkam stage was positioned perpendicular to the base plate. A right angle bracket was affixed to the stage and a carefully positioned counterweight was used to provide stability. The stage was then connected to the liquid nitrogen reserve and temperature control unit. A black cloth was used to cover the sample compartment in order to reduce the effects of stray light.

3.6 X-Ray analysis

The structural characteristics of the fabricated films were obtained using X-ray diffraction measurements. Powder X-ray diffraction measurements were performed using a Siemens D500 diffractometer. The unit comprised of a goniometer that was set up in the Bragg-Brentano geometry with a θ-2θ drive. The X-ray generator was a Kristalloflex model operated at 45kV and 35mA using the CuK αline, (0.15405nm), and a nickel filter (0.015mm) with a solid-state scintillation detector attached to the 2θ-drive. The Cu source generates the X-ray beam at a wavelength of 0.154nm. This beam is then collimated by a slit system which can be varied in order to run the experiments with a proper beam divergence. The diffractometer was interfaced to a PC that controlled the experiment. Routine data collection was generally performed within 30 minutes. The instrument was used to record X-ray diffraction patterns of the fullerene

films before and after the annealing process. Due to the weak diffraction of X-rays by thin films, an alternative procedure to analysing thin films was adopted. This involved deposition of a large quantity of C_{60} or C_{70} inside the Edwards Auto 306 and the subsequent removal of the material from the inside of the dome using a razor blade. This provided greater diffraction intensities as the sample was orientated in all possible directions.

3.7 Atomic force microscopy (AFM)

The surface morphology characteristics of the fabricated films were obtained using Atomic Force Microscopy measurements. AFM measurements were performed using a TopoMetrix Explorer scanning probe microscope (SPM). The unit comprised of a premounted AFM cantilever and tip assembly. The integrated 200x optical microscope, CCD camera and monitor allowed for alignment of the tip and imaging of site selection. The instrument also was capable of being fitted with either a 100μm X-Y or 12μm X-Y fully linearised scanner head. The microscope was controlled by a Pentium PC running Explorer Super-Translater and SPMlab software. The instrument was capable of performing contact, non contact as well as other AFM techniques without any hardware changes. The instrument was used to record AFM measurements of the fullerene films before and after the annealing process. Fullerene samples were sublimed onto silicon wafers (5mm x 10mm in size) using the Edwards evaporator. The fullerene coated wafers were then mounted in a custom made holder so as to ensure the sample surface was positioned at the correct height.

CHAPTER 4

Electroabsorption Experimental Methodology

4.1 Introduction

This chapter presents an analysis of the Electroabsorption instrument and mention some important considerations about its construction. The set-up used is similar to that described by both Boxer, Peteanu and Joseph [47, 48, 49]. In essence it involves passing light from a high-pressure xenon arc discharge lamp, through a monochromator. The radiant energy is then horizontally polarised and focused through a sample under the influence of an externally modulated electric field, housed inside a cryostat. The transmitted light is then detected using a photomultiplier coupled to a lockin amplifier which provides direct measurement of both the total transmission of the sample and of the change in transmission due to application of external field.

4.2 Absorption and electroabsorption

If the optical properties of the sample illustrated schematically in figure 4.1 are considered, the amount of light transmitted at normal incidence to the substrate surface can be described in terms of the sample thickness (d), the absorption coefficient of the material (α) and the surface reflectance (R), according to the following expression [50],

$$I_t = I_o(1-R)^2 e^{-\alpha.d} \qquad \textit{Eqn 4.1}$$

In the above model it is assumed that the reflectance is the same for both front and back reflections, but takes no account of multiple internal reflections.

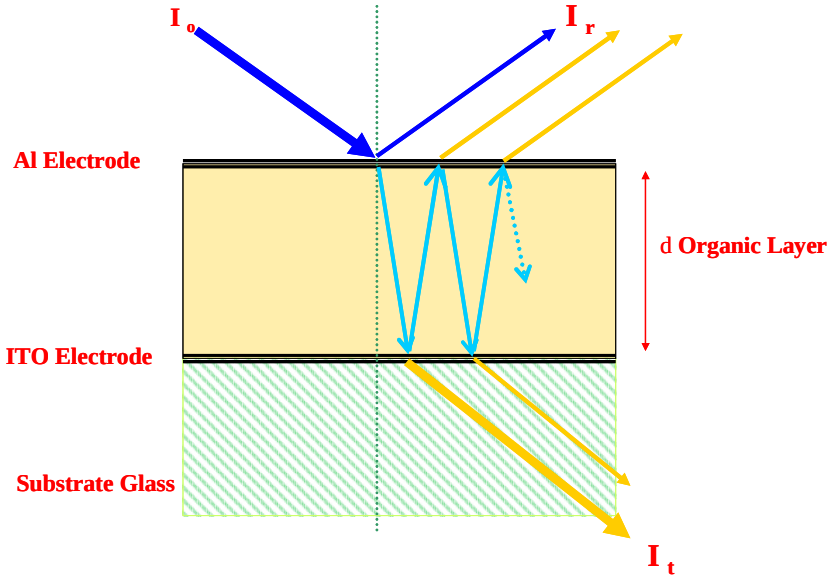

Figure 4.1 Shows the transmission and reflections in a slab of organic material contacted with aluminium top and ITO bottom electrodes. Internal multiple reflections are neglected in calculation the transmitted light intensity.

In the case of a sandwich type structure as shown in figure 4.1, multiple internal reflections occur at the fullerene / Indium Tin Oxide (ITO) layer and also at the interface between the fullerene / Aluminium layer. The change in transmitted light intensity due to the modulating electric field, F, can be approximated as follows;

$$\frac{\partial I_t}{\partial F} = -I_o \exp(-\alpha d)\ \left[\ d(1-R)^2\ \frac{\partial \alpha}{\partial F} + 2(1-R)\ \frac{\partial R}{\partial F}\ \right] \quad \textit{Eqn 4.2}$$

assuming F≠0. Subsequently by dividing Eqn 4.2 by the unperturbed light intensity, i.e. Eqn 4.1, we obtain;

$$-\frac{\Delta I_T}{I_T} = -\frac{\Delta T}{T} = \frac{2}{1-R}\Delta R + d\Delta\alpha \quad \textit{Eqn 4.3}$$

where T is the sample transmission. Examination of Eqn 4.3 reveals that any change in transmission due to an externally applied electric field can actually be composed of two parts. The first part is due to the change in reflectance, known as the Kerr Effect , which is due to a change in refractive index of the material due to the applied field [50]. The second term in Eqn 4.3 is related to the change in absorption of the material and is known as the Stark Effect [50]. In organic semiconductors the contribution from the change in reflectance is very small compared to the change in absorption and can thus be neglected in calculating the electroabsorption signal [50]. Consequently we can write the resulting electroabsorption signal as

$$-\frac{\Delta T}{T} = d\Delta\alpha \quad \textit{Eqn 4.4}$$

where $\Delta\alpha$ is a function of field strength. The details of the Stark effect with specific reference to molecular materials are discussed further in Chapter 5. This chapter outlines the experimental set up designed to measure the spectral distribution of the parameter $\Delta T/T$.

4.3 Instrument Design

The application of electroabsorption spectroscopy to different systems relies on the ability to apply a modulated electric field to the sample under investigation. For the

purposes of temperature dependent measurements this is generally achieved by mounting the sample inside a cryostat. Aside sample compartment considerations of optical and electrical access which will be examined in greater detail later in the chapter, the general requirements of the instrument are similar to those required of any spectrophotometer. As such, it is convenient to examine these spectral components of the instrument first before dealing with the more unique characteristics and implications of incorporating two different cryostats into the system. It should be noted that irrespective of the type of cryostat utilised, a single beam set-up must be adopted. This introduces a possible source of error, since single beam instruments are prone to instrumental fluctuations due to lamp instability.

4.3.1 Spectrometer components

As already mentioned a single beam instrument is generally employed to record the EA spectrum of a sample. A generally schematic of a typical setup is shown in figure 4.2. Using figure 4.2 as a template the individual components of the EA spectrometer will be sequentially examined in greater detail.

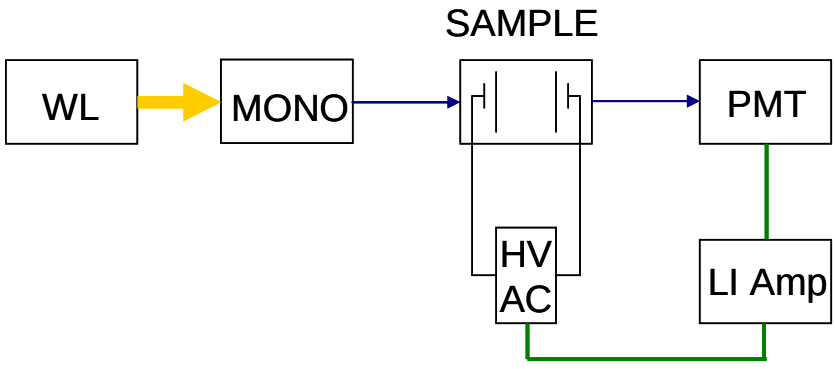

Figure 4.2 The outline schematic of a general EA spectrometer adapted from reference [78]. WL is the white light source; MONO, is the monochromator; PMT is the detector; HVAC is the frequency generator and LI Amp is the lockin amplifier

The sections detailing the sample compartment requirements are dealt with separately from the optical components although there is some overlap with other sections.

4.3.2 Excitation source

Initially a light source must be chosen, the required spectral output of which depends on the sample in question and the wavelength region of interest. For the purpose of this project, all measurements were to be carried out in the visible part of the spectrum. Consequently a broadband white light source such as a Xenon Arc discharge lamp is more than sufficient. For this set-up a LOT Oriel 300 Watt high pressure Xenon Arc lamp(6258) was chosen. In any optical spectroscopy, ensuring that a sufficient intensity of light reaches the detector is of vital importance and in this regard the requirement for an electroabsorption spectrometer is no different. Since in EA spectroscopy the change in the material's absorption is very small compared to the total absorption of the material, variations in the light source may make a significant contribution to the noise of the EA signal. Thus, particularly in EA experiments involving the use of a mechanical chopper, the light source must be sufficiently stable and also be of sufficient intensity so that the signal is not buried in background noise. It is also beneficial if the lamp has a small spot size, so as to enable examination of small areas of samples. The above mentioned light source meets all of the above requirements with the only real disadvantage of having the presence of the high frequency noise associated with all discharge lamps [51]. In general the lamp should be of sufficient intensity such that the jitter never rises above shot noise intensity. The notable exception to this case is the performance of the lamp as it nears the end of its working life [51]. In general, the lamp requires a half hour warm-up period before adequate stability is achieved.

In numerous reported EA measurements [52, 53], the transmitted light intensity is measured using a mechanical chopper with no electric field being applied to the sample. The electric-field-induced change of transmission is then measured without the chopper, and with applied electric field being applied to the sample. This method requires a higher stability of the light source. However in this current set-up the transmitted intensity and the electric-field-induced transmission are measured simultaneously using a lock-in amplifier and thus the requirement for greater lamp stability is not as important.

4.3.3 Spectral dispersion

The second required component of the instrument is a monochromator. The particular choice of monochromator depends on the resolution required to distinguish the absorption bands of a particular sample. In addition the grating must have adequate spectral range to cover the region of interest and ideally be computer controlled so as to allowed easy data collection. Since the instrument will initially involve examination of fullerene C_{60}/C_{70} films, which have absorption bandwidths of approximately 20nm or greater, a monochromator with a resolution of 2nm or better would be sufficient to resolve most spectral features. For this reason a Digikrom CVI CM110, based on the Czerny Turner dual grating design, with a focal length of 110mm was chosen. The instrument is supplied with various slit widths ranging from 0.125mm to 4mm. The maximum spectral resolution of the monochromator was reported to be 0.2nm using a 1200 g/mm grating [54]. Since the set-up would be examining both the qualitative and quantitative aspects of the spectra, it was necessary to compare whether or not an absorption spectrum of fullerene could be reproduced using the EA spectrometer.

While the other spectral components of spectrophotometer system make significant contributions to its characteristics, it is the monochromator which plays the core role in any spectrometer. Figure 4.3 shows the spectra recorded using a commercial spectrometer (Perkin Elmer Lambda 900) compared to a spectrum obtained using a the EA system. There is good agreement between the two recorded spectra and the peak positions of the absorption bands compare well to those cited in literature [32]. The overall line shape of the absorption bands is seen to be well reproduced, although there are some slight differences between the two spectra in particular the region below 2.2eV, which shows a higher absorption for the HOMO-LUMO transition. In addition the peak at 3.6eV is slightly narrower and less intense when compared to the spectrum obtained from the commercial spectrometer.

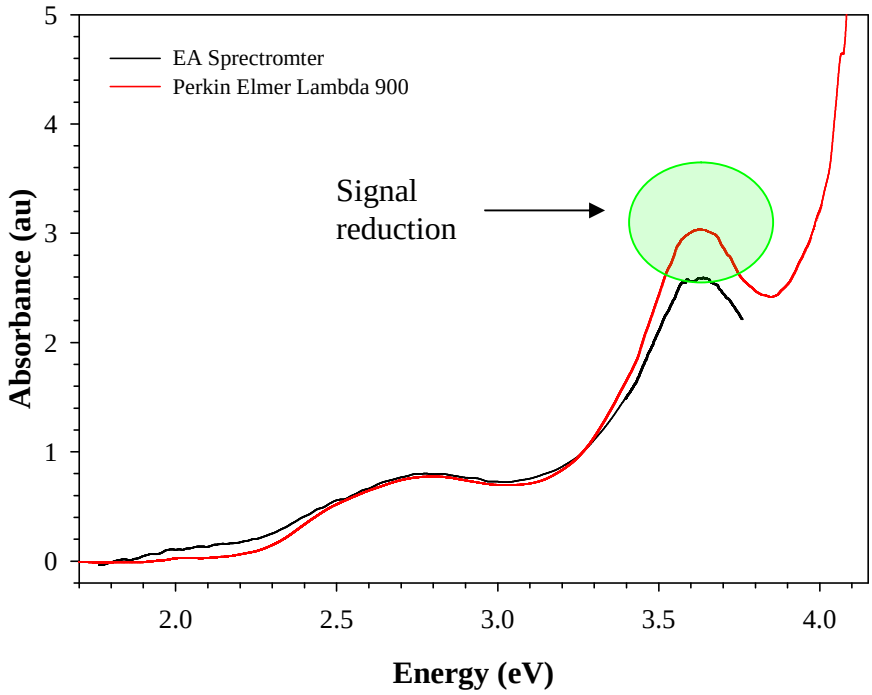

Figure 4.3 The recorded absorption spectrum of fullerene C_{60} using a commercial spectrometer and the home made EA spectrometer. As indicated the slight reduction in absorption feature at 3.6eV is probably due to the single beam nature of the instrument.

These variations in the spectra are most likely due to the single beam nature of the EA spectrometer, and the various spectral cut-offs of the instrument's other spectral components.

4.3.4 Spectral detector

The next component of the system to be decided is the type of optical detector to be used. The two main options available are either a photomultiplier tube or a silicon photodiode, each with its own merits. Irrespective of the type of detector chosen to record an EA measurement, it must measure a large DC signal corresponding to the total transmittance through the sample while also registering a small AC component which is proportional to the change in the materials optical density at the modulating frequency. Depending on the magnitude of the electric field being applied to the sample, the AC component of the signal can be anywhere between four to six orders of magnitude smaller than the DC component of the signal. Thus the ability to recover low noise signals is of major importance in the selection of any detector.

While modern silicon photodiodes offer wide spectral responses with low noise amplification comparable in performance characteristics to photomultipliers tubes (PMT), the preferred choice of detector in applications requiring low noise detection is the photomultiplier tube. Continued improvements in the design of photomultiplier tubes associated with miniaturisation and on board power supplies has also improved their ease of use and reduced the associated cost considerably. Indeed the capital expenditure requirements make the photomultiplier tube the preferred choice of detector. For the purpose of this project an inexpensive Hamamatsu 1P28 A 28mm side

on type PMT was chosen as it provided a wide spectral response, from 1.77eV to 6.7eV, fast response time and a high sensitivity to the low levels of transmitted light associated with a EA signal.

The photomultiplier tube itself was powered by a Hamamatsu C4900 high voltage power supply which is connected to an external power supply of + 15 V DC. This unit has some advantages over its competitors since it is a relatively inexpensive, compact and lightweight on-board power supply. The C4900 high voltage power supply was mounted inside the photomultiplier tube housing and was connected to an external Farnell dual power supply via BNC cables. This external power unit supplies the C4900 with the initial voltage and controls the gain.

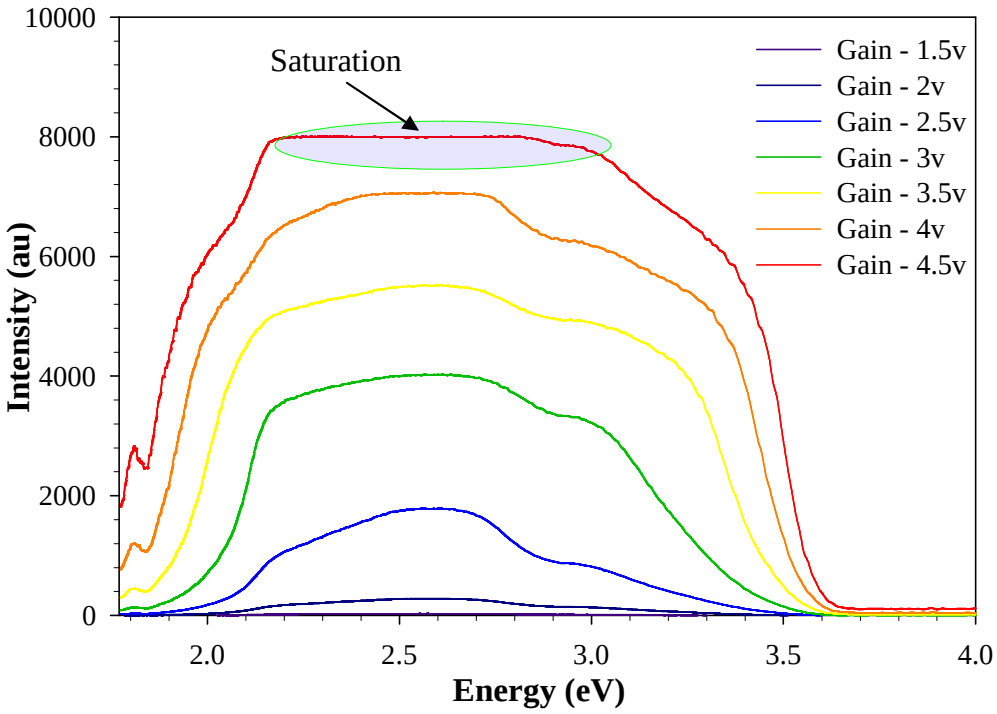

Figure 4.4 The recorded spectra of signal intensity of the photomultiplier tube as the gain is increased. As shown, at the higher gain voltages the spectra start to exhibit a flattening of the spectral profile especially between the energy range of 2.1eV to 3.1eV.

The major advantage of this variable gain control is that the signal from the photomultiplier tube can be adjusted until an acceptable signal to noise ratio is achieved. Aside from the increased noise component of the signal at higher gains the photomultiplier tube can also suffer from saturation as shown in figure 4.4. As shown in figure 4.4 the photomultiplier tube becomes saturated at higher gain voltages. This saturation effect is clearly visible in the spectra as a flattening of the spectral profile between the energy ranges of 2.17eV to 3.1eV. This spectral flattening is most prevalent in the spectra recorded for a gain of -4.5 Volts. It should be mentioned that the above spectra were recorded using a 80-Watt Tungsten Halide lamp.

In the electroabsorption spectrometer the photomultiplier tube was normally set to a gain of between 1 to 3 Volts depending on which excitation source was used as the range provided a reasonable compromise between sensitivity and saturation. Since the Xenon arc discharge lamp has a greater spectral output compared to the Tungsten Halide lamp, scans recorded using it could be obtained at lower gain values.

4.3.5 Lockin amplifier

Given the small size of the change in transmission (AC) signal (10^{-5} to 10^{-6}) relative to the unattenuated transmission (DC) signal it was necessary to employ a lockin amplifier to recover the AC signal from the background noise. The lockin amplifier achieves this signal recovery by multiplying a generated reference signal, either generated internally or supplied externally from a function generator, by the input signal and subsequently passing the output through a low pass filter. This combination of signal multiplication and low pass filtering is known as a phase sensitive detector (PSD). To achieve a maximum output from the PSD, the input wave must be in phase with the reference

signal, although in practise the two signals are minimised by anti-phasing them, and then subsequently adjusting the reference signal by 90^{o}. A more in depth explanation of the underlying principles behind lockin detection can be found in reference [55]. For the purposes of the electroabsorption spectrometer an EG&G model 5210 lockin was utilised. The instrument had an added advantage in that it allowed for the simultaneous monitoring of both the AC and DC component of the EA signal. The actual signal BNC cable was split in two, with one end coupled to the A channel on the front of the instrument, while the second end was connected to one of four available analogue to digital converter (ADC) inputs located at the back of the instrument. Due to the nature of the lock-in process, the output is the root mean squared (RMS) of the selected frequency component's amplitude and thus a correction to the raw experimental data must be made to obtain the real electroabsorption spectra.

4.3.6 Sample geometry.

A crucial aspect of an Electroabsorption spectrometer is its ability to generate a modulated electric field across the sample of the order of 100 kV/cm. This means applying some sort of electrical contact to the sample under investigation. The two most common ways of contacting the sample are either by a co-planar type geometry or in a sandwich type geometry. There are a number of choices depending on the type of sample geometry utilised, either a high voltage supply or a function generator, each with its own merits and disadvantages.

In a coplanar geometry, the sample structure is glass-substrate/ITO/fullerene layer/Al/air. The aluminium is deposited as two contacts separated by a gap of some hundreds of microns or more, between which the field is applied. The light is incident

directly into the organic layer and in this case the electric field is parallel to the substrate plane and thus it is known as a "parallel measurement". A high voltage power supply is an ideal choice as it can induce fields of up to 100 kV/cm in samples relatively easily. An added advantage of this type of supply is that the electrode geometry is much simpler to produce, see Figure 4.5, since higher voltages allow the use of larger electrode gaps, which results in higher transmitted intensities. Consequently these larger gaps allow a greater degree of incident light to reach the detector and thus afford better sensitivity.

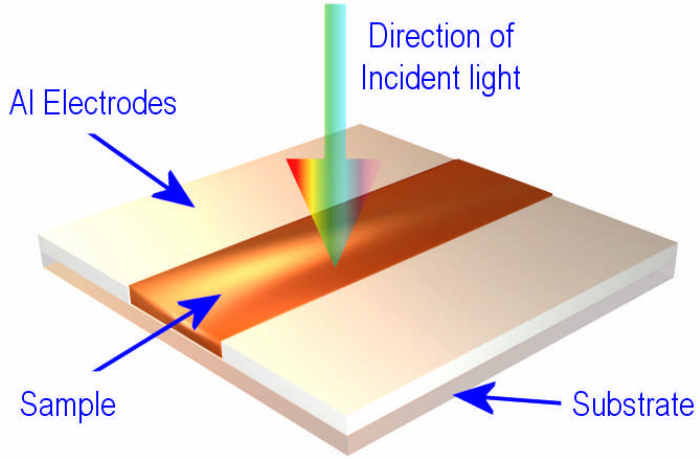

Figure 4.5 Diagram of the "co-planar" electrode geometry. As the model indicates the sample is positioned between two pre-deposited electrodes. The advantage of this design is that it is simple to produce and allows the use of larger spacing between the electrodes, which is allows for a larger transmitted signal intensity.

The only significant reduction in signal intensity is due to the absorbance by the sample and signal intensity is not decreased by the presence of the electrodes, as is the case in the sandwich structures, where light must pass through the sample and the electrodes before it reaches the detector. However a major drawback of utilising this type of

geometry is the need for an expensive high voltage power supply, although a number of attempts were made to fabricate a homemade high voltage supply using a step-up transformer. However the attempts proved to be unsuccessful and a decision was made to try a different approach.

The solution to this problem required a change in the electrode geometry to that of a sandwich structure as shown in figure 4.6. In a sandwich geometry, the sample structure is a glass-substrate/ITO/fullerene layer/Al/air. Light is incident upon the sample from either the glass substrate side or through the aluminium layer. In this the incident light may be transmitted or reflected through the sample depending on the thickness of the aluminium coating. The applied electric field is perpendicular to the substrate plane, so it is called a "perpendicular measurement". In this geometry the gap between the electrodes is reduced to a few hundred nanometres as opposed to 2 to 3mm for "co planar" structures. In fact this gap is determined by the thickness of the film sandwiched between the two electrodes and thus can be controlled during the film deposition.

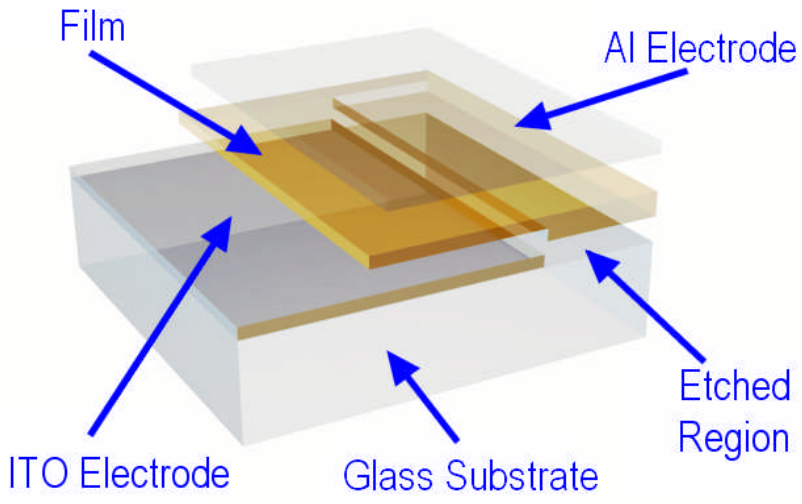

Figure 4.6 Model of the sandwich electrode structure. The glass substrate is coated with a thin transparent layer of ITO, containing a small-etched region, which serves as the bottom electrode.

As mentioned previously, electric field strengths of approximately 100 kV / cm are required to induce Stark splitting. Consequently the reduction in the gap size enables the use of lower voltages, (~1 Volt) to achieve the same Stark effect. Voltages of this magnitude can be easily and routinely obtained from a function generator.

The electrodes used were a commercially purchased transparent pre-coated indium tin oxide bottom electrode, (ITO), and a semitransparent aluminium top electrode.

Figure 4.7 shows the recorded spectral transmission of the ITO substrate where the transmission of the substrate from 1.5eV to 3.75eV is larger than 65 %. The measured sheet resistance of the ITO layer is approximately between 50 Ω/cm^2 to 75 Ω/cm^2, thus assuring a negligible influence on the electrical measurements of the fullerene layer. Prior to film deposition in the vacuum chamber, a pre-cleaning of the substrates was preformed so as to ensure that the substrate was free of dust and chemical impurities.

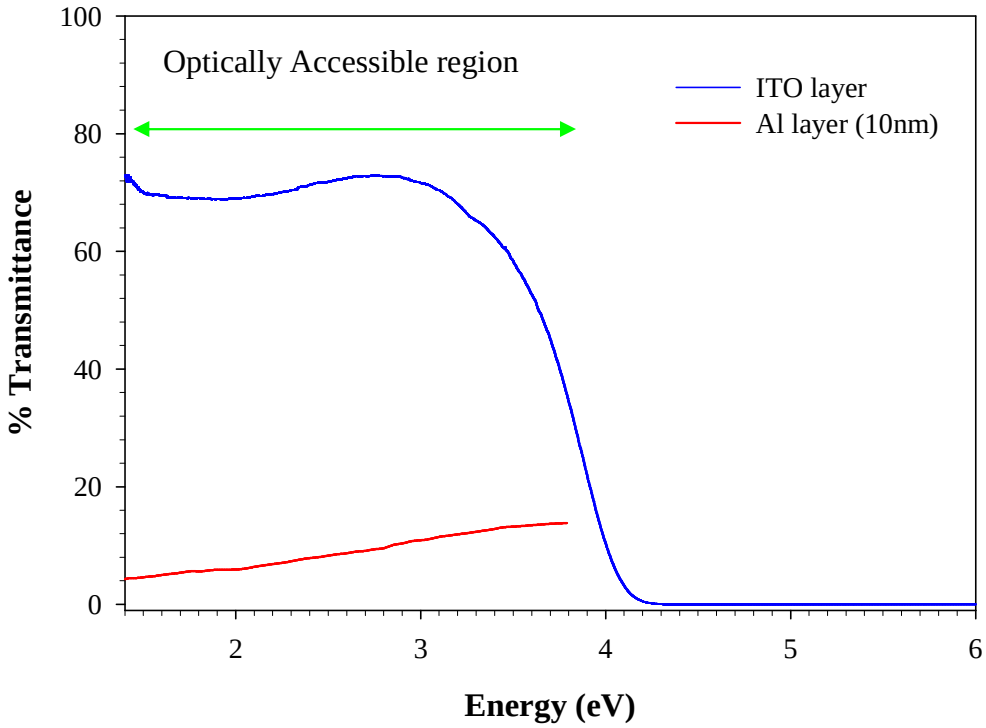

Figure 4.7 The spectral transmittance of the indium tin oxide substrate and top aluminium layer (10nm). The substrates are transparent from 1.5eV to 3.75eV.

The importance of this pre-cleaning step cannot be understated as it provides a means of preventing the occurrence of electrical shorting between the electrodes. There are two parameters which need to be optimised for sandwich type sample geometries. The first is the thickness of the actual organic layer under examination and the second is the choice of the top electrode and its thickness. A thick organic layer ensures that the bulk behaviour of the material is being measured but makes the detection of an EA signal difficult. Similarly a large top electrode ensures good electrical contact with the sample but reduces the intensity of the transmitted light leading to difficulties in signal detection. Another consideration in the choice of the top electrode is whether or not the electrode material possesses any absorption bands in the spectral region of interest. From a spectroscopic view point, an ideal optical electrode should exhibit a flat transmission spectrum in the region of interest and also have a high transmission. For the current set of experiments, Al was chosen as the top electrical contact, since it possesses a flat spectra in the region of interest and is relatively cheap, although its poor transmission ratio does reduce the EA signal intensity (see figure 4.7). The transmission spectrum of the ITO substrate is also relatively flat in the spectral range of interest, with an optically assessable window of up to 4eV, (figure 4.7).

Since the thickness of the aluminium electrode predominately determines the intensity of the signal reaching the detector, an electrode thickness of approximately 10nm was preferred as it afforded a reasonable compromise between signal throughput and acceptable electrical contact with the sample. There are however a number of problems associated with sandwich structure, not least of which is electrical shorting between the electrodes due to film irregularities. A second problem of this design is the reduction in the transmitted light intensity, since the light must pass through the electrodes to reach

the detector while still ensuring good electrical contact with the sample. Although it is possible to perform electroabsorption spectroscopy in a reflection mode, thereby allowing total reflection of light off the top electrode, the difficulties associated with collection of reflected light favoured the transmission set-up.

4.3.7 Electric field application

Depending on the type of electrode geometry, the field generator can be either a high voltage supply or a function generator. For the purpose of this project a sandwich geometry was chosen and thus a SRS DS 345 signal generator was used. The DS345 Function Generator is a 30 MHz instrument that can generate numerous standard waveforms with excellent frequency resolution (1 μHz). Both the function output and a TTL SYNC output are available through floating, front-panel BNC connectors.

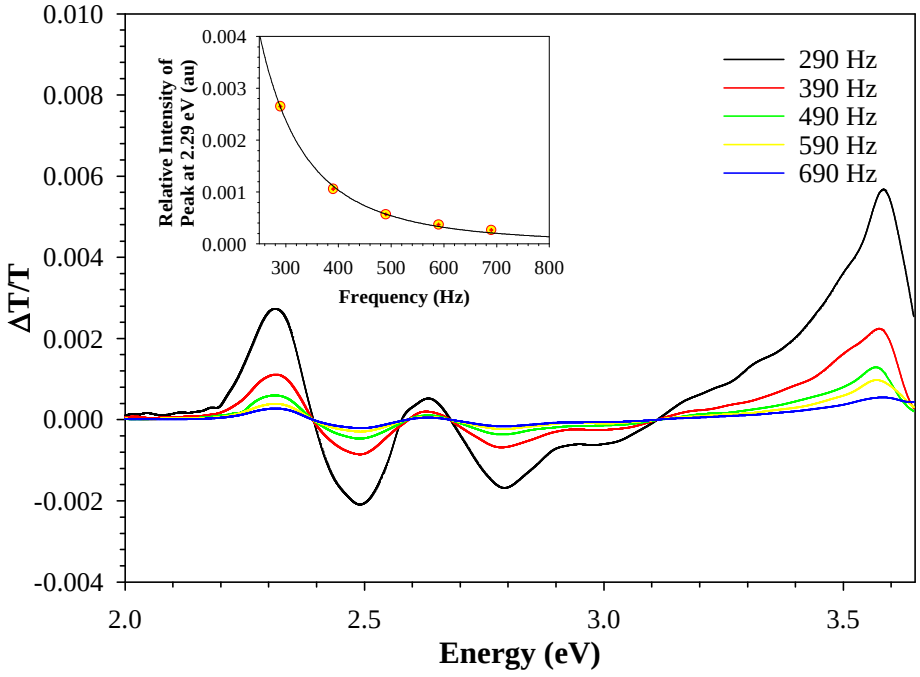

Figure 4.8 The effect of changing the modulation frequency on the ΔT/T signal of C_{60}. As indicated increasing the modulation frequency results in a reduction of the signal strength. The inset shows the plot of peak intensity at 2.29eV as a function of increasing frequency

The amplitude of all function outputs is adjustable from 10 mVpp to 10 Vpp with 3-digit resolution. Since the externally applied field is an oscillating AC voltage it is necessary to choose the field's particular frequency. By changing the modulation frequency of the applied field it may be possible to separate features of different origin, Frenkel excitons or CT excitons. Features arising from the same origin will have the same phase as the electroabsorbance signal. At low frequencies this phase may be the same for all features independent of their origin, however as the frequency increases different phenomena will react to the applied fields on different time scales. While exploration of these changes in phase and relative intensities changes should provide useful information on the structural dynamics of fullerenes it is beyond the scope of this thesis and as such the requirement for the current work is to utilise a single low frequency. Figure 4.8 shows the effect of changing the modulation frequency on the Electroabsorption signal of C_{60}, the exact details of which will be explored in Chapter 5. Based on the data obtained in figure 4.8, frequencies below 290 Hz yield EA signals of higher intensities.

Aside from the frequency dependence of the electroabsorption signal the effect of increasing the external applied field also needs to be investigated. Increasing the field will increase the degree of Stark splitting but care must be taken not to damage the sample due to dielectric breakdown, Figure 4.9. In an ideal sample the electric field is homogeneously distributed in the organic layer. In a sandwich type sample this electric field distribution can be described as:

$$F(x) = -\frac{V - V_{bi}}{d} \qquad \textit{Eqn 4.5}$$

where F(x) is the electric field inside the sample, V is the externally applied voltage, d is the sample thickness, V_{bi} is the built in potential resulting from differences in the

work function of the various electrodes [50]. In chapter 5 it will be shown that the electroabsorption signal, EA(x), is proportional to the square of the externally applied field, and can be written as follows,

$$EA(x) = F^2(x) \qquad \textit{Eqn. 4.6}$$

The applied external electric field which is composed of a DC and AC portion can be written as [56],

$$V = V_{DC} + V_{AC}\cos(\omega t) \qquad \textit{Eqn. 4.7}$$

$$\overline{EA}_{\Omega} = \frac{(V - V_{bi})^2}{d^2} = \frac{1}{d^2}\{V_{DC} - V_{bi})^2 + V_{AC}^2 + 2(V_{DC} + V_{bi})V_{AC}\cos(\omega t) + \frac{1}{2}V_{AC}^2\cos(2\omega t)\}$$

Eqn. 4.8

Upon examination of Eqn 4.8 it can be seen that the EA signal is actually composed of three parts, the first part is the DC component of the EA signal, the second part is the first harmonic of the signal and the third and final part is the second harmonic of the EA signal.

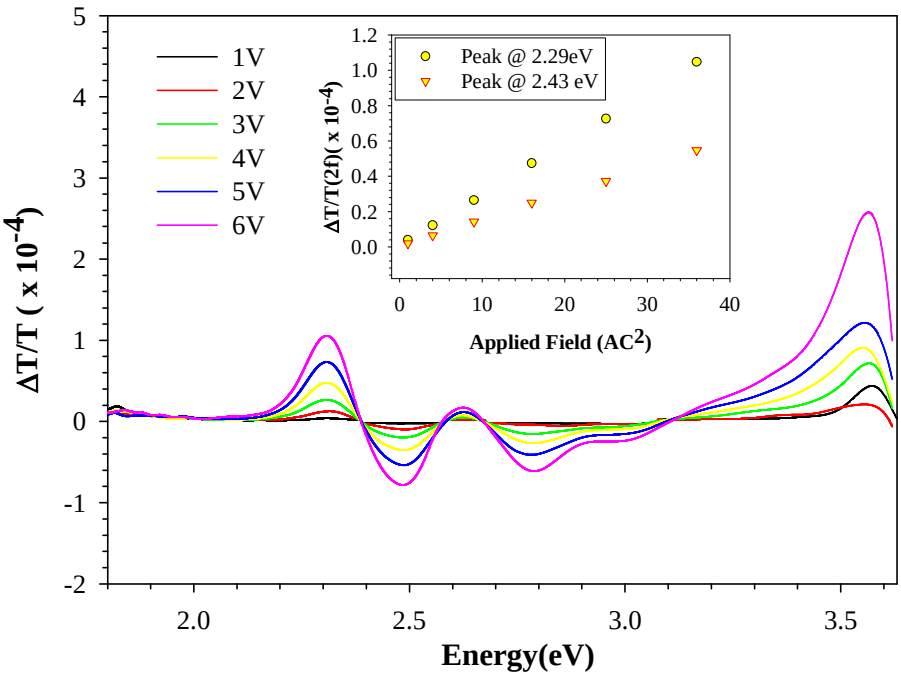

Figure 4.9 The effect of increasing the applied field on the EA signal. The inset shows that the signal response is quadratic in nature**.**

We can define the EA1f and EA2f as the first and second harmonic of the electroabsorption signal and thus they can be written as,

$$EA1f \propto \frac{1}{d^2}(V_{DC} - V_{bi})V_{AC} \qquad \textit{Eqn. 4.9}$$

$$EA2f \propto \frac{1}{d^2}V_{AC}^2 \qquad \textit{Eqn. 4.10}$$

The use of a lock-in amplifier allows for the detection of both the first and second harmonic of the applied electric field frequency. The EA1f signal is proportional to the product of the applied AC and DC bias. The EA2f signal increases linearly with the square of the applied AC bias, as shown in figure 4.9 (inset), and is independent of the DC bias.

4.4 Low temperature electroabsorption spectrometer

A number of properties of semiconductors, such as charge mobility and consequently the material conductivity or the material optical absorption, are temperature dependant and thus the material temperature is a useful parameter to control. Aside from the optical components of the spectrometer, it was necessary to consider the restraints enforced by incorporating an Oxford Instruments CCC1204 closed cycle Helium refrigerator cryostat within the system before being able to design and construct the instrument. An initial constraint is that a single beam set-up must be employed introducing a possible source of error due to lamp instability. The low temperature Stark spectrometer schematic is shown in figure 4.10.

A second constraint enforced by the cryostat is the actual height of the optical access through the cryostat which is positioned 338mm above the base of the cryostat. In the absence of fibre optic coupling, the optical components must be raised to the same

height as the cryostat windows. The working temperature range of the CCC1204 is reported to be between 11K to 330K [57]. The cryostat is capable of being equipped with four optical access ports, although for the purposes of this project only two windows were needed. These windows are at 180° to each other, allowing transmission of light, although the cryostat can be easily converted into a 90° reflection geometry if required. The primary function of the cryostat is to cool the sample to cryogenic temperatures (11K) so as to facilitate low temperature work.

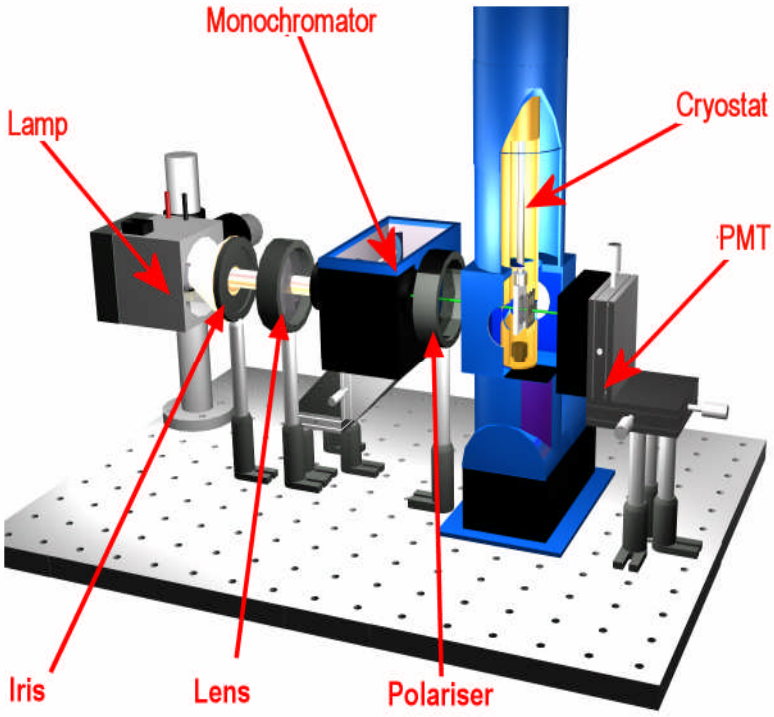

Figure 4.10 A schematic of the low temperature (11K) Electroabsorption spectrometer. The depiction shows a single beam instrument with light leaving an excitation source and being focused onto the entrance slit of a monochromator

To prevent condensation on the windows, both the inner and outer chamber need to be evacuated, which is achieved by means of a rotary backed turbo molecular pump. The inner chamber is purged with helium gas, which acts as a convection medium between

the cold tip and the sample. As previously mentioned the temperature controller regulates the cooling rate of the cold tip by either increasing or decreasing the helium gas flow rate of the compressor.

The controller also serves as a monitor for both the sample holder and cold finger temperature. The cryostat's inner chamber incorporates the sample holder, which is positioned directly in the light path. Once the light had been transmitted through the sample, it then passed through a second set of inner and outer windows before it reaches the detector.

.

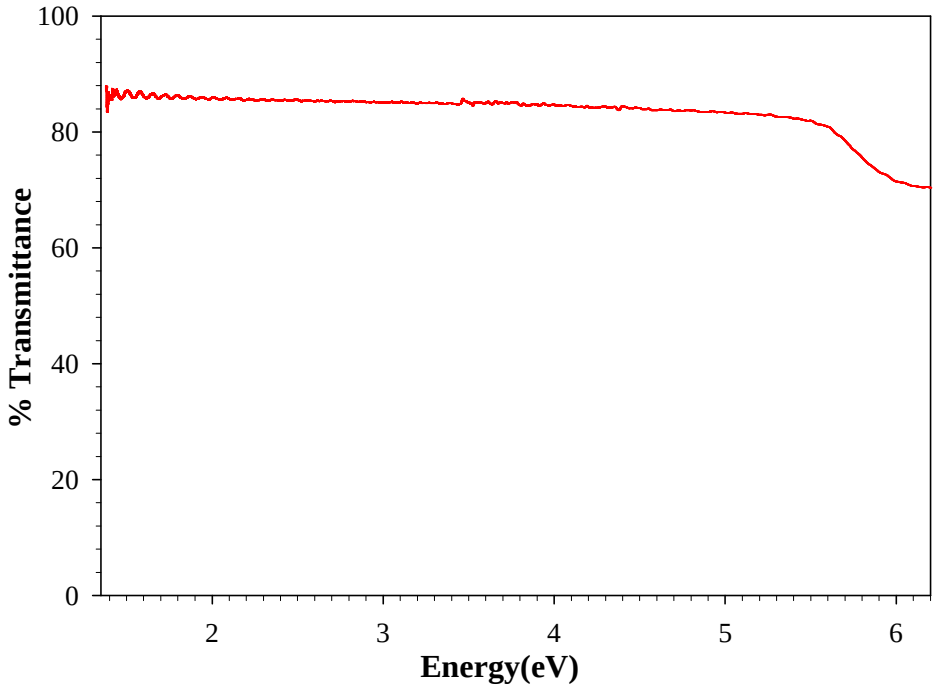

Figure 4.11 The spectral transmission of the cryostats Spectrosil B windows. As indicated the windows are transparent from the ultra violet region upwards. The slight decrease to approximately 90 % in signal intensity is due to reflection from the windows surface.

The spectral transmission of these windows, which are made from Spectrosil B, as measured by the Perkin Elmer Lambda 900 UV/VIS/NIR Spectrometer, is shown in figure 4.11. As shown the windows are transparent from 6.2eV, with a slight decrease

in signal intensity which is due to reflection from the window's surface. Consequently utilisation of these windows places no adverse limitations on the spectral range of the electroabsorption instrument. In the low temperature spectrometer the sample is mounted onto a sample rod which is then top loaded into the cryostat and subsequently surrounded by a helium atmosphere. Electrical contacts to the sample were made using a custom designed holder, described in Chapter 3.

4.5 High temperature electroabsorption spectrometer

During the course of the work it became apparent that in order to observe the peculiar annealing effects associated with the fullerene molecules a second system, which allowed in situ annealing and EA spectra to be recorded at elevated temperatures, needed to be developed. To achieve this, a FTIR600 Linkam heating and cooling stage needed to be incorporated into the system.

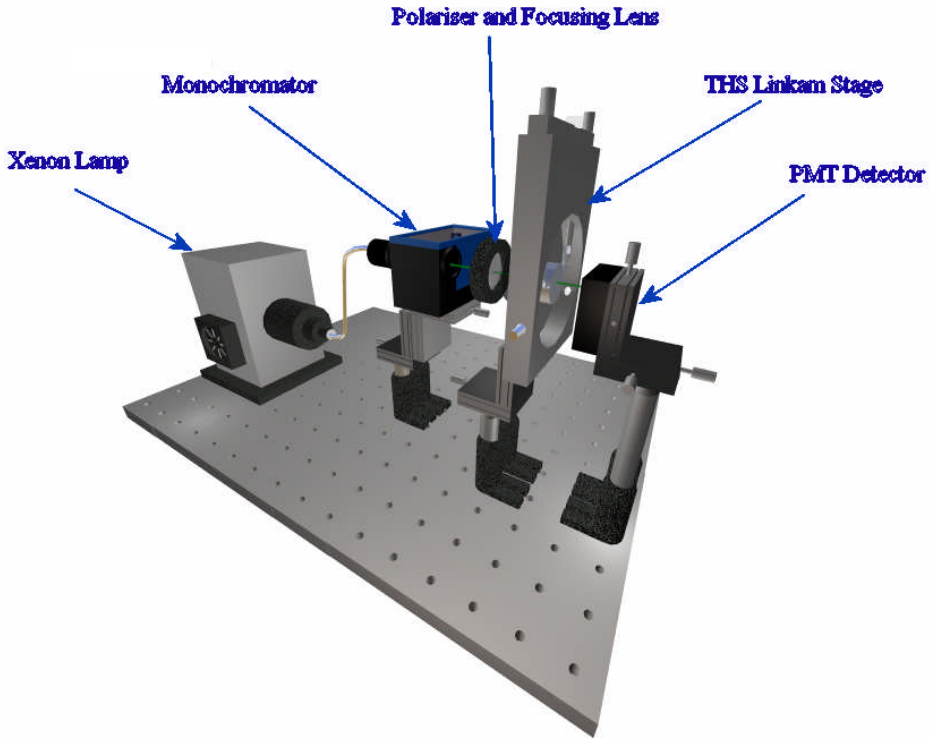

Figure 4.12 Schematic of the high temperature electroabsorption spectrometer incorporating a Linkam THS FTIR 600 heating/cooling stage.

The stage itself allows for the analysis of samples to be conducted from 77K up to 873K, with heating and cooling ramp rates of 130K/min and boasts a temperature stability of greater than 0.1K. Since that stage is designed for use in infra red spectroscopy, the FTIR600 stage can be mounted either horizontally or vertically. The silver block exhibits a high thermal conductivity and has a tapered hole to allow maximum transmittance of radiation without causing any interference. Recycled nitrogen gas is used to purge the stage of moisture and prevent condensation hence, enabling the capture of clear highly resolved images.

The incorporation of this device had a number of implications regarding the overall design. The actual schematic of the high temperature spectrometer is shown in figure 4.12. The utilisation of the Linkam stage had a number of advantages, since thin films could be annealed in situ and their associated spectra recorded. Secondly the stage could also be incorporated in a commercial spectrometer and the equivalent absorption spectrum of the sample could also be obtained either at room temperature or at elevated temperatures, all without disturbing the sample.

4.6 Instrument control and connections

A computer, running a custom written LabVIEW programme is used to control the electroabsorption instrument. Through the use of this program the computer directly controls both the monochromator and the lockin amplifier. Figure 4.13 gives a schematic representation of the entire electroabsorption instrument under computer control. The monochromator is connected via a serial cable (RS 232) to a COM port located at the back of the computer. The lockin amplifier is connected to the computer by a GPIB cable, to a data acquisition card. Both the monochromator and the lockin

amplifier need to be computer controlled due to the complexities involved in performing, and recording, a scan. Aside from the computer control of the instrument there are a number of connections between the various components, which are needed before the instrument is fully functional. Firstly, a modulated voltage needs to be supplied to the sample, housed within the cryostat, by the function generator. The function generator must also supply a reference signal (TTL), to the lockin amplifier, which is connected to the "ref-in" located at the back of the lockin. The third and final connection that has to be made is between the photomultiplier and the lockin amplifier. Since the lockin amplifier is capable of recording both the AC and DC component of the signal simultaneously, the actual signal from the photomultiplier is split in two by means of a "T" male BNC connector.

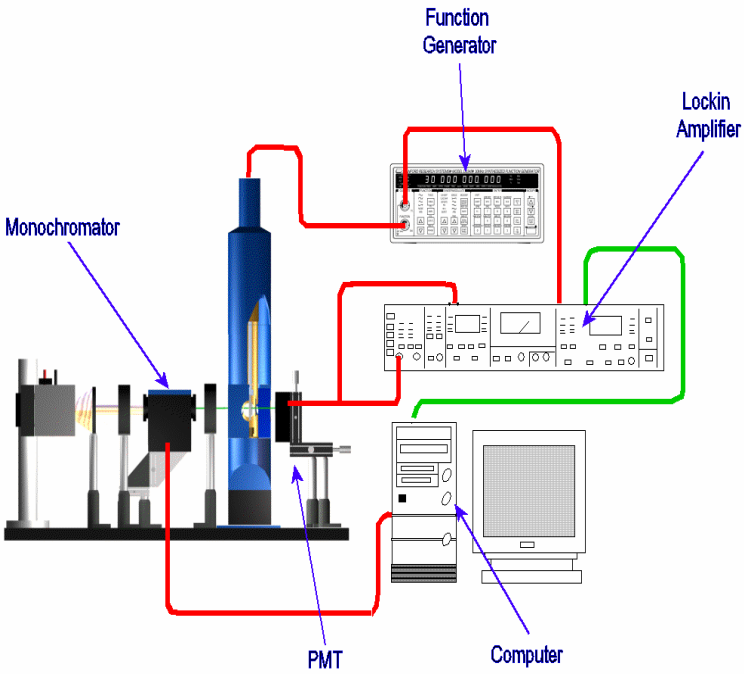

Figure 4.13 Schematic representation of the entire electroabsorption instrument under computer control. Both the monochromator and the lockin are connected directly to the computer. The monochromator is connected via a serial cable (RS 232) to a com port located at the back of the computer. The lockin amplifier is connected to via a GPIB cable, (indicated by the green line), to a data acquisition card occupying one of the computers pci slots.

The first cable is connected to the analogue input “A” located at the front of the lockin amplifier and allows for the measurement of the AC component of the photomultiplier signal. The second cable is connected to one of the analogue to digital converters (ADC) located on the rear of the instrument. Once all the necessary connections have been made, the instrument is fully functional and aside from the initial manual configuration of the function generators frequency and amplitude, the photomultiplier gain and the lockin amplifier sensitivity, it can be completely controlled from the computer through the LabVIEW interface.

4.7 Data acquisition

Owing to the vast amount of data produced during the acquisition of an electroabsorption spectrum, it is necessary to computerise the operation. With regard to the current hardware requirements for the set-up, a computer, (Pentium II) fitted with a ISA GPIB card and a free serial port are needed for communication between the PC and both the lockin amplifier and monochromator respectively. Once the hardware requirements are met the next decision is the choice of programming language used to code the control program. For the purposes of this set-up a graphical user language called LabVIEW was used. It is an excellent choice since it is well integrated with the DAQ interface card and has excellent built-in libraries for data acquisition and for performing real-time calculations. LabVIEW is a program development environment, similar to BASIC. However, LabVIEW is different from this application in one important respect. BASIC uses text-based languages to create lines of code, while LabVIEW uses a graphical programming language, G, to create programs in block diagram form. Instead of text code it uses icons or graphical symbols, which can be

connected together to form a program. LabVIEW is a general-purpose programming system with extensive libraries of functions and subroutines. LabVIEW also contains application-specific libraries for data acquisition, GPIB and serial instrument control, data analysis, data presentation, and data storage. There is also an option which allows animation of the execution. This shows how data passes through the program, making debugging and program development easier [58]. The LabVIEW application consists of two interfaces referred to as the front panel and the Block Diagram. The Front Panel is the window the user observes when the program is running. It contains a toolbar of command controls and status indicators for running and debugging VIs (Virtual Instruments). It also contains two palettes, which are used when building and designing the program. The tools palette contains the tools used to edit and debug VIs and the Controls Palette is used to place controls and indicators on the front panel of the VI.

4.7.1 Electroabsorption front panel

The front panel of the program is divided up into two sections and is designed to allow the user to alter various settings of the instrument. In the instrument set-up panel, figure 4.14, various parameters of the monochromator's set-up can be controlled. This panel also contains an initiator switch for the monochromator as well as the COM port and step size settings for the monochromator, all of which can be adjusted as required. This panel also gives feed back on the status of the monochromator, returning an error code if the monochromator has not initialised properly. Important to note is that once this portion of the program is activated, it is impossible to operate the rest of the program.

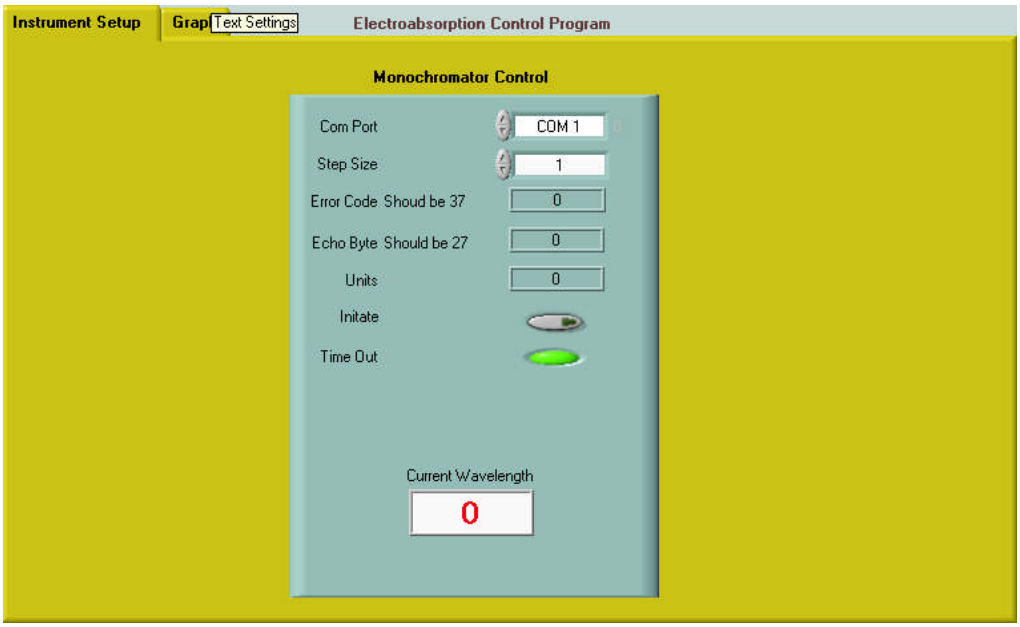

Figure 4.14 Picture of instruments set-up control panel. From this panel it is possible to define certain parameters and initialise the monochromator. Once this section of the program is activated it is impossible to enable any other parts of the program.

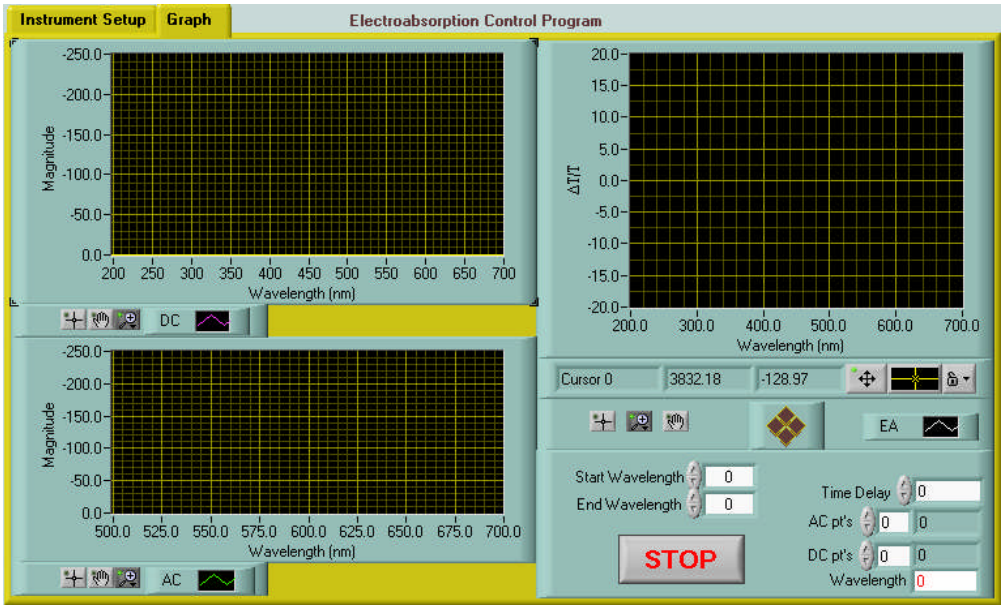

Figure 4.15 The graph panel of the electroabsorption program. This is the main control panel of the program as it contains the controls settings for both the lockin amplifier and monochromator. As shown it allows parameters like the spectral range and number of data points sampled to be controlled.

Although the primary function of the graph panel, figure 4.15, is to provide a visual representation of the recorded data, it also allows control over a number of different instrument parameters. These parameters include the spectral range of the scan and the number of data points to be sampled by the lockin amplifier during the scan. It is also possible to adjust the time delay between sampling. Increasing or decreasing the number of data points allows the signal to noise ratio to be optimised. As already mentioned the primary function of this panel is to afford a visual display of the data. The two graphs located to the left-hand side display the recorded DC and AC signals, while the graph on the right hand side displays the calculated EA signal. When a scan is complete, the data is then write-recorded to a file in ASCII format, which can then be imported into spreadsheets or other programs for further analysis and presentation.

4.7.2 Electroabsorption block diagram

The block diagram of the electroabsorption control program contains the actual coded program. It can be separated into four routine sequences. The first sequence involves initialising the monochromator, figure 4.16. This section of the program was adapted from a program designed for use with the monochromator and was incorporated into the overall electroabsorption control program [59]. As shown in figure 4.16, the monochromator routine is composed of a number of subroutines, which are performed in alphabetical order.

Routine (a) configures the serial port to the following parameters, baud rate of 9600, a parity of 1, number of data bits to 8 and the number of stop bits to 1. The settings used were reported to be the most reliable by the monochromators manufacturer [54].

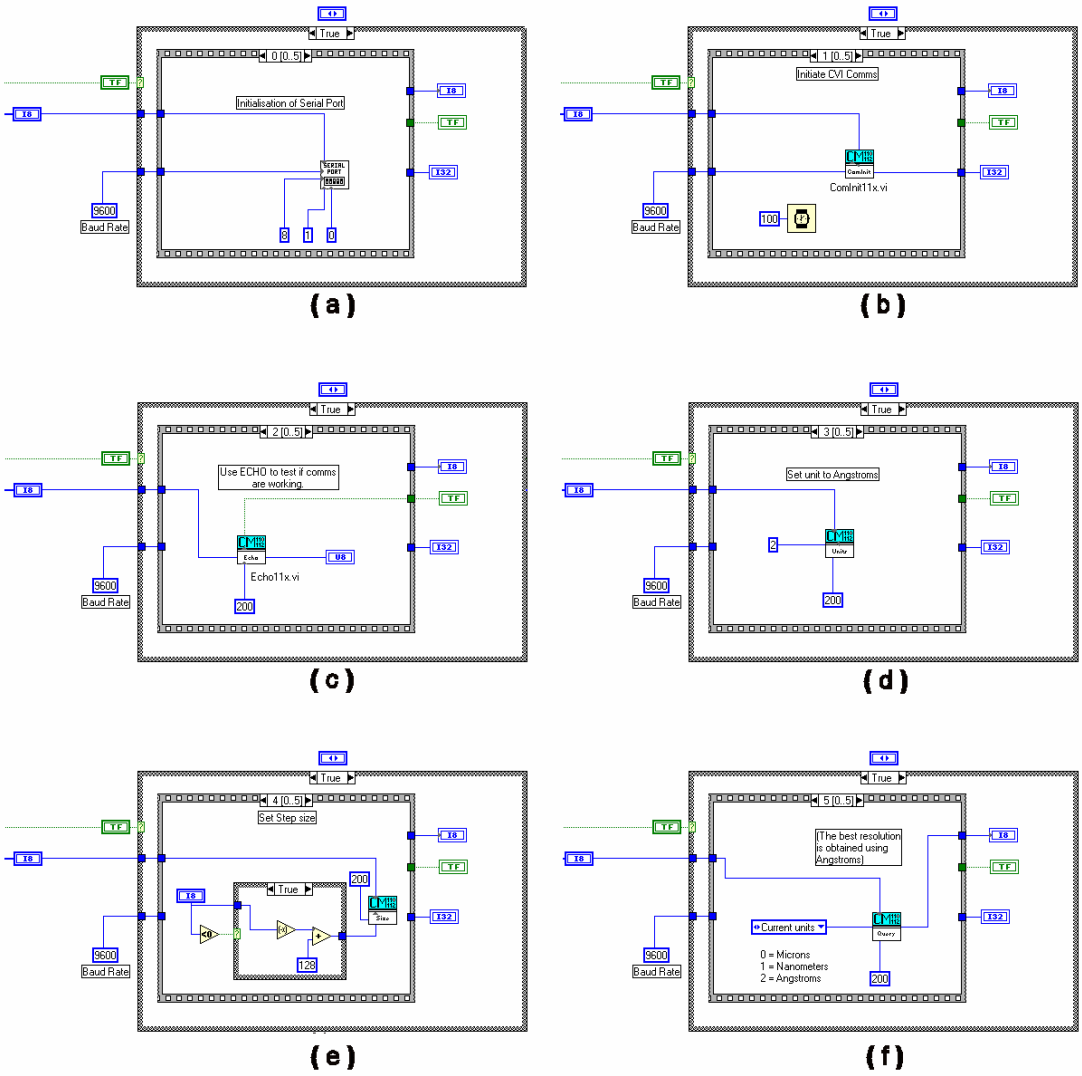

Figure 4.16 The block diagram for the first sequence of electroabsorption program. This section of the program was supplied with the monochromator and was incorporated into the overall program. Its function is to control the initialisation of the monochromator.

Routine (b) initialises the monochromator communication with the computer. After the communication link has been established, Routine (c) uses an ECHO command to test the communication link. An error code is displayed if there are any failures between the monochromator and the computer. If no error code is return the program then uses Routines (d) and (e) to set the monochromator units and step size to Angstroms respectively. Finally routine (f) uses a QUERY command to check units. Once the

initialisation is complete this section of the program is deactivated by the user and in doing so allows the rest of the program to be activated.

The second sequence involves collection of the DC data using one of the lockin amplifier's ADCs on the rear panel, as shown in figure 4.17.

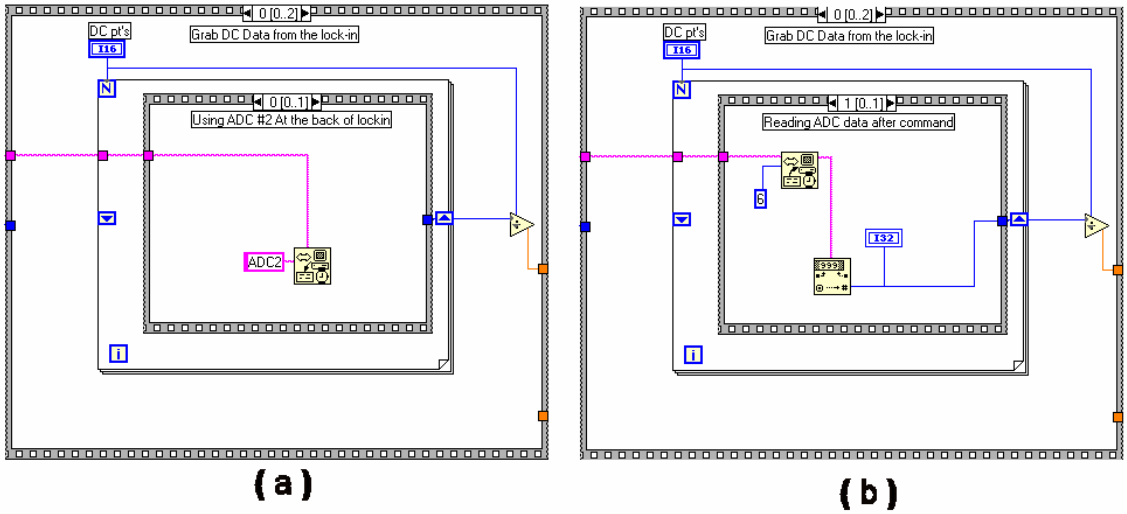

Figure 4.17 The second sequence of the electroabsorption control program, which is involved in the collection of DC data from the lockin amplifier. Panel (a) shows a write command being used to instruct the lockin amplifier to record the DC data at ADC channel 2. Panel (b) shows a read command being used to instruct the lockin amplifier to transmit the recorded data to the computer.

As shown in figure 4.17, panel (a) uses a GPIB WRITE command to tell the lockin to record the data presented at ADC channel 2. Subsequently panel (b) uses a GPIB READ command to tell the lockin to transmit the data to the computer. This string is then converted to a decimal number by the routine. Both these routines are contained in a FOR-LOOP, which allows a number of data points to be recorded and averaged for each wavelength. The third sequence of the electroabsorption program involves collection of the AC data using the lockin amplifiers "X" function, as shown in figure 4.18.

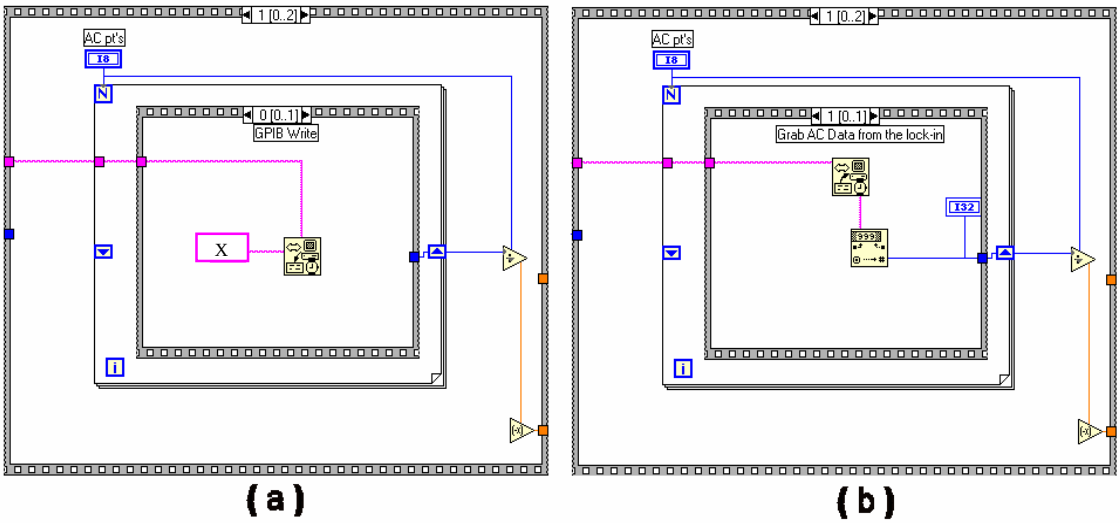

Figure 4.18 The third sequence of the electroabsorption program. Panel (a) shows the use of a GPIB WRITE function to instruct the lockin amplifier to record the magnitude of the data at the "A" input. Panel (b) shows the utilisation of a GPIB READ command, which instructs the lockin amplifier to transmit the recorded data to the computer.

Routine (a) uses a GPIB WRITE command to tell the lockin record the magnitude of the data presented at "A" input. As already mention previously the magnitude of the AC component is presented as a DC value. As before routine (b) uses a GPIB READ command to tell the lockin to transmit the data to the computer. This string is then converted to a decimal number by the routine. Again both these routines are contained in a For Loop, which allows for a number of data point to be recorded and averaged for each wavelength. It should be noted that before each scan the phase of the signal was auto adjusted to the reference to yield a maximum deflection on the front panel of the lockin. This was achieved using the auto-phase function on the lockin amplifier. Both the AC and DC sub-routines are embedded in the fourth and final routine sequence of the main electroabsorption program, as shown in figure 4.19. The primary function of this main routine is to step the monochromator after collection of each data point.

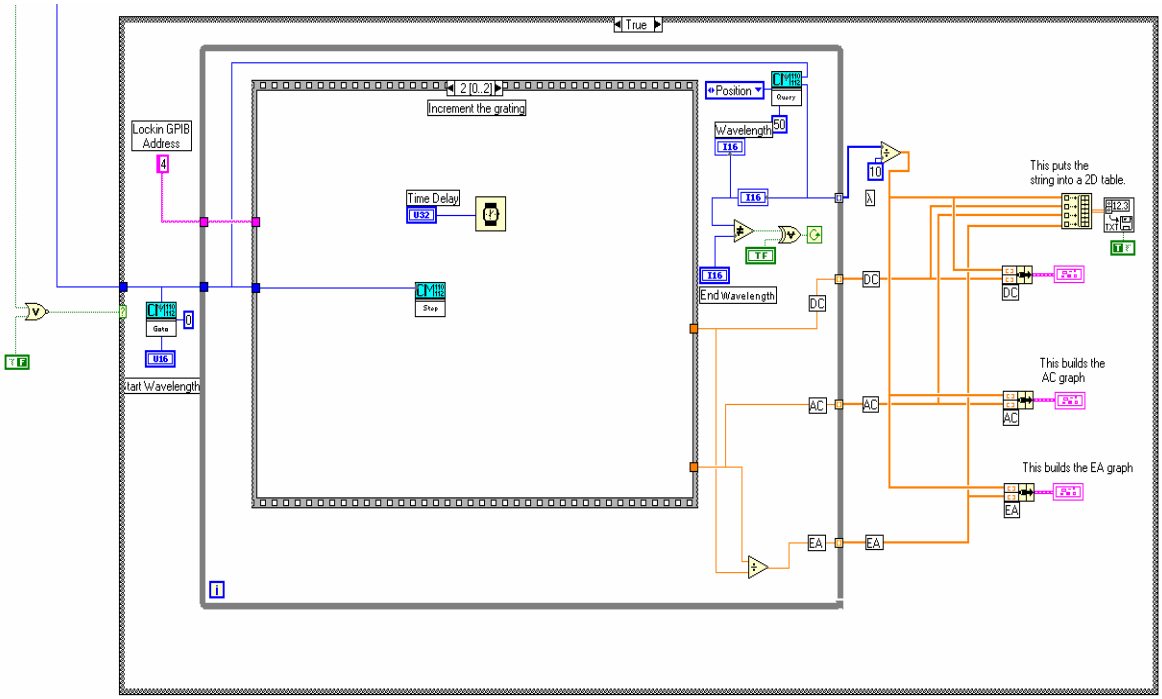

Figure 4.19 The fourth routine sequence of the electroabsorption control program. The primary function of this routine is to step the monochromator after collection of each set of points. Once a scan is complete the routine saves the complied data as a text document and also generates the three x-y plots on the graph panel.

Once a data point has been recorded and transmitted to the computer it is compiled into a tabular array. This process is repeated until the scan has finished. Upon completion of a scan, the data is saved as a text document and used to generate the three xy plots on the graph panel.

4.8 Summary

Overall the construction of an electroabsorption spectrometer is an extremely complex undertaking involving the optimisation of an optical signal and the subsequent electronic recovery of very small changes in a materials transmitted intensity as a result of an applied field. A fairly sophisticated computer program is required to automate the

control of the instrument and also to allow for the collection of data. In spite of these difficulties and with no commercially available alternative on the market the construction of an electroabsorption spectrometer is warranted since extremely valuable information on the electronic properties of a material can be obtained through its application. For the purpose of this study the instrument is used to collect information on the degree of change transfer between fullerenes in the solid state. Although adequate for this study, the instrument does have some limitations, which may hinder its applications in the investigation of other systems. These limitations are primarily as a result of the spectral cut-offs associated with the use of glass machined components. These glass components could be replaced with quartz optics thus extending the working range of the instrument, allowing a greater diversity of molecular systems to be studied.

CHAPTER 5

Electronic Spectroscopy and Excitonic Processes in Fullerenes

5.1 Introduction

Building upon the information presented in chapter two, the focus of this chapter is to examine the electronic properties of fullerenes in both the isolated and solid state. A convenient method for examining the electronic properties of a material either in solution or solid form is electronic spectroscopy. A key point of chapter two was that there are still a number of unanswered questions regarding the electronic properties of solid state fullerenes and in essence the question is whether the delocalised electrons remain on a single molecule or whether they are distributed across the solid. Thus the aim of this chapter is to address the role of excitonic processes within solid state fullerenes.

5.2 Bouguer Lambert Beer law

In 1729 Bouguer discovered that as light passes through a material the reduction in light intensity is directly proportional to the radiation flux and sample thickness [60]. This formulisation was later extended to include gas and solutions based systems by Lambert and Beer in 1760 and 1852 respectively [60]. Combined, these results comprise the Bouguer Lambert Beer law, which states [61],

- $A = \log (I_o/I) = \varepsilon\, c\, l$ *Eqn 5.1*

where, A is the absorbance of the material, I_o is the intensity of the incident light, I is the intensity of the transmitted light, ε is the molar extinction coefficient or molar absorptivity in $cm^2\ mol^{-1}$ and l is the path length in cm. For many purposes, particularly analysis involving the examination of thin films, the law can be applied in its exponential form [62],

- $I = I_o\, e^{-\alpha d}$ *Eqn 5.2*

where α is the absorption coefficient of the material and *d* is the film thickness. The relationship between α and ε is**,**

- $\alpha = 2.303\, \varepsilon\, c$ *Eqn 5.3*

The strength of the absorption band can be described by ε_{max} of the material and the actual shape of an electronic absorption band results from coupling between the electronic energy levels and energetically close vibronic sublevels. The ε_{max} value of a material can be calculated by the wavelength weighted area under the absorption band [63]. This quantity is known as the dipole strength and it represents the electronic transition probability of the absorption band which results from the temporary electric

dipole generated as a consequence of the promotion of an electron from a low to high energy state.

5.3 Theory of electronic spectroscopy

Electronic spectroscopy is the term used to describe the phenomenon of the absorption of photons in the ultraviolet (UV), visible (vis) or near infra red (NIR) region of the electromagnetic spectrum. In molecular spectroscopy the absorption of a photon of light results in an electronic transition within a molecule, where electrons are promoted from the ground state to a higher electronic excited state [61]. These electronic transitions which are characteristic by absorption in the near infra-red, visible or ultraviolet region of the electromagnetic spectrum result in changes in energy of order 1eV or more and provide a measure of the probability of promoting electron from the HOMO to LUMO at a given photon energy ie exciting a molecule from its ground state to its excited state [61]. For each energy state associated with an electronic transition both singlet (S) and triplet (T) excited states are possible. In singlet states the spins of the paired electrons are anti-parallel, whereas a triplet state arises if the spins are parallel. It is important to note that not all transitions between individual states are allowed and quantum mechanical selection rules allow for transitions between S→S, and T→T processes but not S→T and T→S [62]. Molecular ground states are usually singlet in character and thus most excitations are to singlet excited states. Triplet states are usually formed by intersystem crossing from an excited singlet state, such as S_1, rather than by direct excitation from the S_0 ground state. It should be noted that under certain conditions, transitions which are normally forbidden by the selection rules become allowed as a

result of vibronic coupling and weak forbidden transitions appear in the molecular spectrum [64].

In molecular solids possessing relatively small binding energies like fullerenes which consist of electronically neutral closed-shell π conjugated electron systems held together by weak van der Waals forces, excitons play a fundamental role in determining the material's optical properties. An exciton is the term used to describe a specific electronic excitation, which corresponds to a bound state of an electron and a hole [65]. Excitons may be classified as either Frenkel or as Wannier Mott(WM), depending on the separation radius of the electron and the hole. Small radius Frenkel excitons represent an electronic excited state of a crystal in which the electrons and holes are placed on the same molecular site as distinct from the larger radius WM excitons, in which the electron and the hole are separated by a larger distance.

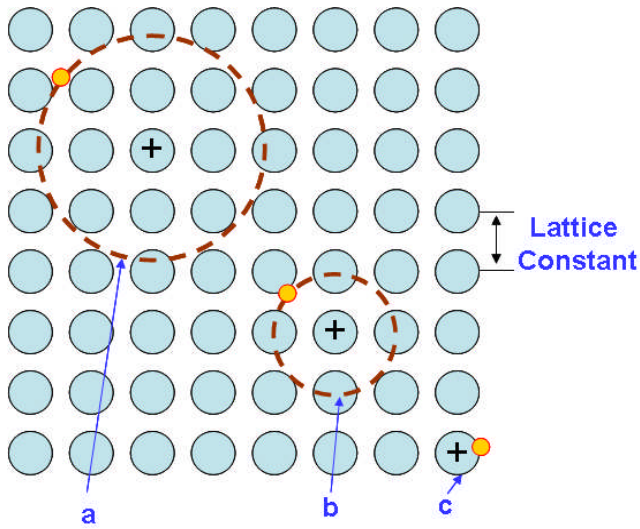

Figure 5.1 (a) Shows the separation of the electron and hole which is larger than the lattice constant which is characteristics of Wannier Mott excitons. (b) Shows the case for a Charge transfer exciton with the electron and hole located on different molecular sites. (c) Shows a Frenkel exciton electron-hole pair that is located on the same molecular site, where the orbit of the electron in the excited state is smaller than the separation of the molecules.

Wannier Mott excitons are more common in inorganic crystals and only play a minor role in organic molecular crystals since the interaction between the molecules is much smaller than between atoms in inorganic crystals [50]. Of greater importance in organic molecular crystals is the role of Charge Transfer excitons, which can be described as an intermediate between the FE and WM excitons, and involve some degree of intermolecular charge transfer in the excited state. Electronic transitions arising from the neutral crystal ground state to a CT exciton state are normally extremely weak. As a result of the low oscillator strength associated with CT excitons, and also due to the energy level of the CT exciton transitions being in the same range of the highly allowed Frenkel exciton transition, it is generally difficult to observe the CT transitions in standard absorption spectroscopy. However, these CT excitons are much more sensitive to electric fields and can therefore be observed using techniques like electroabsorption spectroscopy [67].

5.4 Electronic spectroscopy of isolated C_{60} and C_{70}

The electronic spectra of both C_{60} and C_{70} were recorded using the Perkin Elmer Lambda 900 UV/Vis/NIR spectrophotometer described in Chapter 3. With regard to the solution spectrum of C_{60} the first noticeable low energy feature is the HOMO-LUMO transition at 1.9eV. As mentioned in the previous chapter, given the icosahedral symmetry of fullerene C_{60}, this electronic transition should be dipole forbidden since it has a zero transition dipole moment. However, as a result of Hertzberg-Teller vibrational coupling and Jahn-Teller distortions there is a relaxation of the selection rules and consequently a broad vibrationally rich absorption band from 1.93eV to 2.75eV becomes weakly allowed and consequently the C_{60} solution exhibits a characteristic burgundy colour.

Examination of the absorption spectrum of C_{60} solutions reveals a number of characteristic features as shown in Figure 5.2. To date one of the most detailed analysis of the isolated absorption spectrum of C_{60} in hexane has been reported by Leach et al [32].

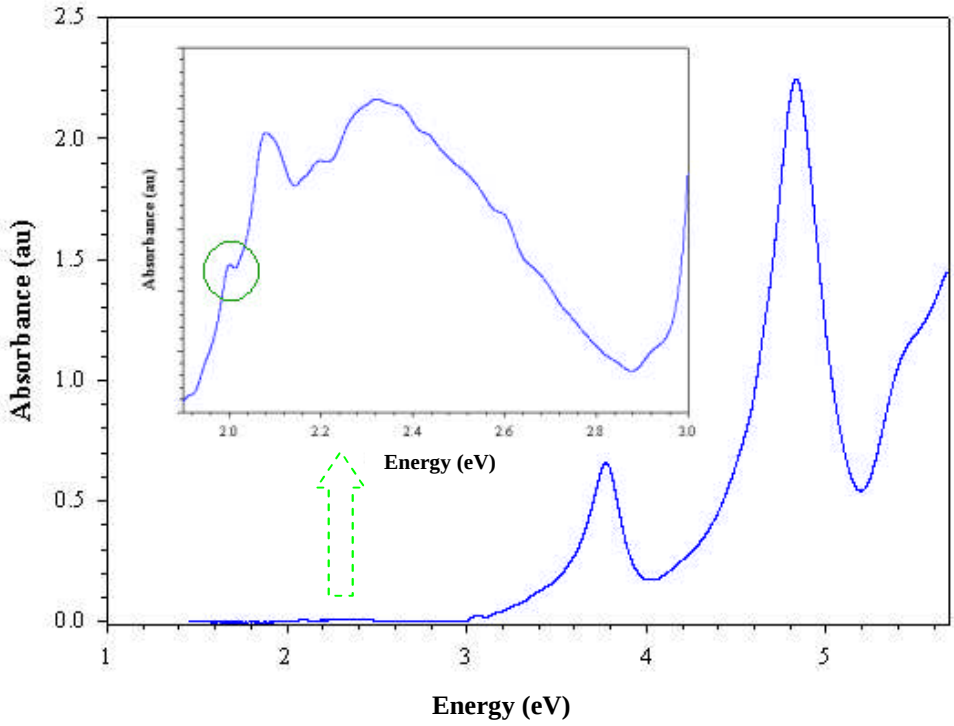

Figure 5.2 The absorptions spectrum of C_{60} in hexane. The insert shows an expanded portion of the spectrum in the region of 1.9eV to 3.0eV. The h_u to t_{1u} or HOMO-LUMO transition is indicated by the circled area at approximately 1.9eV.

The authors examined the absorption spectra of C_{60} from 1.7eV to 6.5eV and within this region, they divided the absorption spectrum into four sections. The first section covered the spectral range between 3.54eV to 6.52eV to which consists of 3 absorption bands centred at 3.78eV, 4.84eV and 5.87eV. The second region identified was that containing weaker bands from 2.88eV to 3.54eV which the authors attributed to electronic transitions which exhibit some vibrational structure. The third region identified covers

the 1.93eV to 2.88eV range with the most intense feature centred at 2.29eV. This range exhibits numerous superimposed peaks and shoulders which have been credited to various vibronic transitions and this vibrational structure has been assigned to the effects of Hertzberg-Teller distortions. The fourth and final section identified encompasses the 1.79eV to 1.93eV portion of the spectrum which consists of 3 extremely weak bands which result from the vibronic features of the spin forbidden singlet to triplet transition. Similar to the analysis conducted by Leach et al [32], the absorption spectrum of C_{70} has also been extensively studied [29, 37]. Figure 5.3 shows the isolated absorption spectrum of C_{70} recorded in hexane.

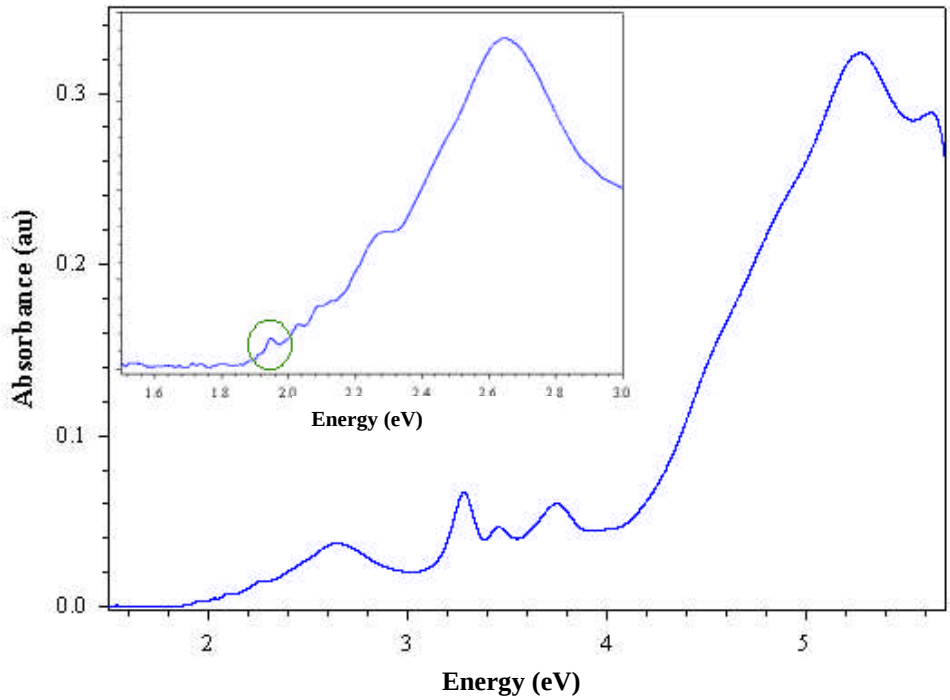

Figure 5.3 The absorption spectrum of isolated fullerene C_{70}. The insert shows an expanded portion of the spectrum in the region of 1.5eV to 3.0eV. The a_2" $-e_1$ or HOMO-LUMO transition is indicated by the circled area at approximately 1.87eV.

Examination of C_{70} absorption spectrum shows marked differences from that of C_{60}. One of the most noticeable differences is that it extends further into the low energy region. Also evident are a number of sharp features which result from electronic transitions some of which are vibronically coupled. An in-depth account on the various electronic transitions of C_{70} is provided by Shumway et al [29], who identified a number of transitions ranging from 1.87eV to 3.92eV. The authors attributed that the first transition on the low energy side of the spectrum was located at 1.87eV and resulted from the dipole allowed a_2" –e_1 or HOMO-LUMO transition. It should be noted that depending on the theoretical calculations the HOMO-LUMO of C_{70} may be non degenerate or two fold degenerate. However the closeness in energy of other nearby orbitals means that a degeneracy of 3 may be more realistic. The authors ascribed the second feature at 1.92eV to an e_1"-a_1 allowed transition. Subsequent features located at 2.00eV and 2.07eV, were identified as resulting from vibronic coupling of the A_1' vibrational mode with the a_2" –e_1 and e_1"-a_1 electronic transitions [29].

5.5 Solid state fullerene environment

The weak van der Waals interactions between organic molecules, like fullerenes in the solid state, result in relatively low charge mobility even for single crystals when compared to inorganic crystals and consequently the absorption spectrum of the molecular crystal tends to be similar to that of the isolated molecules. The electronic structure of the fullerene molecules only experience a small perturbation as one moves from the isolated molecule to the solid state environment, which is evident by the similarity of their relative spectra. With regard to C_{60}, figure 5.4 shows the comparison of the absorption spectra in film and in solution. Inspection of the spectra reveals that

the onset of the absorption in the solid state is slightly red shifted compared to that of the isolated molecule, but it has a vibrational structure similar to that of isolated molecule [68]. In the higher energy region, 3.2eV to 5.5eV, the solid state spectrum shows the presence of all the molecular transitions associated with the isolated molecules but as before slightly red shifted compared to the isolated molecule [69]. Such a red shift is commonly observed in molecular aggregates, but as the molecular transitions are largely unchanged it is possible to describe C_{60} as a molecular solid in which the molecular wavefunctions are minimally perturbed as a result of their crystalline environment.

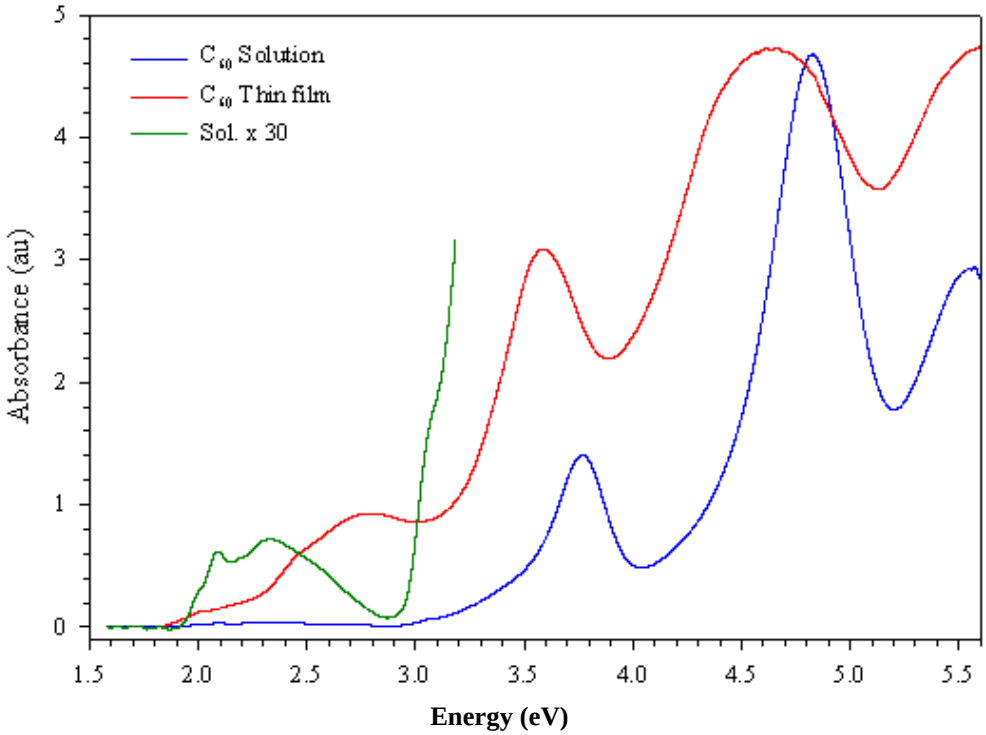

Figure 5.4 A comparison between the solid state absorption spectra and isolated molecular spectrum of fullerene C_{60}. The green curve is a magnified portion of the solution spectrum.

However the region from 2.2eV to 3.0eV in the solid state spectrum displays a strong new double feature at 2.45eV and 2.75eV which is absent from the isolated molecule's spectrum. The proposal that this photoexcited state is not molecular in nature is supported by photoconductivity and electro-absorption measurements [43, 70].

Electroabsorption measurements preformed by Kazaoui et al demonstrated that this feature actually arises from a number of charge transfer states where the transition occurs between the HOMO of one molecule to a higher unoccupied state of another molecule whose wavefunction derives from a mixture of the molecular state with those of its next nearest neighbours [43]. This unique solid state feature is the first indication that the material's electronic properties may be influenced by its crystalline environment and as such merits investigation.

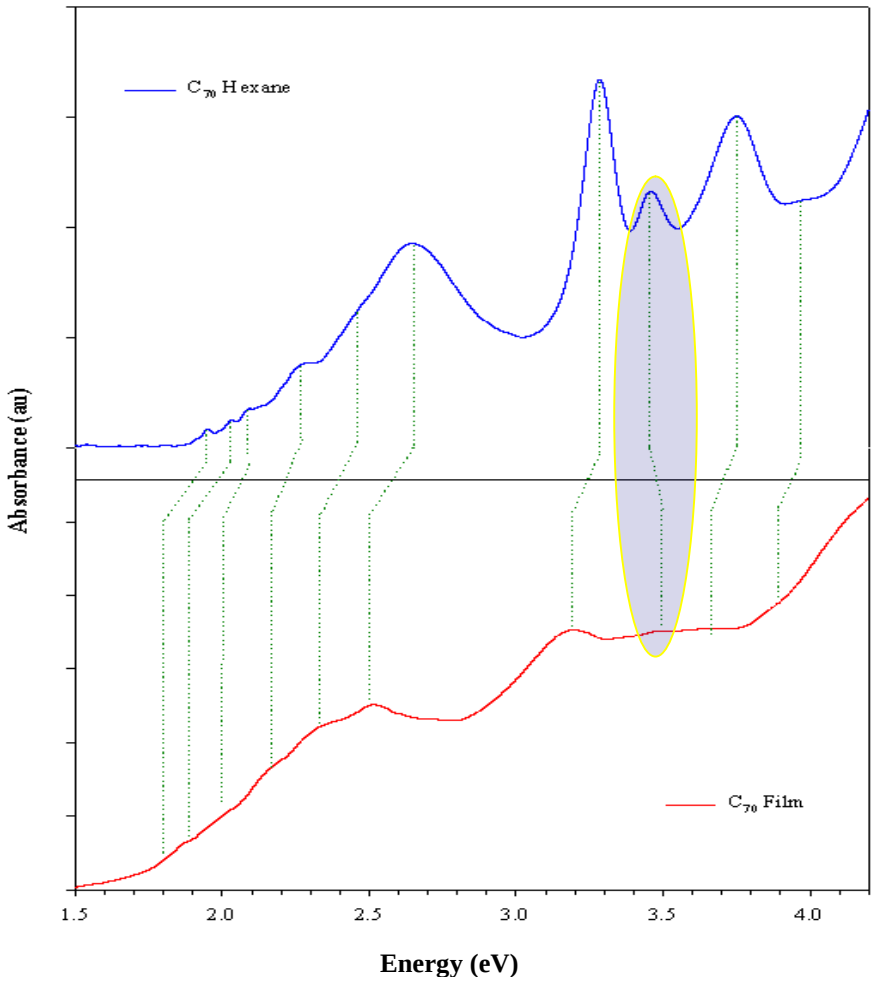

Figure 5.5 The compared absorption spectra for C_{70} in both solution and solid state environments. The dotted lines indicate the corresponding transitions in both the film and solution. The highlighted region indicates the e_1' – a_1' transition which uniquely experiences a shift to the higher energy.

In contrast to C_{60}, comparison of the isolated molecular and the solid state absorption spectrum of fullerene C_{70} shows a striking similarity between the two, which supports the opinion that solid C_{70} is a nearly ideal molecular solid, figure 5.5 [71]. However, upon closer inspection it is observed that the thin film absorption spectrum is broadened and red shifted when compared to the isolated molecular spectrum [37]. One noticeable exception to the trend is the feature located at 3.47eV attributed to the $e_1' - a_1'$ transition, which exhibits a blue shift of approximately ~40meV. Although Ichida et al offer no reasoning for this blue shift, reference is made to the possible involvement of CT excitons in this band [37]. Aside from this blue shifted transition the overall structure of the solid state spectrum exhibits good correspondence with the isolated molecular spectrum.

As one moves from the isolated to condensed environment, one noticeable difference between C_{60} and C_{70} is that solid state C_{70} lacks a distinct observable peak due to CT excitons. As mentioned previously solid C_{60} exhibits an electronic transition at approximately 2.5eV with an oscillator strength comparable to the allowed transitions located above 3.0eV. This new solid state feature that is characteristic of CT excitons and which is composed of an electron and hole being separated at the adjacent molecules in the lattice is absent from solid state spectrum of C_{70}. The absence of this feature can be explained by the lower symmetry of C_{70} which renders the HOMO-LUMO transition dipole allowed.

Since the intramolecular S_0-S_1 transition in C_{60} located at 1.9eV is symmetry forbidden and the next lowest allowed intramolecular transition is the S_0-S_2 which is located at about 3.0eV, there exists a wide energy gap between these two transitions. The CT band associated with the sold state interaction is observable at 2.5eV as a strong

absorption band midway between these two transitions. However in C_{70}, while the HOMO-LUMO transition is forbidden, there exist numerous orbitals of close lying energy where allowed transitions may occur and consequently the absorption spectrum exhibits numerous transitions above the HOMO-LUMO, masking any features arising from CT excitions and as such eliminating the possibility of observing a distinct CT band in solid C_{70}. This inability to identify certain CT bands by UV/Vis spectroscopy necessitates a more sensitive technique, such as Electroabsorption spectroscopy.

5.6 Stark effect

While absorption spectroscopy provides an enormous amount of information on the structural and electronic properties of a material under investigation the direct optical observation of CT excitons is very difficult, due to their very small associated transition dipole moment. As a result the CT excitons tend to be masked by Frenkel excitons (FE) in the optical absorption spectrum. Fortunately, CT excitons are very sensitive to electric fields, and as such they can be observed using Electroabsorption or Stark spectroscopy. As mentioned earlier the Stark effect is the term used to describe the change in transmission of a sample as a result of an applied electric field [73]. Alternative terms like, electroabsorption, electrochromism and electro-optic absorption are also found in literature to describe the same effect [74], but in this thesis the term electroabsorption (EA) will be used to describe the phenomenon.

Electroabsorption spectroscopy uses an external electric field to perturb the electronic wavefunctions of a material resulting in its electronic excited states experiencing a shift in energy. The net result of this shift is the coupling of energy levels with each other and the formation of new states. These minute changes in the electronic energy levels,

can then be subsequently measured by monitoring changes the materials absorption spectrum. Normally, for organic molecular crystals the change in the absorption spectrum, ($\Delta T/T$) due to energy shift and change in the wavefunction is in the order of 10^{-6}~10^{-4}. The strength of the applied electric field in electroabsorption spectroscopy is normally of the order of 10^5V/cm which is relatively small when compared to the intramolecular or atomic electric fields intrinsic within a molecule (normally at 10^8V/cm).

Under the influence of an electric field a highly polarisable molecular state will interact to a greater extent with other states. These interactions result in changes in the molecular state energy, oscillator strength and wave function. Inspection of electroabsorption spectra yields detailed information on two parameters associated with an optical transition. The first is the change in the dipole moment, $\Delta\mu$, and the second is the change in polarisability, Δp, associated with an electronic transition from its initial ground state to its final excited state. This change in the dipole moment provides a useful measure of the amount of charge transfer associated with a particular optical transition. The change in polarisability, Δp, supplies quantifiable information on an optical transition sensitivity to an externally applied electric field and thus is particularly important in understanding the electronic properties of a material. It is possible to theoretically calculate these parameters, but the results are estimates and tend to be inaccurate. Thus electroabsorption spectroscopy can provide information beyond that afforded by absorption and emission measurements

5.7 Electroabsorption theory

The first theoretical work which focused on utilisation of electroabsorption spectroscopy to measure changes in the charge distribution between the ground and excited state in molecules under the influence of an external electric field was described by Liptay in the early 1970's [73]. As already described, electroabsorption spectroscopy uses an electric field to perturb the electronic wavefunctions of a material resulting in its electronic excited states experiencing a shift in energy. The net result of this shift is the coupling of energy levels with each other and the formation of new states. These minute changes in the electronic energy levels can then be measured by monitoring changes in the materials absorption spectrum. The field induced change ΔE(F) of a molecule's transition energy as it responds to an electric field can be described as [75],

$$\Delta E(F) = -\Delta\mu.F - \frac{1}{2}F.\Delta p.F \qquad \textit{Eqn 5.4}$$

where, F, μ, and p are the externally applied electric field, dipole moment and polarisability respectively. The electroabsorption spectrum of a material is basically the difference between the absorption spectrum in the presence and absence of an applied electric field. This change in the absorption coefficient as a function of transition energy for a molecule under the influence of an externally applied electric field can be described as a Taylor expansion truncated at the quadratic term, since the change in energy associated with higher order terms is negligible [76],

$$\Delta\alpha = \frac{\partial\alpha}{\partial E}\Delta E + \frac{1}{2}\frac{\partial^2\alpha}{\partial^2 E}\Delta E^2 \qquad \textit{Eqn 5.5}$$

where Δα is the change in absorption resulting from an applied electric field, and (ΔE) is the change in energy of the molecular states due to the Stark effect. The electric field induced change in a system's molecular eigenstates results from two contributions known as the linear and the quadratic Stark effect. The contribution made by the linear

Stark effect results from the polarization induced change in energy of the surrounding medium by the permanent dipoles [76]. This change in energy of a permanent dipole in an electric field and can be expressed as follows;

$$\Delta E = \Delta\mu . F \qquad \textit{Eqn 5.6}$$

where F is the applied electric field and μ is the permanent dipole moment equal the transfer of a charge, q, across a distance, r, ie μ = (q.r). This is known as the linear Stark effect since the shift in energy of the permanent dipole due to an induced electric field, is linear with the field. Consequently by substituting the above expression back into equation (5.5) it is possible to describe how the absorption is changed as a result of the linear Stark effect,

$$\Delta\alpha = \frac{\partial\alpha}{\partial E}\Delta\mu.F + \frac{1}{2}\frac{\partial^2\alpha}{\partial^2 E}(\Delta\mu.F)^2 \qquad \textit{Eqn 5.7}$$

In a system with an even distribution of permanent dipoles, the first term in equation (5.7) can be set to zero, since it has to be averaged over all the possible orientations of the permanent dipole moments. However the second term in equation (5.7) cannot be zero when averaged over all the possible orientations with respect to the direction of the applied electric field and so the contribution of the linear Stark effect follows the second derivative of the absorption spectrum,

$$\Delta\alpha = \frac{1}{2}\frac{\partial^2\alpha}{\partial^2 E}(\Delta\mu.F)^2 \qquad \textit{Eqn 5.8}$$

It should be noted that while the linear Stark effect arises as a result of the permanent dipoles, there may still be some contribution from centrosymmetric molecules, particularly in organic molecular crystals containing impurities.

The first derivative contribution to the electroabsorption spectrum arises from the change of molecular polarisability (Δp) and is known as the quadratic Stark effect. As

mentioned previously if a sample consists of randomly orientated dipoles as is the case in evaporated solids, $\Delta\mu.F$ is equal to zero. Consequently the only contribution to the linear term in ΔE in equation 5.4 comes from the polarisability. This reduces equation 5.4 to the form;

$$\Delta E = -\frac{1}{2}\Delta p.F^2 \qquad \textit{Eqn 5.9}$$

In essence equation 5.9 is known as the quadratic Stark effect since it represents the energy shift of the molecular eigenstate which is proportional to the change of polarisability and quadratic in the external field. By substitution of equation 5.9 into equation 5.5 we obtain;

$$\Delta\alpha = -\frac{1}{2}\frac{\delta\alpha}{\delta E}(\Delta p.F^2) + \frac{1}{8}\frac{\delta^2\alpha}{\delta^2 E}(\Delta p.F^2)^2 \qquad \textit{Eqn 5.10}$$

In equation 5.10, the second term is neglected because the change of the polarisability is normally small and the contribution from the higher order term is negligible. Thus the contribution to the electroabsorption spectrum arising from a change in polarisation is approximated by

$$\Delta\alpha = -\frac{1}{2}\frac{\delta\alpha}{\delta E}(\Delta p.F^2) \qquad \textit{Eqn 5.11}$$

In essence equation 5.11 shows that the electroabsorption signal is proportional to the square of the electric field and its spectrum follows the first derivative of the absorption spectrum.

Since an EA spectrum can be expressed as a convolution, and a convolution can be expressed as a sum of derivatives of each Gaussian band describing an electronic transition, the EA spectra can be fitted with the derivatives of the absorption spectrum. Figure 5.6 shows the resultant first and second derivatives of a Gaussian curve. Electroabsorption spectra which can be fitted using a first derivative term indicate the presence of Frenkel type excitons in the material. This derivative term arises due to the

molecular polarisability interacting with the externally applied field and inducing a dipole moment normally in the direction of the field. Since this field induced dipole moment is orientated with respect to the field, the transition band shifts to either a higher or lower energy [47].

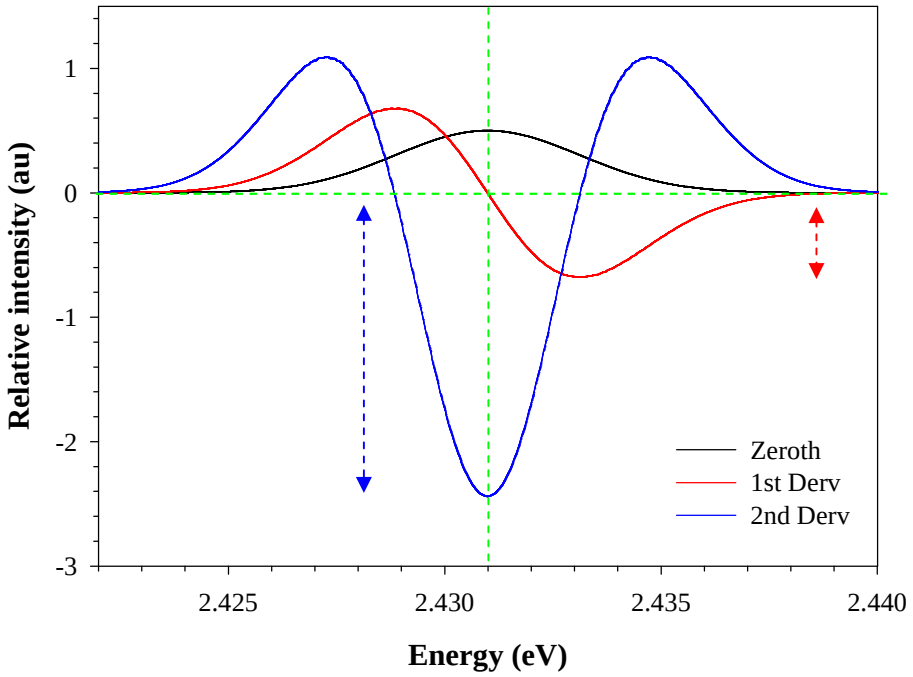

Figure 5.6 The zeroth, first and second derivatives of a Gaussian curve. The red broken arrow indicates the relative magnitude of the first derivative term. The blue broken arrow indicates the relative magnitude of the second order contribution.

The resulting difference between the line shape for the "field-on" and "field-off" is just a first derivative curve. The presence of a second derivative line shape in an EA spectrum is indicative of charge transfer species [47]. The random orientations of the dipole moments with respect to the applied field have the effect of spreading of transitional energies associated with the excitation band. The difference between the broadened "field-on" transitional band and the unperturbed band simply follows a

second derivative lineshape. Through the use of electroabsorption measurements it is possible to determine the change in the optical absorption coefficient. If the field-off optical absorption spectrum is known then it is possible by fitting the electroabsorption spectrum with Eqn 5.5 to determine the relative magnitudes of ΔE and $(\Delta E)^2$ of the individual states [50]. Thus based on the information yielded through the analysis of an EA spectrum it should be possible to distinguish between Frenkel excitons states and states which have a significant CT character in a material.

5.8 Electroabsorption spectroscopy of fullerenes

The first reported application of electroabsorption spectroscopy in examining fullerene C_{60} was provided by Pichler et al in 1991 [77]. The authors described the spectrum as being dominated by Frenkel type excitons since its overall shape seemed to follow the first derivative of the absorption spectrum with strong features identified at 2.5eV and 2.75eV as well as a numerous finer structures. Initially this would seem to be a reasonable assumption since the low energy EA spectrum does resemble a first derivative lineshape. However this interpretation contradicted the available data since Pichler also reported clear indications of solid state effects in the form of peak broadening and stronger tailing in the solid state absorption spectra. Based on traditional models these solid state effects would follow a second derivative line shape. The following year, Jeglinski et al, seemingly unaware of the previous work performed by Pichler, reported the EA spectra of C_{60} between the spectral region of 2eV to 5eV and also proposed that the EA spectrum of C_{60} resulted from Frenkel type excitons [78]. They identified prominent peaks at 2.37eV and another at 3.49eV as well as higher energy features at 4.37eV and 4.7eV. In the work the authors assign the EA features at

3.5eV and 4.7eV to the corresponding absorption transition at 3.6eV and 4.7eV, while also speculatively assigning the feature at 2.4eV to an allowed A_g-H_g transition.

However subsequent work conducted by the Petelenz group in Poland [79] introduced the possibility of the involvement of CT states, since integration over energy of the EA spectra did not return a polarisability weighted absorption spectra. They reported that the negative lobes at 3.0eV and 4.0eV of integrated EA spectra could not derive from Frenkel like excitons. Thus a subsequent second integration of the EA spectra would be required in order to obtain an absorption spectra, indicating the possible existence of CT states. Soon afterwards Hess and co-workers examined the EA spectra of both isolated and molecular C_{60} and extended the work further to include analysis of fullerene C_{70} [80]. Similar to interpretation by Pichler, Jeglinski and Petelenz, the author also ascribed the EA feature at 2.5eV as deriving from Frenkel type excitons. A different interpretation of the origins of the fullerene C_{60} spectral EA feature at 2.4eV was suggested by Kazaoui et al [43].

Using a semi empirical model originally proposed by Sebastian et al for conducting polymers [74], they deconvolved the EA spectra into a summated series of weighted first and second derivatives of the absorption spectrum [43]. In order to reproduce the EA spectrum of C_{60} they described the EA spectra as being composed of number of overlapping second derivative type contributions, centred at 2.43eV and 2.7 eV. Like Hess and co workers [80], the work was also extended to include C_{70}, identifying a number of features specific to the solid state environment, in particular the features at 1.85 and 2.3eV. This hypothesis that CT excitons are the dominant source of these spectral features was later further supported by numerous subsequent works reported by the Petelenz group in Poland [81].

The presented spectra for C_{60}in figure 5.7 compare well with those cited in literature for similar type films.[81, 82, 43] As mentioned towards the beginning of this chapter, this thesis will focus solely on the low energy solid state features in both C_{60} and C_{70}. Examination of the C_{60} spectrum in the low energy region shows a number of distinct features, of particular note are the ones located at 2.4eV and 2.7eV.

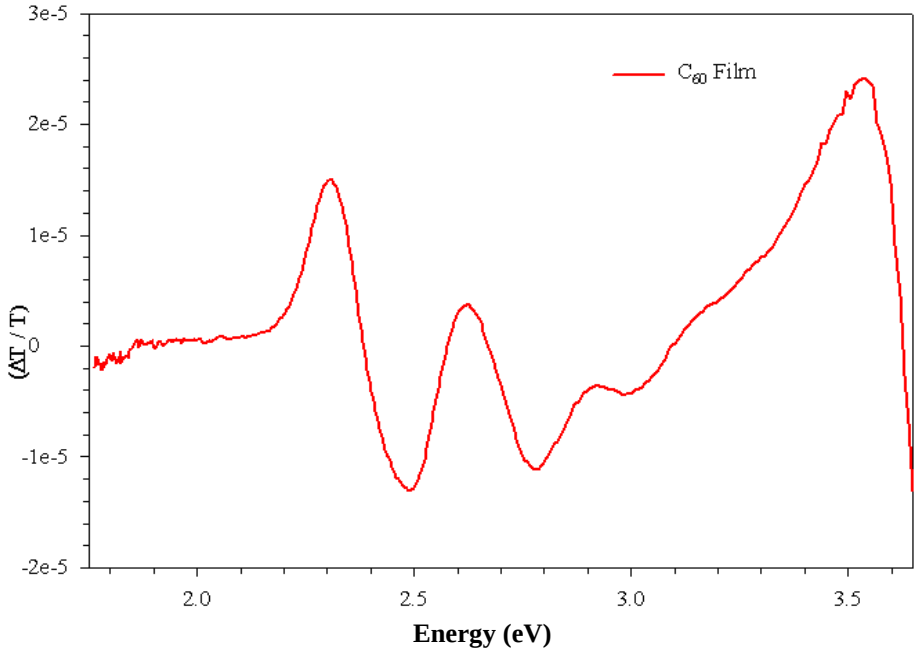

Figure 5.7 The electroabsorption spectrum for a typical 400nm C_{60} thick film in the region of 1.75eV to 3.65eV with a field strength of $1.5x10^5$V/cm,.

Unlike previous works, Kazaoui described the feature centred at 2.43eV as a CT state resulting from a series of off diagonal charge transfer states created by the transferring of an electron from the HOMO of one molecule located at the origin of the lattice to the LUMO of its nearest neighbour [43]. According to the authors the feature at 2.7eV results from a forbidden intramolecular excitation which is activated by coupling between nearest neighbour CT states.

Inspection of the C_{70} spectrum, figure 5.8, reveals a strong feature centred at 2.26eV which has previously been assigned to a coupling between a CT state and the nearby allowed Frenkel 1e'1 state at 2.45eV [88]. The distinctive second derivative feature shape of the EA feature at 2.26eV implies that it is of CT origin, although the source of its intensity is less certain. Depending on the theoretical calculations of the HOMO and LUMO, they may be either non degenerate or twofold degenerate, but since there are other orbitals which are very close in energy to both the HOMO and the LUMO it may be more appropriate to use an effective degeneracy of 3.

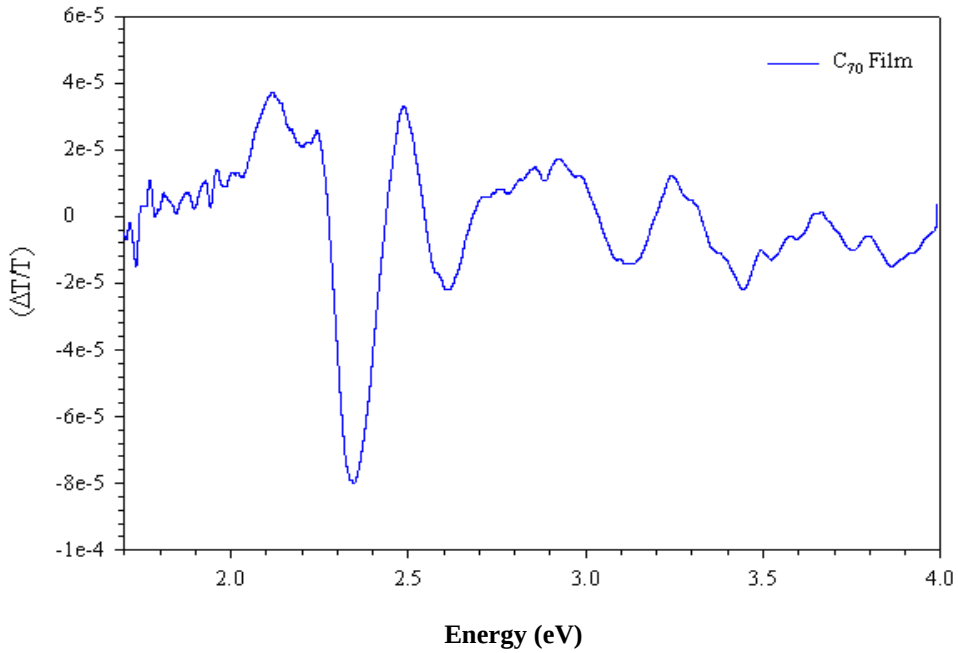

Figure 5.8 The typical a recorded EA spectrum for a 300nm film of C_{70} in the 1.75eV to 4.0eV region with a field strength of 1.3×10^5 V/cm.

In crystalline C_{70} the calculated energy of the nearest neighbour states may be directly compared with the position of the lowest and presumably the most intense CT state, i.e. the feature at 2.26eV. The fact that in C_{70} the CT states are located at lower energies

than those of C_{60} is a consequence of the lower ionisation potential and higher electron affinity of the molecule.

It is important to note that the above semi empirical model takes no account of mixing between Frenkel and CT states and it assumes that the EA signal originating from Frenkel and CT states can be effortlessly discerned and well separated in energy scale. This interpretation requires that CT states be viewed as perfectly localized electron-hole pairs, with no allowance for charge delocalisation between different molecules. However, as suggested by Kazaoui [43] and later demonstrated by Petelenz [83], the EA signal of the CT states does not have to follow the second derivative of the absorption spectrum and in fact the first-derivative shape is equally credible when the CT exciton lies close to the Frenkel exciton in energy. For this condition to arise the absorption bandwidth of an individual eigenstate must be smaller than the separation between the zero-field eigenstates. Thus, when the energy difference between two excited states (e.g. Frenkel excitons) is comparable to the absorption bandwidth of one of the individual states, the semi-empirical procedure for interpreting EA spectra may be over simplistic. In spite of this, while the values cannot be taken to be absolute measures of the individual parameters, the semi empirical model does provide an approximate qualitative guideline for calculating the change in dipole moment and polarisability associated with a transition.

CHAPTER 6

Spectroscopic and Thermal Analysis of Fullerene Films

6.1 Introduction

This chapter presents the electronic spectral analysis obtained from thermal treatment of fullerene films exposed to various temperature regimes. In fullerenes, like many molecular solids, the intermolecular electronic interaction is strongly thermally activated and this behaviour should be reflected in a temperature dependence of the materials optical properties. The change in the rotation of the molecules around their lattice positions as a result of passing though the phase transition means that there will be alterations in the intermolecular interactions between the molecules. These changes in the lattice parameters would be expected to affect the CT integrals and consequently their effects should be readily observable in the intermolecular optical excitations of the

material. Understanding the temperature and therefore structural dependence of these interactions can potentially lead to a mechanism to optimise them for potential applications.

6.2 Temperature effects on sample transmittance

The colour and consequently the absorption spectrum of an object can depend on its temperature, a phenomenon known as the thermochromic effect or thermochromism. It refers to a reversible increase or decrease in a material's optical density as a function of temperature [60]. In order to investigate how this thermal dependence arises it is necessary to reconsider the attenuation of beam of light as it passes through an absorbing medium as described earlier in Chapter 4,

$$I = I_o \; e^{-\alpha d} \qquad \textit{Eqn 6.1}$$

where I_o is the incoming intensity on the front surface of the sample, I is the transmitted light intensity, d is the sample thickness and α is the absorption coefficient of the sample at that particular wavelength. Assuming a constant illumination on the front surface of the sample and a constant film thickness, the quantity which is responsible for the thermal effects associated with changes in the transmitted intensity is due to the absorption coefficient, α. Thus since a material's absorbance is related to its transmittance as described by the Beer-Lambert law [63], variations in the absorption coefficient arising from thermal effects result in changes in the absorption spectrum of a material. Consequently investigating the thermal properties of a material's absorbance provides accurate information on any reversible thermochromic effects associated with the material.

6.3 Thermal effects on absorption bands

As mentioned in chapter 4 the absorption of light in the visible region of the spectrum is caused by low level electronic transitions, whereby an absorbed photon excites an electron from one energy level to another. The Gaussian shape of the absorption coefficient and thus the absorption band itself, is provided by the expression [84],

$$\mu(\varepsilon) = \mu_{max} exp\left(-\frac{1}{2}\left(\frac{\varepsilon-\varepsilon_0}{\Delta\varepsilon}\right)^2\right) \qquad \textit{Eqn 6.2}$$

where μ_{max} is the peak amplitude, ε_0 is the energy of the maximum absorption peak and $\Delta\varepsilon$ is the full width half maximum. With regard to the thermochromism of a material, while thermal differences will result in changes in peak height and peak width of the material absorption band, the integrated area of the band will remain constant [63]. The integrated area, A, of the Gaussian band can be obtained by the following expression, [84].

$$A = \left[\frac{\mu_{max}}{\sqrt{2\pi\Delta E}} exp\left[-\frac{1}{2}\left(\frac{\varepsilon-\varepsilon_o}{\Delta\varepsilon}\right)^2\right]\right] \qquad \textit{Eqn 6.3}$$

Thus any thermal dependent fluctuations in the integrated area of an absorption band are as a result of non-thermochromic processes occurring in the material. In fullerenes, aside from any thermochromic processes which may occur as a result of temperature variations, there should also be additional effects which depend on temperature dependent intermolecular coupling. These additional effects result from the alterations in the electronic CT integrals due to changes in the crystalline packing associated with the phase transition temperature of the material. It is this sensitivity of fullerenes to their crystal packing which will be probed using electronic spectroscopy.

6.4 Modelling C_{60} electronic spectra

The previous section introduced the approximation of a single optical excitation using a Gaussian curve. However, in general the electronic spectra of molecular solids are comprised of a number of overlapping electronic transitions.

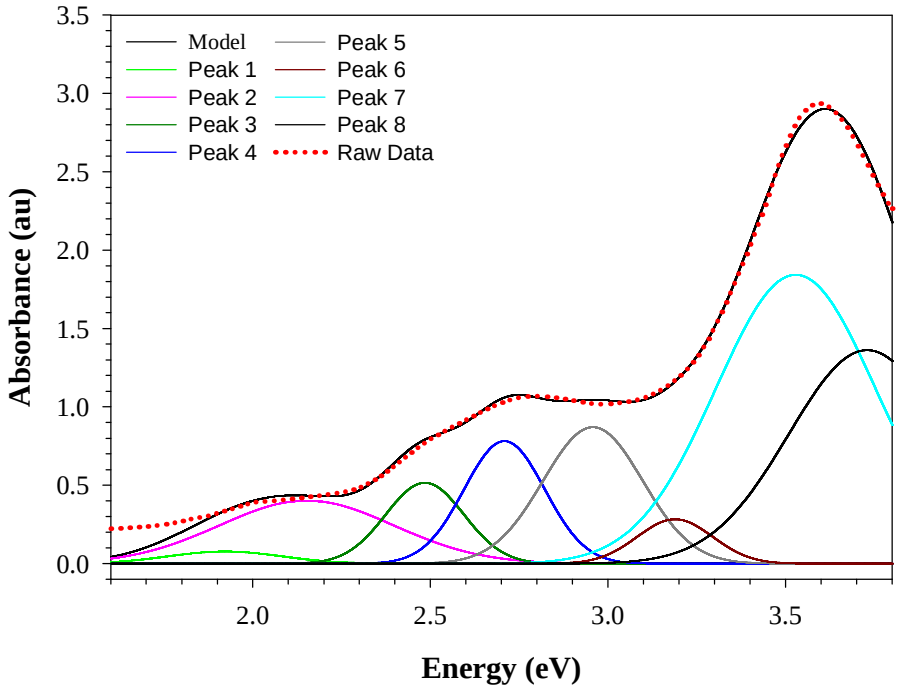

Figure. 6.1 The absorption spectrum of a thin film of C_{60} fitted with a number of model Gaussian bands in the low energy region.

Consequently in order to better understand these electronic contributions of each of the bands to the overall spectrum, it is generally useful to fit the electronic spectrum with a number of overlapping Gaussian bands. This provides a quantifiable measure of each band's contribution to the overall spectrum. From previous works its has been shown that C_{60} has a number of low energy electronic transitions [32], and a number of previous works have focused on the identification of these electronic transitions [43].

Table 6.1 The measured peak amplitude, centre and FWHM for the modelled C_{60} thin film absorption spectra. The values shows in brackets reflect those cited in literature [43].

Peak	Amplitude	Energy(eV)	(Lit)	FWHM
1	0.0773	1.9205	(2.04)	0.3758
2	0.4014	2.1501	(2.20)	0.5783
3	0.5154	2.4831	(2.43)	0.2596
4	0.7809	2.7072	(2.70)	0.2677
5	0.8707	2.9563	(2.94)	0.3307
6	0.2829	3.1874	(3.20)	0.2493
7	1.8431	3.5273	(3.50)	0.5288
8	1.3616	3.7283	(-----)	0.5193

In this present work the values reported by Kazaoui et al, for the electronic transitions in fullerene C_{60} will be used as a reference. In order to reproduce the absorption spectrum of C_{60} in the 1.6eV-3.8eV region eight overlapping Gaussian bands needed to be introduced. The absorbance data was then modelled using the SYSTAT software package, "Peak Fit 4.1" [84], using starting values as cited in literature [43] and a least squares fit. The resultant fitted spectrum and the constituent bands are shown in Figure 6.1. On inspection of the fitted data as shown in Table 6.1, the calculated parameters are found to agree well with the reference values. The small discrepancies between the observed data and the model are due in some part to the inherent errors in the fitting procedure and also possibly from instrumental factors. Of the eight bands, the peaks centred at 2.48eV and 2.70eV are of greatest interest as they have been identified as being charge transfer in origin and the focus of this work is directed primarily at these charge transfer species. While the feature at 2.48eV is higher in energy, (0.05eV), than the reference value, (see table 6.1), it is the overall magnitude of the peak which is of greater interest since it is used in EA spectroscopy to estimate by band resolution the

change in dipole moment associated with the transition. The interest in these features arises from the fact that they have no counterpart in the solution absorption spectrum and thus they are the first indication of intermolecular solid state effects in a condensed environment.

6.5 Modelling C_{70} electronic spectra

Similar to the analysis of C_{60}, the absorption spectrum of C_{70} was also de-convoluted into a number of separate Gaussian bands. Using parameters cited in literature [43] as the starting point, each peak was fitted in the same manner as C_{60}. Figure 6.2 shows the resultant fit and associated bands while the individual parameters are tabulated in Table 6.2 and compared to the literature values.

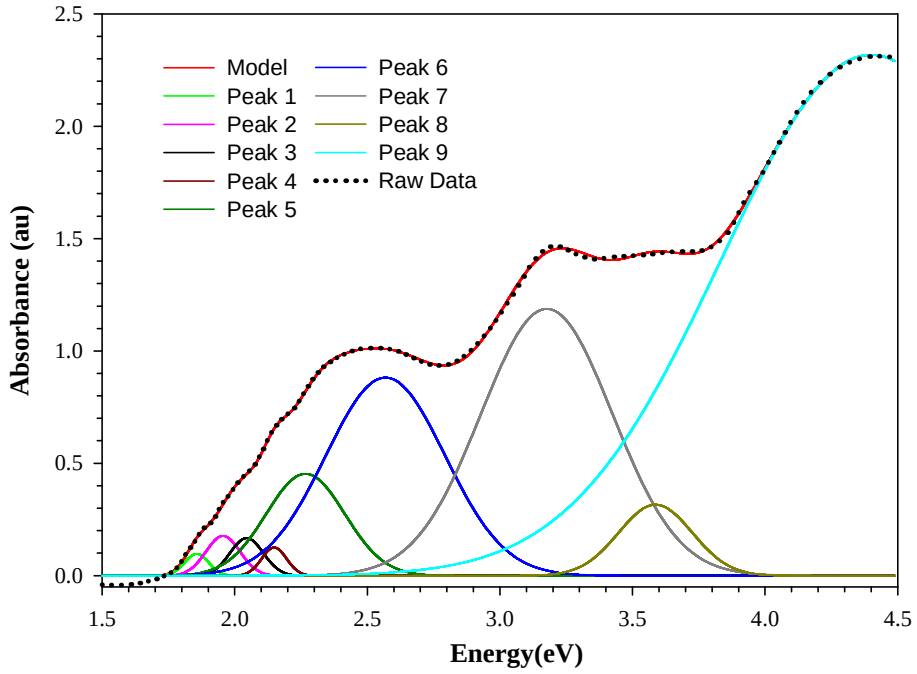

Figure 6.2 The modelled absorption spectra of a C_{70} fullerene thin film obtained be using 9 individual Gaussian functions.

Analysis of the data shows that the calculated model agrees well with the literature values. Of particular interest is the band centred at 2.26eV which has been ascribed to the CT eigenstate occurring at the (1,0,0) and (0,0,½) position [43].

Table 6.2 The measured peak amplitude, centre and FWHM for the modelled C_{70} thin film absorption spectra. The comparative values in brackets are those reported by Shumway et al [29]

Peak	Amplitude	Energy(eV)	(Lit)	FWHM
1	0.0966	1.8548	(1.83)	0.1059
2	0.1764	1.9540	(1.89)	0.1513
3	0.1667	2.0434	(2.01)	0.1474
4	0.1252	2.1469	(2.15)	0.1099
5	0.4529	2.2652	(2.30)	0.3490
6	0.8811	2.5667	(2.53)	0.5294
7	1.1872	3.1749	(3.20)	0.5835
8	0.3153	3.5848	(3.60)	0.3270
9	2.3185	4.3983	(-----)	1.3327

Although the band energy is somewhat lower than the expected reference value, (0.04eV), the calculated energy of the peak is in agreement with values report by Kazaoui et al thus providing an indication of the degree of variance among calculated models. Besides this feature, all of the other peak energies are in agreement with the literature values and as such the model is deemed to be acceptable. In both C_{60} and C_{70} the variance between the calculated models and those cited in literature can be due to a differing crystallinity associated with the different film production methods.

6.6 Reversible electronic spectroscopy of C_{60}

The effect of sub ambient thermal treatments on the absorption bands of fullerenes, in particular C_{60}, have been previously reported [85]. In general these works have focused on cooling the samples to 77K and subsequently measuring the absorption spectrum. It has been established that the feature at 2.7eV experiences a marked increase in oscillator

strength on passing through the first order phase transition (260K) whereby the C_{60} lattice changes from an fcc to a sc phase [85]. The findings show that the feature at 2.7eV is sensitive to changes in the lattice structure. In order to reproduce these temperature dependant absorption spectra, a Linkam Heating/Cooling stage was incorporated within the Perklin Elmer Lambda 900 Uv/Vis/NIR spectrophotometer as described in Chapter 3. An added advantage of this setup was the ability to optically monitor the effects of the thermal processing on a sample continuously in an inert environment, (Argon or Nitrogen). The in situ nature of the setup alleviated any problems normally associated with handling, transferring and repositioning samples during scans. A shown in figure 6.3, increasing the temperature of a C_{60} film (from 77K to 323K) results in a gradual loss of oscillator strength of the individual peaks at 2.43eV and 2.70eV. These features are believed to result from a series of intermolecular CT states. Also evident is the gradual decrease in the feature at 3.59eV, which derives from an intramolecular allowed transition. Inspection of the peak height of the two features at 2.43eV and 3.59eV shows that there is a decrease in the peak height with increasing temperature, which is in good agreement with the findings reported by Minami et al [85]. Of particular note is the noticable change in the peak height of the feature at 2.43eV, which coincides with the phase transition temperature of C_{60}, as shown in figure 6.4. In contrast the peak at 3.59eV displays a more gradual decrease in peak height and a far less obvious break around the phase transition. At temperatures below the phase transition, 260K, the C_{60} molecules lose two of their three degrees of rotational freedom. The remaining rotation around the four (111) axes is somewhat hindered, since one of the molecule's electron deficient pentagonal faces aligns itself with the electron rich hexagonal face which in turn acts to stabilise the sc structure.

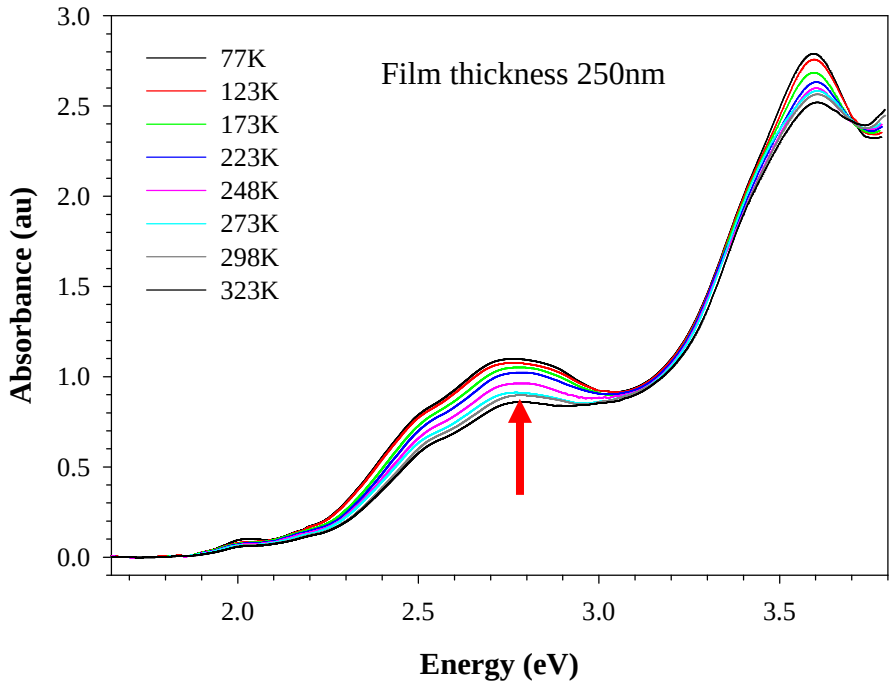

Figure 6.3 The normalised temperature dependence of the absorption spectrum of C_{60} in the 1.6 to 3.8eV region**.** The arrow indicates the increase in oscillator strength as the temperature decreases**.**

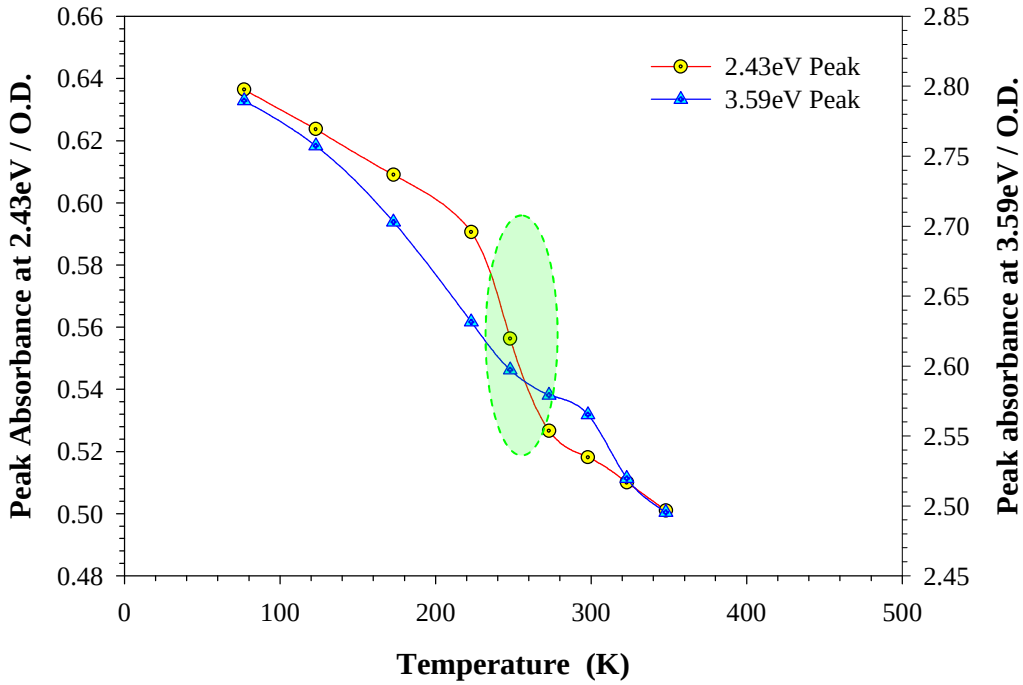

Figure 6.4 The peak absorbance at 2.43eV and 3.59eV as a function of temperature. The shaded region indicates a break in the peak absorbance associated with the first phase transition of C_{60}.

This simple cubic crystalline structure which can be described by the space group Pa3 which contains four C_{60} molecules per unit cell with coordinate locations of (0,0,0), (½,½,0), (½,0,½), (0,½,½) and a lattice constant of 14.17Å [25]. Evident from figure 6.4 is the greater susceptibility of the CT peak at 2.43eV to changes in the crystalline environment. This would be expected since the extent of intermolecular interaction will depend on the relative orientations of the molecules within the lattice. Thus the CT integrals will display a greater receptiveness to modification of the lattice than Frenkel like excitons such as that at 3.59eV which is indicated by abrupt change in the peak height of the 2.43eV feature in figure 6.4.

A question which must be addressed is whether or not these low temperature effects are reversible upon cycling through the phase transition. In order to elucidate this question the absorption spectrum of the film was measured at room temperature. The film was then cooled to the desired temperature for a period of 30 minutes.

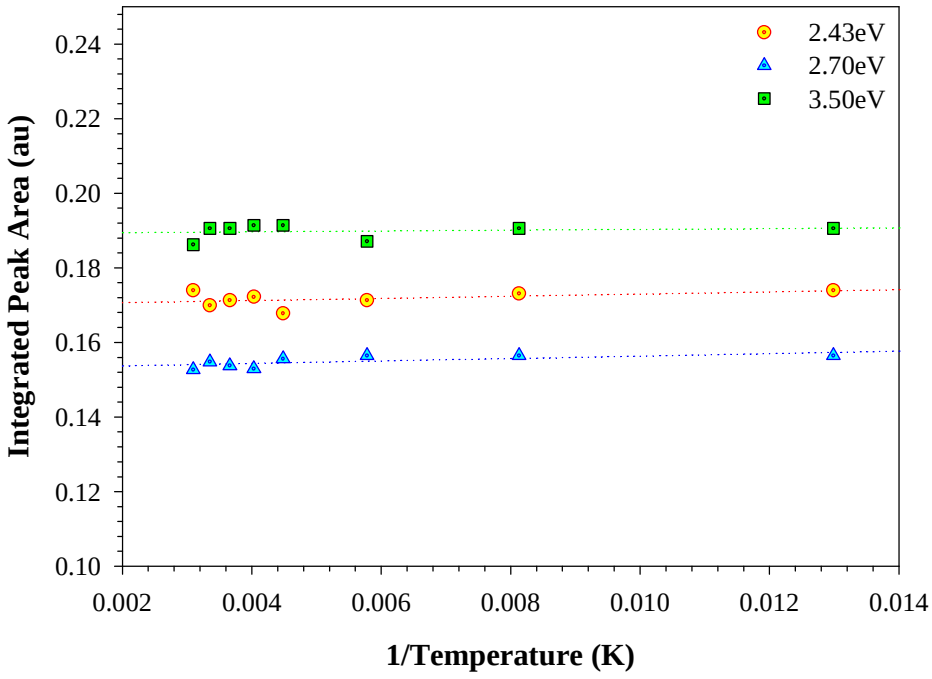

Figure 6.5 The integrated peak area for the peaks at 2.43eV, 2.70eV and 3.5eV as a function of temperature. The broken lines indicate the best fit lines of the data.

After this time had elapsed the film was then allowed to equilibrate back to room temperature and its absorption spectrum was subsequently re-measured. The integrated area of each peak after a thermal cycle was then calculated using band analysis of each spectrum and plotted as a function of temperature. As shown in figure 6.5, the integrated area remains constant for the three peaks throughout the temperature cycling of the film. This indicates that while the material's electronic properties exhibit some variation as a result of passing through the phase transition, the changes are temporary in nature. Thus it implies that in the low temperature regime, the processes responsible for these changes are completely reversible and display no long term alterations in the material's properties.

6.7 Reversible EA measurements on C_{60}

While the above data reveals the temperature dependence of the feature at 2.43eV it provides no information on the extent of charge delocalisation within the lattice. As discussed in Chapter 4, in C_{60} the first indication of interaction between individual molecules in the condensed state is the appearance of two new features in the absorption spectrum centred at approximately 2.5eV and 2.8eV which are absent in the isolated molecular spectrum. Although the identification of the origins of these states has been somewhat contentious in the past, as discussed in Chapter 4, they are now generally regarded to arise from a series of CT states [43]. Generally the intensity in the optical absorption spectrum of these CT integrals is usually small since they are limited to intermolecular overlap and in general they are often buried under intense vibronic artefacts resulting from intramolecular excitations. While C_{60} is an exception to this generalisation, since the intermolecular interactions are observable in the solid state

spectrum, it is particularly significant in the spectrum of C_{70} where the CT feature at 2.3eV is masked by numerous close lying allowed transitions obscuring the CT band in the absorption spectrum of solid C_{70}. In electroabsorption spectroscopy these small absorption intensities of the CT integrals are compensated by their high sensitivity to electric fields and thus electroabsorption spectroscopy provides a valuable tool for their study [86].

With regard to the temperature dependence of C_{60} of these two features, Kazaoui et al reported a discontinuity in solid state absorption features intensities at 260K upon cooling, while the first intramolecular allowed transition at 3.5eV experienced a steady increase [87]. The authors associated this discontinuity with the reordering of the lattice from a sc to an fcc crystalline structure. The indication is that the solid state specific absorption is influenced by the molecular orientation of the interacting molecules.

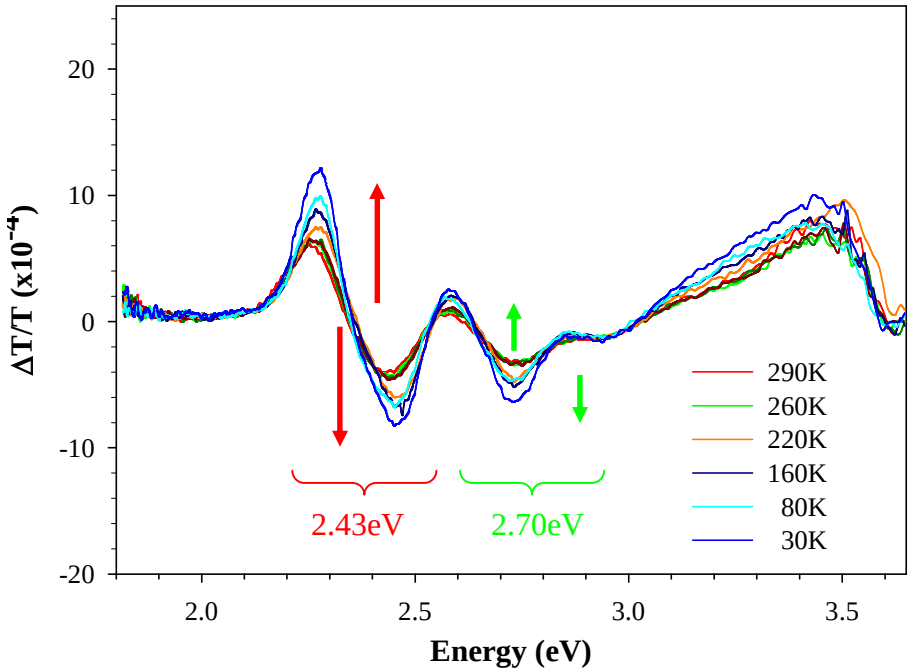

Figure 6.6 The effect of decreasing temperature on the EA signal of fullerene C_{60}. The arrows indicate the directional increase in intensity of the feature centred at 2.43eV, 2.70eV and 3.5eV. The inset shows the comparison between spectra recorded at RT and 30K.

These molecular orientations can also explain why the CT states are more sensitive to temperature changes than Frenkel type excitons. At a finite temperature a degree of orientational disorder is expected which leads to a spread in values of the CT integrals over a range of energies and thus results in a spread in energies of the eigenstates of CT origin [43]. As the temperature of the system is increased the extent of the orientation disorder also increases and the degree of intermolecular overlap decreases. As a consequence the absorption spectrum broadens and the EA signal experiences a reduction in intensity [43]. Allowed Frenkel type excitons in contrast only show a weak temperature dependence since they only weakly depend on their molecular orientation since they are intramolecular in origin [43]. However forbidden Frenkel excitonic states in a similar fashion to CT states critically depend on intermolecular overlap and thus are very temperature dependant since they depend on electron exchange [43].

Examination of the temperature dependence of the Electro absorption spectrum of C_{60} in figure 7.1 shows that upon cooling there is a marked increase in intensity of a number of spectral features. The feature centred at ~2.43eV which has previously been ascribed to an admixture of CT and Frenkel states experiences a large increase in intensity upon cooling. Kazaoui et al proposed that the CT states were in fact not localised charged pairs but were eigenstates of the crystal resulting from contributions from various charge configurations [43], and that different eigenstates deriving from the same set of localised CT configurations are split by the off diagonal interactions in the CT integrals [88]. As a result of this off diagonal coupling the CT integrals critically depend on the relative orientation of the molecules and the temperature dependence of these splittings would be expected to be quite strong. This is consistent with the interpretation that lowering the temperature increases the extent of intermolecular overlap as a result of

decreased orientational disorder resulting from the molecules adopting orientations that minimize intermolecular repulsion [86].

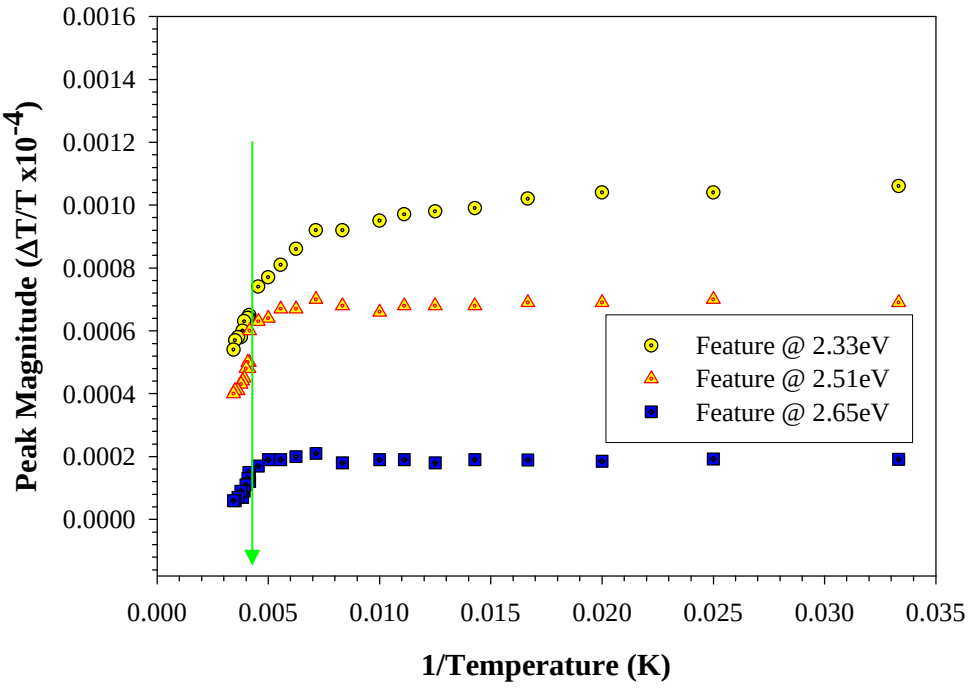

Figure 6.7 The absolute peak magnitude of the features at 2.33eV, 2.51eV and 2.65eV as a function of temperature. The green arrow indicates the non linear change in the relative intensities around the phase transition point at 250K.

Pac et al described the feature at 2.7eV as resulting from the same (½,½,0) CT local parentage as the 2.43eV feature, split by off diagonal interactions [81]. Similar to the peak at 2.43eV it also experiences an increase in intensity as a result of lowering the temperature although not as strikingly. Inspection of the relative peak magnitudes as a function of decreasing temperature, shown in figure 6.7, shows that at approximately 250K the change in the relative intensity of the peaks becomes non linear indicating the abrupt transition of the lattice from an fcc phase to an sc phase and consequently the introduction of a greater degree of orientation ordering. In the low temperature sc phase the molecules are frozen in well defined relative orientations in which the carbon-carbon

double bond located at the edge of one molecule is directed towards the centre pentagonal face of its nearest neighbour. In fact the border line between these phases is not as clear cut and it is known that sc and fcc phases can co-exist over a range of temperatures [89]. Consequently at a finite temperature there exists some disorder below the phase transition and some residual order above it, thus leading to a gradual change between order and disorder in a fullerene film. The data in figure 6.7 highlights the susceptibility of these CT features to changes in the local environment. It should be noted that the temperature changes observed reflect the relative orientations of the fullerene molecule associated with a gradual transition from complete orientational disorder at high temperatures to an ordered phase at low temperatures and not their structural spacing [88].

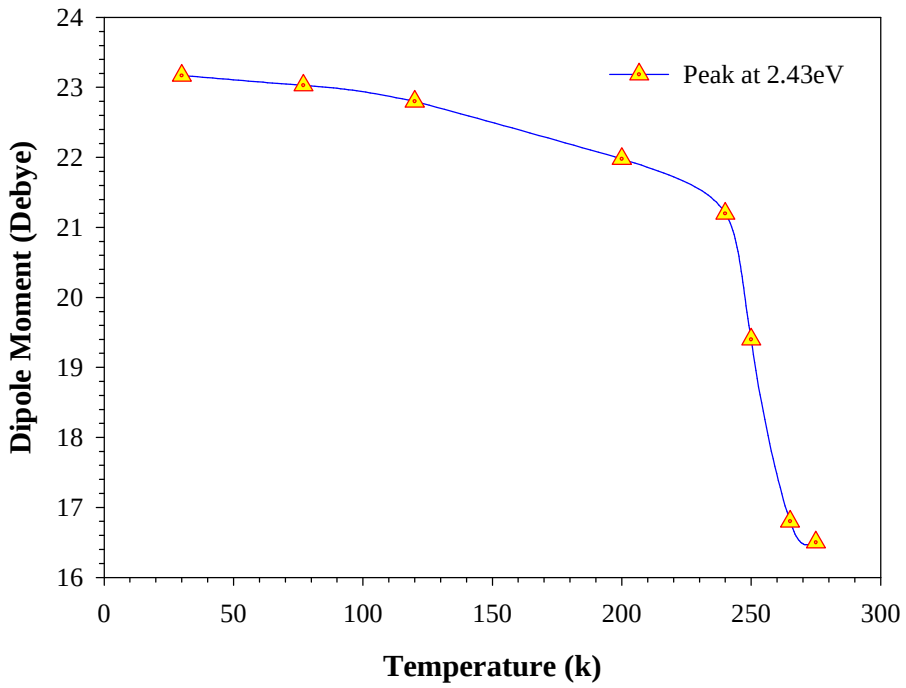

Figure 6.8 The calculated dipole moments for the peak at 2.43eV as a function of temperature. A large change in the dipole moment is observed around the phase transition

In order to relate these changes to the changes in the crystalline structure it is necessary first to calculate the dipole moment for the 2.43eV peak since it is thought to derive from a nearest neighbour electron charge transfer. This is achieved by fitting the EA spectrum with weighted derivatives of the absorption bands. Figure 6.8 shows the calculated dipole moments for the peaks at 2.43eV. Once these dipole moments have been calculated it is necessary to convert these values into meaningful lattice parameters. This can be achieved by adopting the approach utilised by Kazaoui whereby it was assumed that half of the charge is transferred from one molecule to its nearest neighbour [43]. In the fcc crystalline structure at room temperature the calculated dipole moment for the feature at 2.43eV was 16.8D which equates to an electron-hole separation distance of 7.0 Å.

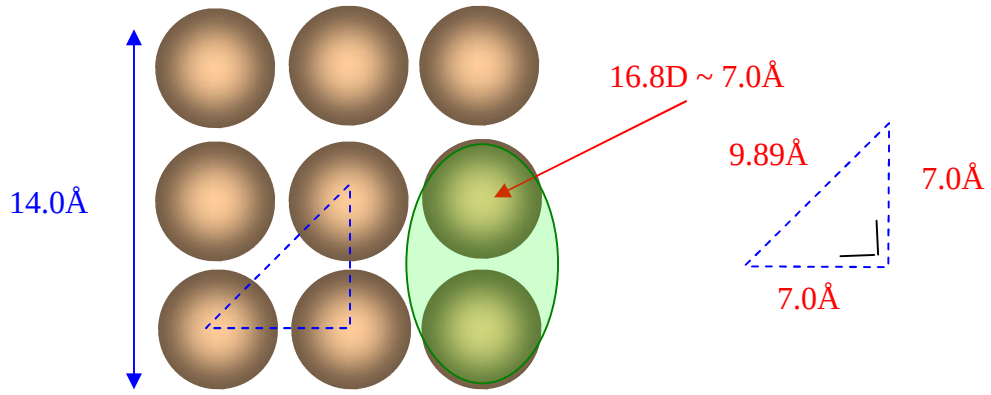

Figure 6.9 The fcc crystalline structure of C_{60} at room and also the relationship between a CT dipole moment and the equivalent lattice constant. The above diagram neglects to show the out of plane molecules in an fcc lattice.

Applying Pythagora's rule of right angle triangles allows the diagonal CT distance to be determined, see figure 6.9. Based on the calculated dipole separation of 7.0Å, for the

nearest neighbour, the fcc lattice constant is calculated to be 14.0Å. This is smaller than the actual lattice constant of 14.17Å as cited in literature [25]. This discrepancy may arise from the calculation of the dipole moments whereby there is an uncertainty of 10% associated with fitting the EA data with second derivates of the absorption band to the EA signal. That aside, the analysis does provide a useful indication of dimensions of the room temperature crystalline unit cell structure. While the crystalline structure of solid C_{60} above the phase transition temperature is the fcc structure (Fm3m), below this temperature the structure is an sc structure (Pa3).

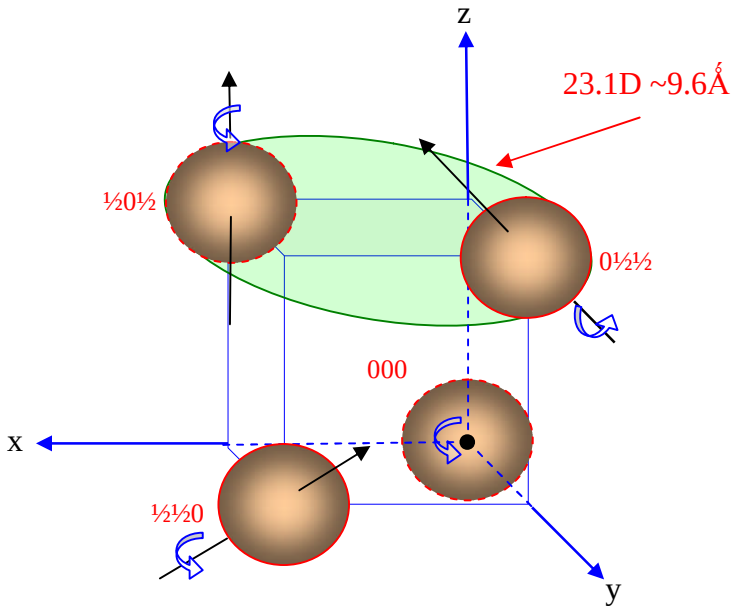

Figure 6.10 Shows the sc unit cell for C_{60}. In this structure there are four molecules all with their twofold axis aligned parallel to the cubic edges.

As the temperature of the solid is lowered the relative molecular orientation of the molecules becomes important with each of the four molecules obtaining a specific (111) rotational direction, figure 6.10, the net result of which is the reduction in the material's

crystal symmetry. As a result of this realignment the C_{60} molecules at these lattice sites are no longer equivalent and the lattice constant decreases by 0.013nm [25].

Again assuming that half of the charge is transferred from one molecule to its nearest neighbour, the calculated dipole moment of 23.1D of the sc phase at 77K equates an electron-hole separation of 9.6Å, figure 6.10. This value while slightly higher than that calculated by Kazaoui, compares well to the literature value for the C_{60}-C_{60} nearest neighbour distance of 10.02Å

6.8 Irreversible electronic spectroscopy of C_{60}

Based on the susceptibility of the CT integrals to low temperature fluctuations the study is extended into the higher temperature regimes in order to monitor the affect of temperature variations on the CT integrals. At room temperature the C_{60} molecules exhibit rapid rotation through all three degrees of rotational freedom. As a result of this rapid rotation around their lattice positions there is no orientational ordering of the solid and all the molecules appear equivalent during measurements which require a longer time to perform than the rotational period ($t>10^{-11}s$) [25]. In such a solid the molecules can arrange themselves in either an fcc or an sc lattice structure. The room temperature fcc crystalline structure can be described by the space group Fm3m and contains one C_{60} molecule per primitive unit cell with a lattice constant of 14.17Å [25]. This room temperature crystalline structure is preserved down until the phase transition temperature, where a transition to an sc structure occurs. While the effects of the transition from a low temperature regime to a room temperature crystalline structure are well defined, the effects of raising the temperature above ambient on the crystalline structure are less well understood.

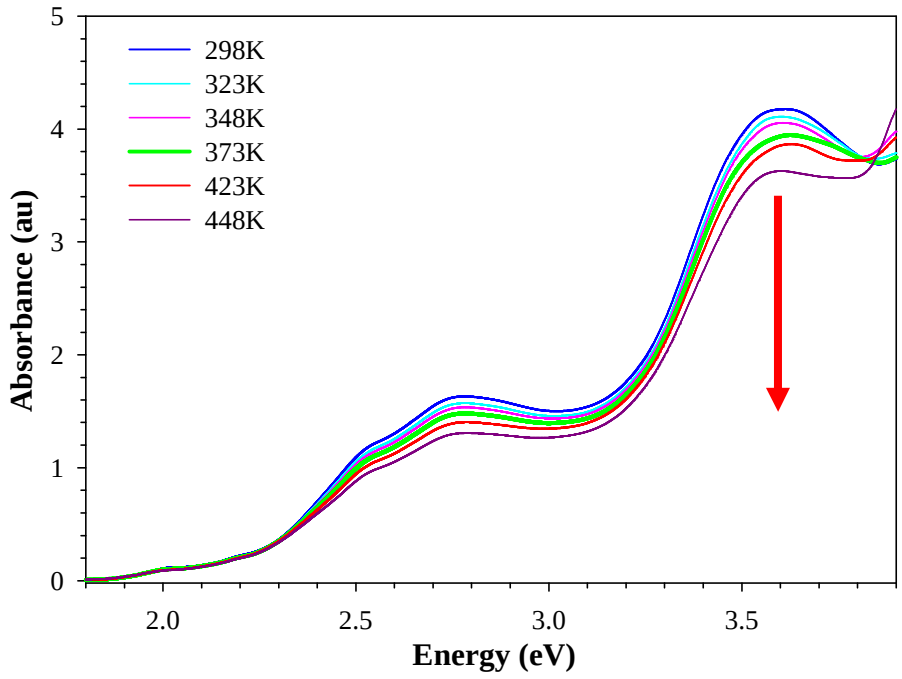

Figure 6.11 The normalised temperature dependence of the absorption spectrum of C_{60} in the 1.8 to 3.9eV region. The arrow indicates the decrease in oscillator strength as the temperature increases.

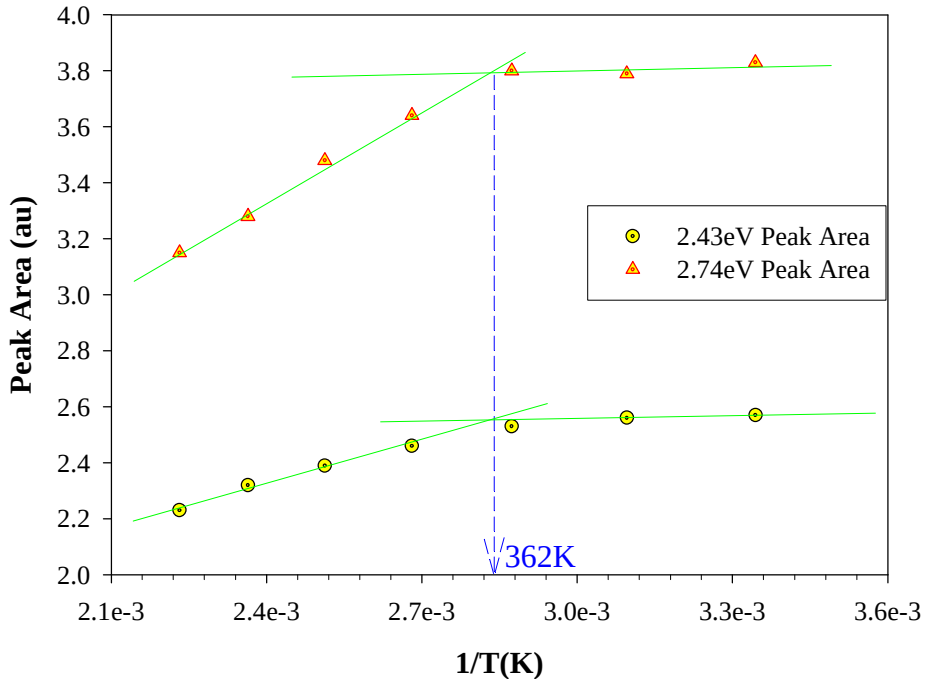

Figure 6.12 The integrated area of each band as a function of inverse temperature. As indicated on the graph an inflection point is observed at an equivalent temperature of 362K.

As can be seen in figure 6.11, increasing the temperature of the material results in a loss of oscillator strength of the individual peaks. In fact Gaussian band analysis of the two features of primary interest, (2.43eV and 2.70eV) shows that in the low temperature regime (RT-348K), while there is a decrease in the peak height, while the integrated area of the bands remains roughly constant. Thus indicating that the reduction in peak intensity results from a reversible thermochromic effect, see figure 6.12. However as the temperature of the material is increased, a steady decrease in the integrated area of each band is observed, providing evidence of another process occurring. Indeed plotting the integrated area of each band against temperature reveals the onset of an inflection point at 362K. The steepness of the slope for the peak centred at 2.74eV may indicate a greater susceptibility of this CT integral to high temperature treatments than the mode at 2.43eV. In either case, below this inflection point it is still possible to recover the original signal intensity upon cooling of the sample to room temperature. However, subjecting films to temperatures exceeding this point leads to the permanent irreversible loss in oscillator strength for the individual modes. As shown in figure 6.12 the extent to which the reduction occurs would seem to depend on the temperature.

6.9 Irreversible EA measurements on C_{60}.

While the low temperature dependence of the electroabsorption characteristics of C_{60} and C_{70} have been reported previously, no work to date has focused on the effect of high temperatures on the respective EA signals. Since in fullerenes the CT states control the electronic properties of the bulk material and given the susceptibility of the CT states to temperature changes, investigation of the effect of high temperature treatments on these properties is merited. Akselrod et al demonstrated that temperature can affect a change

in the intermolecular interaction both reversibly and irreversibly, pointing towards the potential to manipulate and therefore optimise the electronic properties of these materials [90].

The temperatures chosen, maximum 473K, were sufficiently below the sublimation temperatures (707K for C_{60} and 739K for C_{70}) of each fullerene so as not to result in any undue loss of material from the substrate due to heating. Additionally the experimental set up used, described in chapter 4, has a maximum working temperature range of 77K to 448K. The films were heated to set temperatures for a period of 10 minutes before a scan was recorded. This was to ensure a constant stable temperature gradient across the sample. Due to the nature of EA spectroscopy, scans normally take between 10 to 15 minutes depending on the range and/or resolution required.

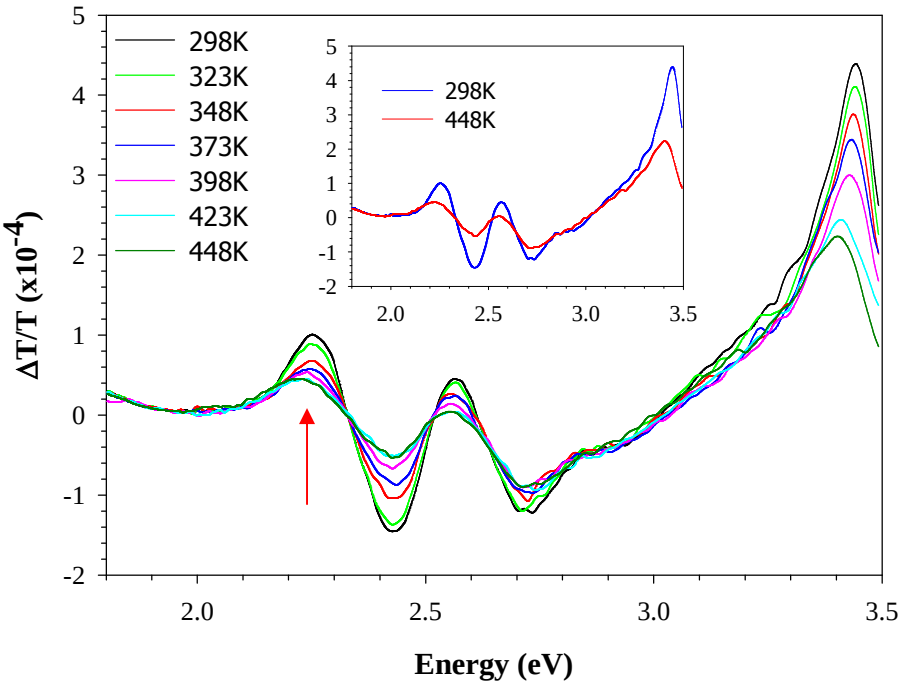

Figure 6.13 The high temperature dependence EA signal of C_{60}. Asides from the obvious intensity decrease there is also a red shifting of the spectral features. Of particular interest is the more pronounced reduction in intensity of the 2.43eV mode compared to other spectral features.

Similar to the data previously shown, the most prominent features are the ones located at 2.43eV at 2.70eV. As discussed in the previous section, decreasing the temperature results in these spectral features becoming stronger. By analogy it is reasonable to assume that a similar inverse trend would occur at higher temperatures where by these modes would become weaker and broader, akin to a thermochromic effect. However as shown in figure 6.13, unlike the trends observed at low temperatures, where there is a consistent sharpening of all the CT states, in the high temperature regime an unexpected trend is observed. It is noticed that certain CT states experience a greater reduction of their spectral modes when compared to other nearby CT integrals. Initially as the temperature is raised from RT to 323K there is a relatively minor decrease in the overall oscillator strength of the entire EA signal. A somewhat similar response is observed upon increasing the temperature to 348K, although the feature at 2.43eV experiences a slighter larger decrease than the rest of the features. Increasing the temperature even further reveals the gradual reduction of the feature at 2.43eV compared to the other features, in particular the mode at 2.7eV. This is interesting in that it would suggest that the feature at 2.43eV may be more susceptible to changes in the local environment than its counterpart at 2.7eV. Further temperature increases result in even greater reductions in peak strength of the feature at 2.43eV while the reduction at of the 2.7eV feature is far less pronounced in comparison. The feature at ~3.5eV also experiences a gradual decrease in intensity as result of increasing temperature. There is also an apparent red shifting of the state, which is similar to the affects observed in the electronic spectroscopic data. While Pac et al ascribed the origin of these two features at 2.43eV and 2.7eV as resulting from the same CT state split by off diagonal coupling [82], the

current data supports the theory originally proposed by Kazaoui, whereby the two features arise from two separate series of CT states [43].

6.10 Reversible electronic spectroscopy of C_{70}

Given the susceptibility of C_{60} to changes in the local environment, and given the similarities between the two molecules it would seem reasonable to assume that a similar process might also govern the electronic properties of C_{70}. In order to elucidate whether or not this is the case the study is extended to investigate the effects of thermal modification on C_{70} lattice. Unlike C_{60} the presence of a CT state in the solid state absorption of C_{70} is masked by numerous close lying intramolecular excitations.

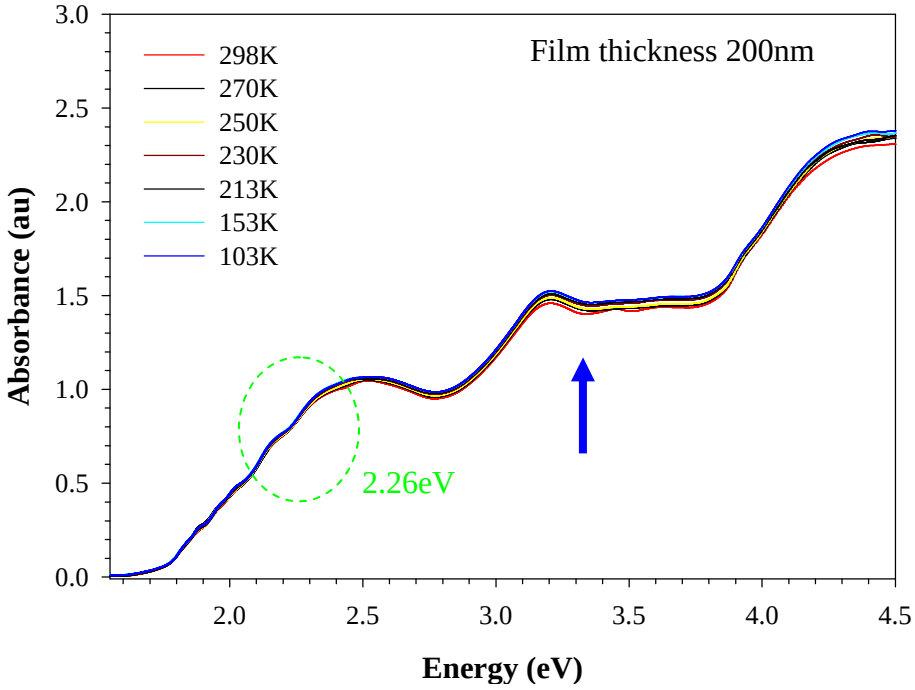

Figure 6.14 The low temperature dependence of the absorption spectrum of C_{70} in the 1.5eV to 4.5eV region**.** The arrow indicates the increase in oscillator strength as the temperature decreases**.**

As a result of the relatively small CT integral being buried under vibronic artefacts, the thermal dependence of the absorption spectrum is expected to be weak since the intense

intramolecular excitations do not critically depend on the molecular orientation. Figure 6.14 shows the absorption spectra of a C_{70} film being subjected to successively lower temperatures. As can be seen there is a small increase in the oscillator strength across the entire spectrum although the increase is not as dramatic as that observed in C_{60}. However this would be expected given the relative independence of the intramolecular excitations on temperature.

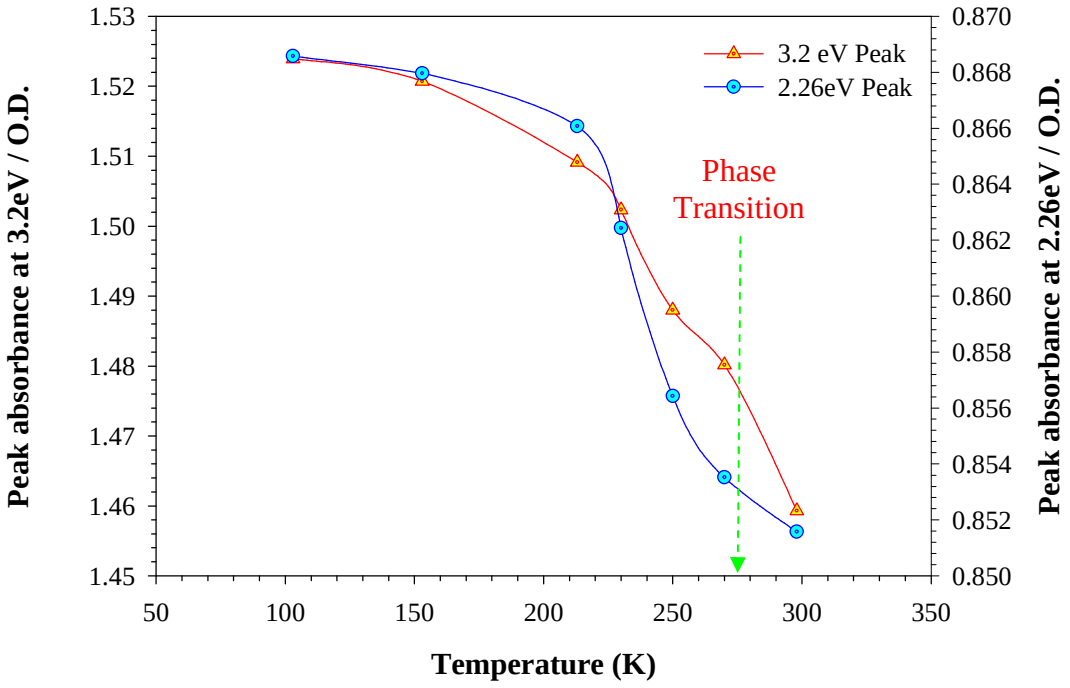

Figure 6.15 The peak absorbance for the feature at 2.26eV and 3.2eV as a function of temperature. The broken green line indicates the reported phase transition in C_{70}.

Plotting the relative peak absorbance for both the CT state at 2.26eV and the intramolecular excitation at 3.5eV reveals the thermal dependence of the film. Of note is the sharp increase in the peak height of the 2.26eV feature with decreasing temperature starting at approximately 250K. This inflection point is somewhat lower than the cited in literature of 280K, but the width of this transition has been reported to

vary by up to 50K [25]. It is believed that at this temperature the free rotation of the molecules around the c-axis becomes frozen. At these temperatures the crystalline structure is thought to adopt a monoclinic structure with an angle of 120^{o} and a unique c-axis which lies parallel to the intermediate temperature hcp or rhombohedral structure [25]. Above this phase transition, in the intermediate range from 280K to 340K the molecules begin to align around their long axis and the crystalline structure develops a certain degree of anisotropy. This intermediate temperature phase derives from an elongation of the high temperature fcc structure along a unique (111) direction. This directionality results from the molecular rotational "freezing out" of the axis perpendicular to the long axis during and consequently a rhombohedral structure develops which can be described by the space group R3m [40].

Although the changes in the absorption spectrum of C_{70} were smaller than those observed in C_{60} it was still important to determine if these effects were reversible.

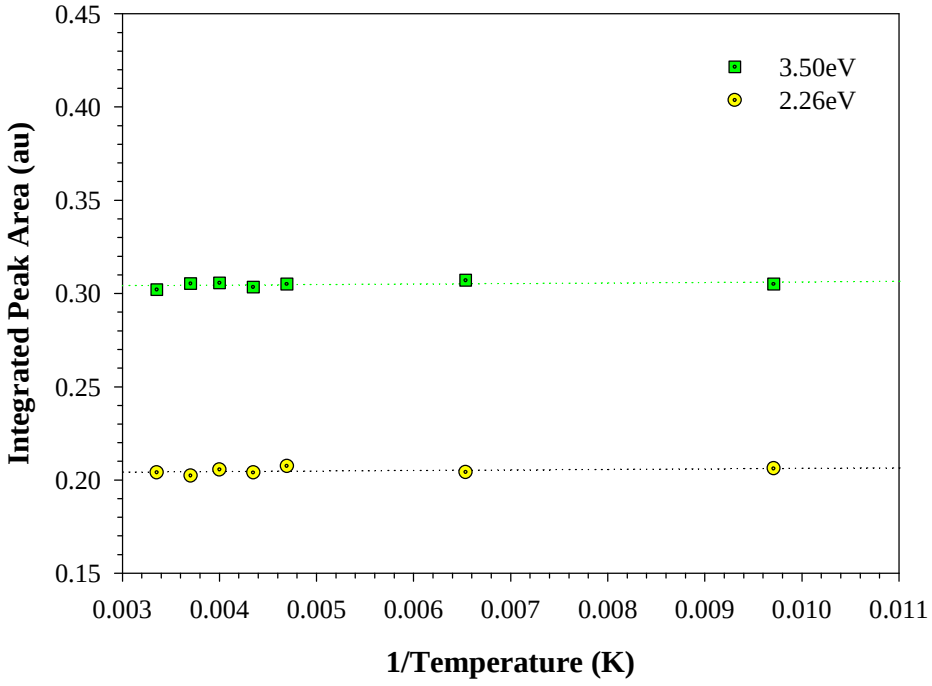

Figure 6.16 The integrated peak area for the peaks at 2.26V and 3.5eV. The broken lines indicate the best fit lines of the data.

Thus in order to investigate whether these processes were reversible in C_{70} a similar approach to the one used for C_{60} was adopted. From the data shown in figure 6.16 the changes in the absorption as result of low temperature fluctuations would seem to be reversible, since the integrated area for each band remains constant. As shown in figure 6.16, the integrated area remains constant for the two peaks irrespective of the temperature cycling of the film. Interpreting the data in figure 6.16 implies that changes in the electronic properties of C_{70} as a result of the low temperature cycling procedure are not permanent.

6.11 Reversible EA measurements on C_{70}

A noted in the previous section, C_{70} has a much more complex phase behaviour than is exhibited in fullerene in C_{60} with the existence of a stable monoclinic structure dominating at low temperatures, in which no molecular rotation occurs around the long axis. However as the temperature is raised through the phase transition temperature at 280K, the molecules begin to freely rotate around their long axis and the crystal lattice adopts a distorted hexagonal structure (hcp). Raising the temperature above the phase transition at 337K results in even further rotational motion freedom whereby free rotation around all molecular axes is allowed. Figure 6.17 shows the experimentally observed temperature dependence of the C_{70} EA signal. Inspection of the data reveals a clear increase in intensity of the feature at 2.26eV, with small variations in the other high energy spectral features. This feature has been previously ascribed to an off diagonal coupling of the (1,0,0)/(0,0,½) CT state [43]. The recorded data compares well with the cited references although the feature at 2.01eV, does display a stronger temperature dependence than previously reported.

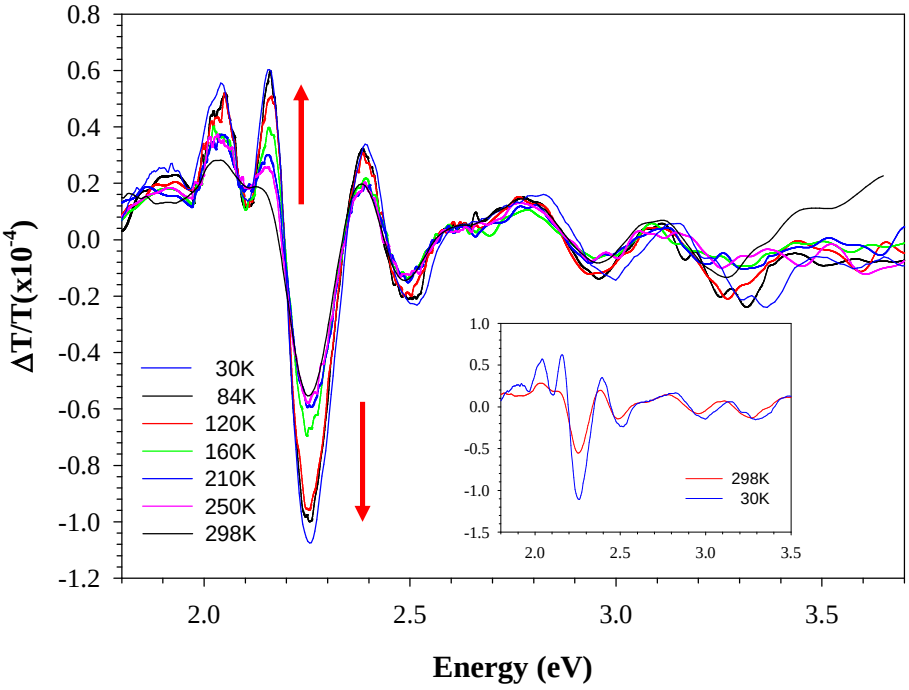

Figure 6.17 The temperature dependence of the EA signal for C_{70}. The arrows indicate the increase in relative intensity of the 2.26eV feature as the temperature is lowered. The inset shows the comparison between the EA signal recorded at RT and at 30K for clarity purposes.

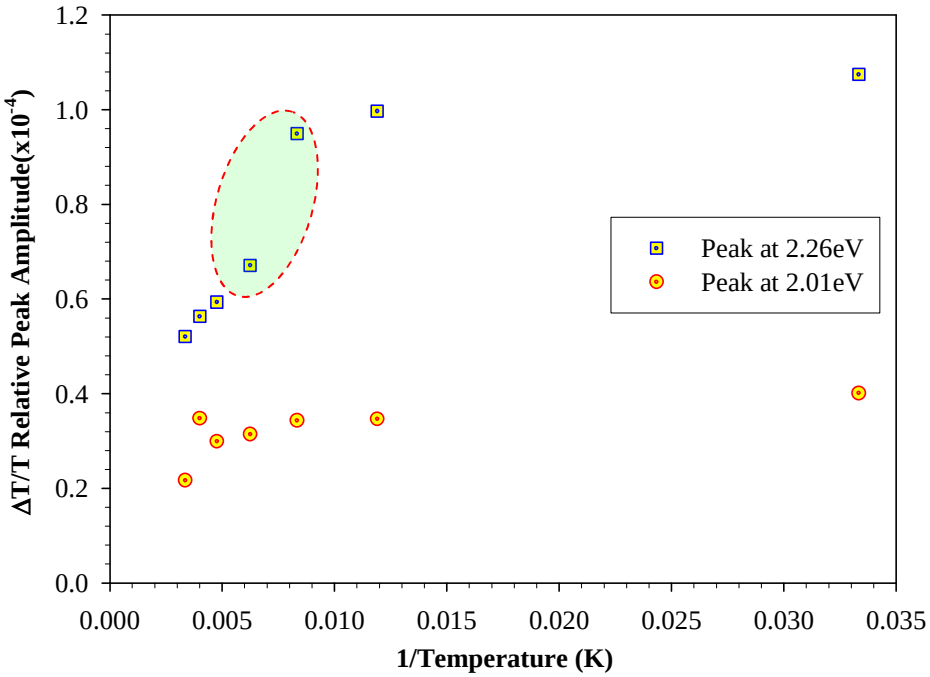

Figure 6.18 The temperature dependence of the CT state at 2.26eV and the tentatively assigned forbidden Frenkel exciton at 2.01eV. The shaded area indicates the gradual transition of the lattice from an hcp to monoclinic phase.

The actual origins of this are uncertain although the zeroth derivative line shape has prompted authors to speculate that it may result from a forbidden Frenkel exciton becoming allowed under the influence of the electric field [88]. Evident from figure 6.18, is that the CT state at 2.26eV is more susceptible to temperature changes than the Frenkel state at 2.01eV. As indicated, the structural transition in C_{70} from a hcp phase to a monoclinic phase is a gradual which is consistent with the reported findings of Petelenz [88]. The current experimental results exhibit a much larger transition range than that predicted by the Petelenz model although these inconsistencies may be due to the estimates inherent in the predicted model [88]. Similar to the case for C_{60}, the above findings provide evidence that the CT states in C_{70} are more sensitive to changes in temperature than Frenkel type excitons.

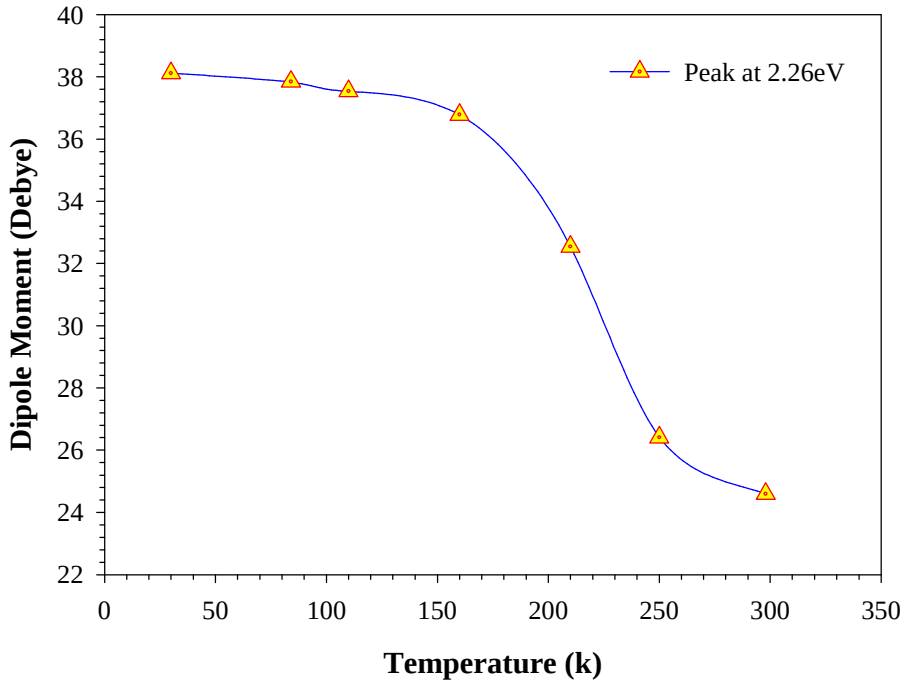

Figure 6.19 The calculated dipole moments for the peak at 2.26eV as a function of temperature. A large change in the dipole moment is observed around the phase transition

The implication of these results is that through thermal modification of the crystalline lattice it is possible to manipulate the degree of CT interaction and it thus possibly offers a way of controlling the materials bulk properties. In order to allow a correlation to be drawn between the materials EA signal response and the change in its crystalline structure it is necessary first to calculate the dipole moment for the charge transfer peak at 2.26eV. This was achieved in a similar manner to those calculated for C_{60}. Figure 6.19 shows the calculated dipole moments for the peaks at 2.26eV as a function of temperature. At 77K the dipole moment of the feature at 2.26eV was calculated to be 37D. It should be noted that this is somewhat larger than the value previously reported by Kazaoui, of 32.5D [43]. Some discrepancy would be expected as a result of the different fitting procedures employed to determine the dipole moment. That aside this value represents an electron hole separation of approximately 15.4Å which is comparable to crystallographic data and provides an indication that the interpretation is consistent.

6.12 Irreversible electronic spectroscopy of C_{70}

Extending the study to the high temperature regime reveals that the material's behaviour to a thermal treatment is somewhat different to that of C_{60}. Evident from figure 6.19 is the reduction in oscillator strengths as the temperature increases, although the reductions are far less pronounced than those observed for C_{60} films. However a semi empirical band analysis of the feature at ~2.30eV, which has been identified previously as the primary CT in C_{70}, seems to exhibit only a minor temperature dependence when compared to the feature at 2.57eV even though CT states should be more sensitive to

orientational disorder. This seemingly minor temperature dependence of the CT state may be as a result of the vibronic masking of the CT feature.

.

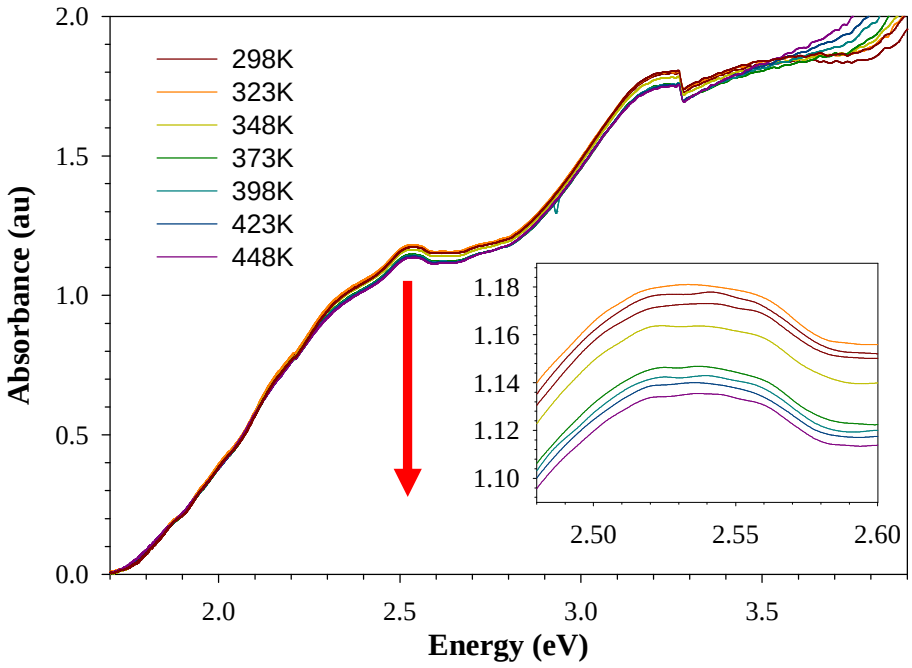

Figure 6.19 The evolution of the temperature dependence of C_{70}. The inset shows an expanded region from 2.48eV to 2.6eV for clarity. Feature at 3.25eV is due to lamp change over

A plot of the relative peak area of the two features as a function of temperature shows that the changes observed are reversible up to a temperature of 340K and as such are deemed to be thermochromic in nature. However on exposure to temperatures above 340K there is a gradual decrease in the integrated area of each peak indicating that the decrease in oscillator strength is as a result of a non-reversible process occurring. It is known that in the crystalline structure of C_{70} both fcc, hcp phases can co exist in addition to large concentrations of defects [45]. It is generally accepted that there are three temperature regimes for crystalline C_{70}; high, intermediate and low. In the high temperature regime (temperatures above 340K), molecules experience free rotation through degrees of rotation and stack into an fcc phase. Intertwined within this fcc

phase is another coexistent hexagonal hcp phase as indicated by numerous stacking faults in the crystalline structure. The stacking sequence of the planes follows a ABCABC for the fcc structure and ABABA for the hcp structure.

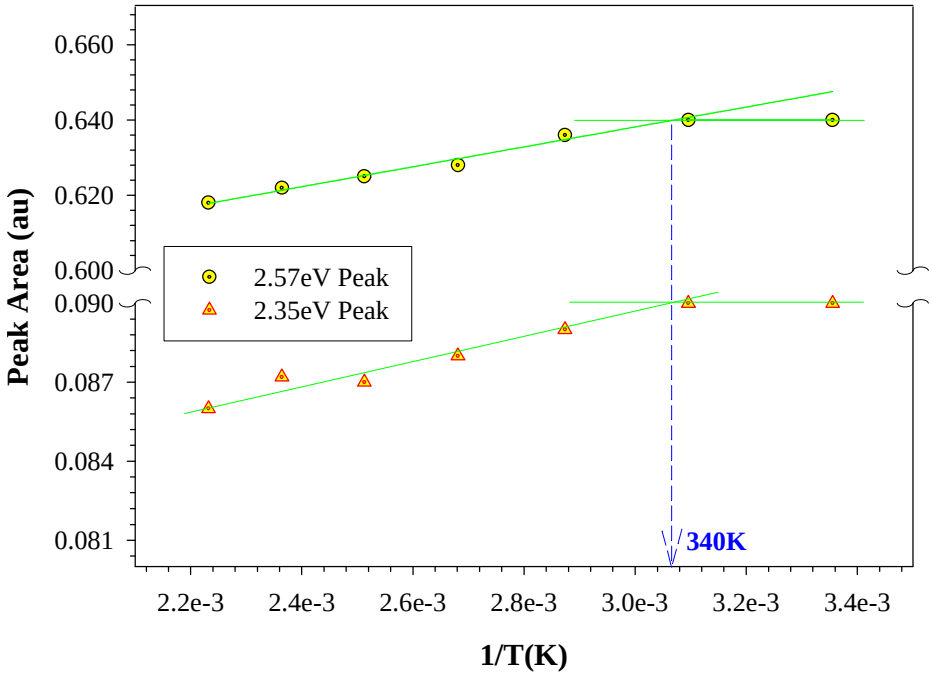

Figure 6.20 The integrated peak areas for the features at 2.35eV and 2.57eV as a function of temperature. As indicated on the graph the peak areas remains approximately constant and thus reversible until 340K where an inflection point is observed suggesting the presence of an irreversible process taking place.

There are only minor differences between these structures since the distance between the C_{70} molecules in both phases is practically identical, with the only difference being the planar stacking along the (111) direction. Based on the reports on the thermal properties of C_{70}, Prassides tentatively suggested that heating a sample of C_{70} to approximately 350K would provide sufficient energy to convert the rhombohedral phase to the fcc phase [41]. The hypothesis was based on the fact that temperatures of approximately

350K would provide sufficient energy to overcome the potential barriers associated micro-strains and defects in the film. Other works reported this phase transition occurring at lower temperatures, 337-340K which they attributed to the molecules being able to rotate about axes other than the long axis [45, 91].

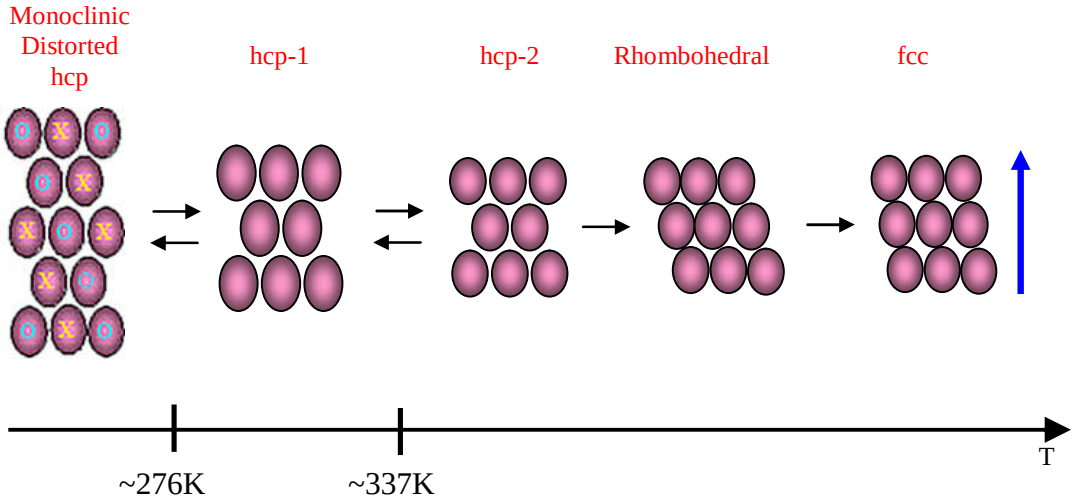

Figure 6.21 Shows the phase diagram for C_{70} with its possible transitions as adapted from [25]. The blue arrow indicates the (111) stacking direction for all unit cells.

Given the variation in literature regarding this phase transition, it is likely that the inflection point at 340K in figure 6.20 may reflect the initial stages of this phase orientation. The gradual decrease in the integrated peak area of the 2.53eV feature implies that the process itself is irreversible and as such non-thermochromic in nature. Inspection of the feature at 2.30eV reveals a similar irreversible trend associated with peak area reduction as a function of increasing temperature, although the relative change in magnitude is smaller when compared to the feature at 2.57eV. That aside the reduction in peak area does indicate a certain sensitivity of this CT state to structural changes in lattice as a result of a increasing the temperature of the system.

6.13 Irreversible EA measurements of C_{70}

Figure 6.21 shows the effect of increasing the temperature on the EA signal of C_{70}. Similar to that observed in C_{60}, there is a gradual reduction in the peak strength as the temperature is increased. As previously noted the primary feature associated with CT states in C_{70} is located at 2.26eV, which Kazaoui postulated as arising from eigenstates of (1,0,0)/(0,0,½) CT parentage [43].

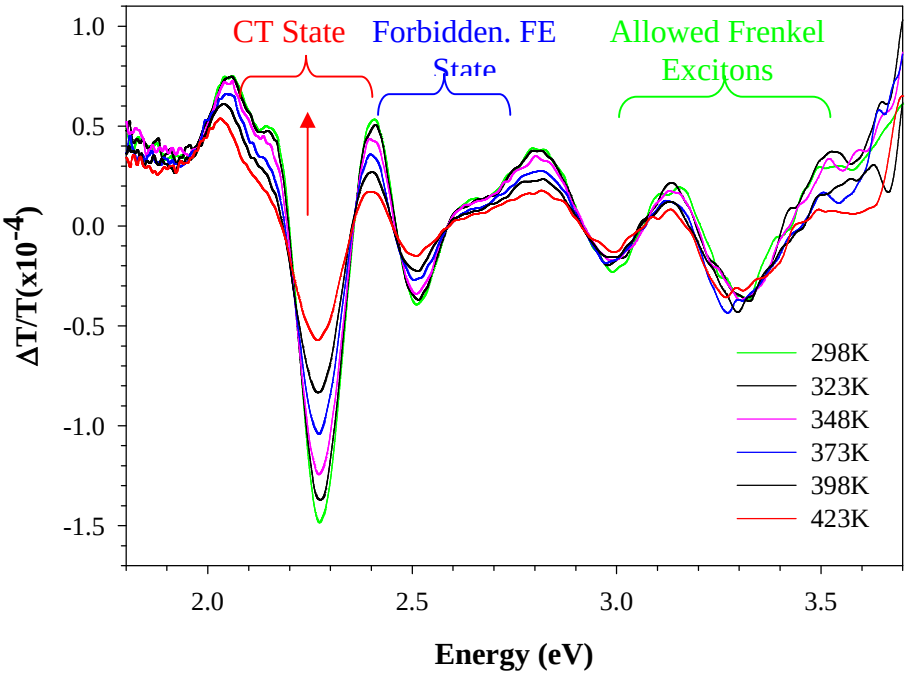

Figure 6.22 Shows the effect of heating on the EA signal of C_{70}. Evident is the marked decrease in the feature at 2.26eV with increasing temperature associated with the CT state. Also noteworthy is the much weaker temperature dependence of the forbidden Frenkel Excitons (FE) located at 2.45eV. Little change is observed in the intensity of the allowed Frenkel excitons, which supports the theory that they not dependant on their molecular orientation

While there is an overall gradual decrease in the relative strength of most of C_{70} EA features, it is the CT state at 2.26eV which experiences much larger reductions when compared to nearby Frenkel type excitons. Similar to the situation observed in the low

temperature EA measurements the sensitivity of the CT states at higher temperatures should be dependant on relative molecular orientation. This degree of orientational disorder would be expected to increase as a result of increasing temperature, especially at temperatures around the phase transition. The overall net affect of this increased disorder would be a broadening of the absorption spectrum and a reduction in the EA signal amplitude. Inspection the data in figure 6.22 reveals this predicted trend whereby the CT at 2.26eV experiences a reduction in signal intensity as result of increasing temperature. In addition to the changes experienced by the CT states, some of the low energy Frenkel also exhibit temperature dependence, in particular the features at 2.45eV. While the temperature dependence of the allowed Frenkel states is predicted to be small, the excitonic transfer integrals for forbidden states are governed by electron exchange and as such their existence will depend on their molecular orientation and consequently on the temperature [88]. Unlike the allowed states, which are governed by dipole-dipole interactions and thus for the most part remain unaffected by molecular orientations, the forbidden states are very sensitive to orientational disorder and thus exhibit substantial temperature dependence.

6.14 Conclusion

The data from the low temperature measurements on C_{60} and C_{70} revealed that the CT states associated with both molecules are strongly influenced by their local thermal environment, when compared to the Frenkel type excitons. The indication from the electronic analysis of both C_{60} and C_{70} films is that the changes in the electronic properties of the material's are reversible in nature below a specific temperature, ie 362K for C_{60} and 340K for C_{70} and indeed in this regard the films can be cycled through

various thermal treatments without experiencing any loss in oscillator strength. The effect is similar to the one observed in the low temperature regimes and the process is deemed to be thermochromic in nature. However exposure to thermal treatments above these temperatures results in irreversible changes in the optical properties of both C_{60} and C_{70}. Apparent form the optical absorption data is the loss in oscillator strength of all the eigenstates. Peak area analysis for both C_{60} and C_{70} reveal sharp decreases above these transition temperatures indicating the changes are irreversible. The electroabsorption analysis also shows a similar trend associated with the CT states. In particular the feature at 2.43eV in C_{60} experiences a dramatic loss in strength compared to other states, indicating that the origins of this state have a greater susceptibly to temperature fluctuations. The electroabsorption analysis on C_{70} also revealed a susceptibility of the CT to temperature changes. The data would seem to indicate that the films have undergone a thermally induced process which is inhibited at lower temperatures and that the observed changes in the optical properties of the material are due to a structural reordering of each material's crystalline environment. It is this thermal modification or annealing process which will be structurally investigated in the next chapter.

CHAPTER 7

Annealing effects in Fullerene Films

7.1 Introduction

This chapter presents the data obtained from spectroscopic measurements of films which have been thermally treated resulting in irreversible effects i.e. annealed films. As outlined in chapter 6, the electronic process in both C_{60} and C_{70} critically depend on their temperature dependent crystal packing. It was shown that these thermal processes were either reversible or irreversible depending on the treatment temperature. In this chapter the focus is placed on the irreversible effects associated with the high temperature treatments with particular emphasis being placed on the thermally induced changes in the crystalline structure. Supportive evidence of the annealing effect is also

presented based on crystallographic measurements and morphological analysis of both materials.

7.2 Electronic evidence for annealing in C_{60}

In Chapter 6 the effects of temperature on the optical properties of solid state C_{60} were examined. While the effect of low temperatures on the optical absorption of C_{60} has been well documented, studies describing the effects of increasing the temperature of the sample to above ambient conditions are much less common. The high temperature data presented in Chapter 6 indicated the presence of an inflection point at 362K and subjecting films to temperatures exceeding this value resulted in a permanent loss in the material's oscillator strengths.

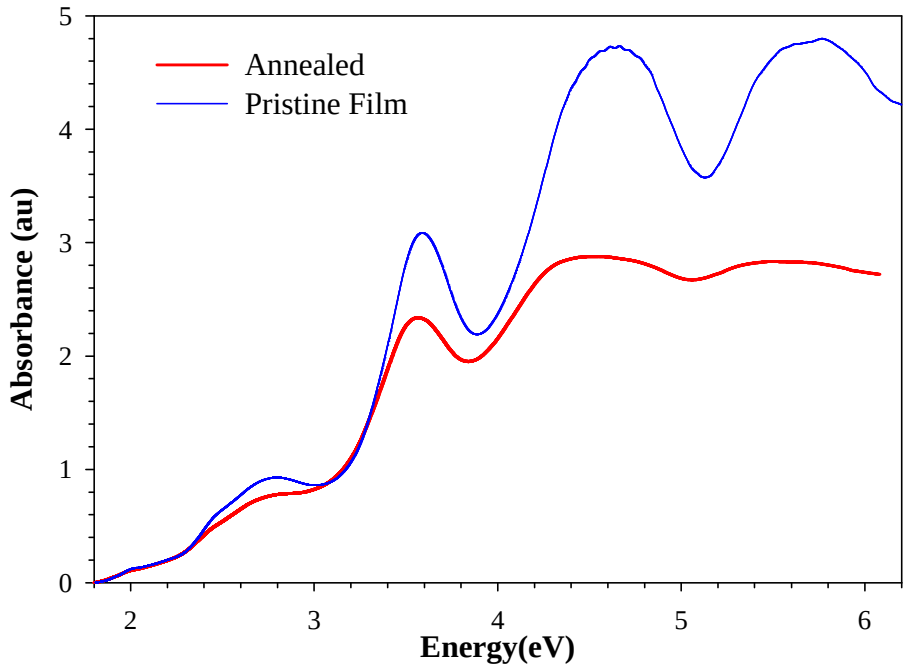

Figure 7.1 The comparison between a pristine C_{60} film and it the subsequent effect of exposing the films to thermal treatment. A continuous red shifting and reduction in the allowed transitions oscillation strengths are indicative of an annealing process.

The data is consistent with the findings of Akselrod et al who ascribed the observed reductions in oscillator strengths as being due to an annealing process [90]. In fact the most drastic indication of a change is in the comparison between the optical absorption of a pristine film before and after temperature conditioning at 473K for 1 hour, shown in figure 7.1 for a C_{60} film. Initial inspection of the data in figure 7.1 reveals an expected continuous red shifting of the features which is indicative of an annealing effect although the extent to which shifting occurs is not as dramatic as that reported by previous authors [90, 91]. Also evident in Figure 7.1 is a marked overall decrease in the oscillator strengths of the features between 3.1eV and 6.2eV. Although not as notable, there is also a decrease in intensity of the features centred around 2.75eV. As discussed in Chapter 6, it was demonstrated by Kazaoui et al [43] that the state at ~2.75eV is derived from a coupling of the nearest neighbour charge transfer states with the forbidden Frenkel manifold. It was also noted that while the HOMO LUMO at 2.01eV remains unaffected, all the other solid state features experience a continuous red shifting of their energies, although not entirely evident from figure 6.5. Based on these observations it can be conjectured that the loss in oscillator strength and continuous red shifting maybe due to a closer packing of the molecules in the solid state phase. It has been demonstrated that the spectral positioning and oscillator strengths of the π transitions in C_{60} can be affected by its crystalline packing [93]. These variations arise from the various coulombic attractions between molecules in different packing arrangements. The large reductions in the oscillation strengths of the allowed transitions in the high energy region of the spectrum, 3.5eV to 6.2eV, provide additional support for the idea that the films are annealed. The observed data is consistent with the changes observed in thermally annealed films.

An interesting anomaly was found regarding the length of time required to induce this annealing effect. In the published work by Akselrod et al [90], increasing the length of time the films were subjected to a thermal treatment favoured larger reductions in the oscillation strengths of all the electronic transitions. The results presented here are consistent with the findings as reported by Akselrod and in essence the findings show that at temperatures above 362K, longer heating cycles result in larger decreases in oscillation strengths, as shown in figure 7.2. By comparison, films subjected to thermal treatments below 362K exhibited little time dependence of the reversible reductions in oscillator strengths.

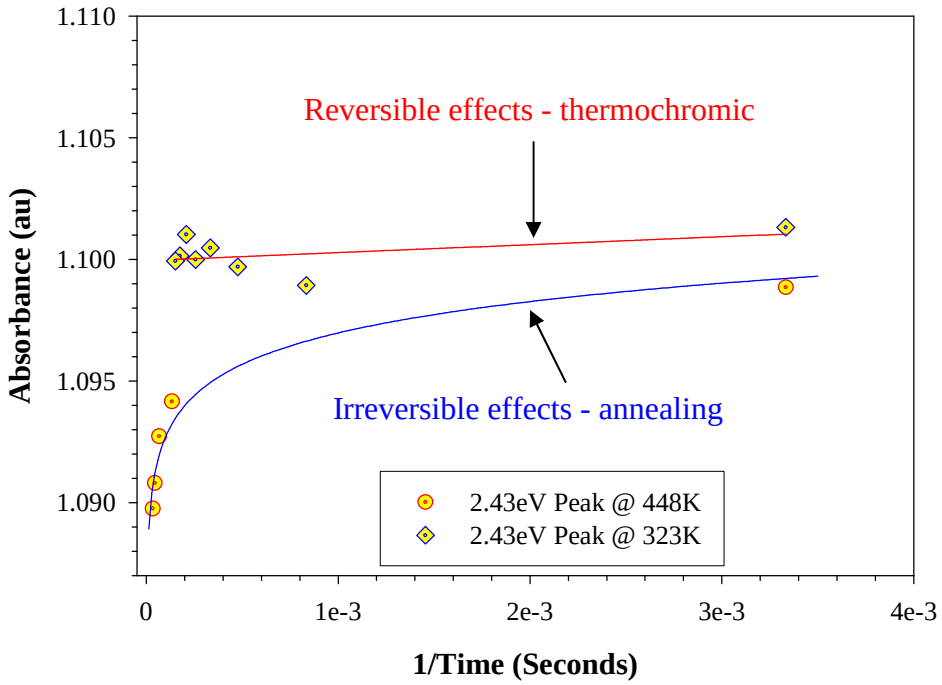

Figure 7.2 The decrease in intensity of the 2.43eV peak as a function of time. As indicated below 362K the peak height remains roughly constant while above 362K there is a gradual decrease in the peaks intensity.

Inspection of the data in figure 7.2 reveals that samples subjected to temperatures below 362K exhibit only minor fluctuations in oscillation strength for the mode at 2.43eV as a

function of the heating time indicating that the observed reversible changes are thermochromic in nature. However above 362K, increasing the duration of the heating cycle results in a gradual irreversible decrease in the mode oscillator strengths, thus implying the annealing effect is time dependant.

The nature of the annealing affects would suggest the molecular orientation has a role to play. Given the CT integral's sensitivity to relative molecular orientation, investigation of the EA spectral data should provide an indication of the changes in the materials electronic properties associated with the annealing process.

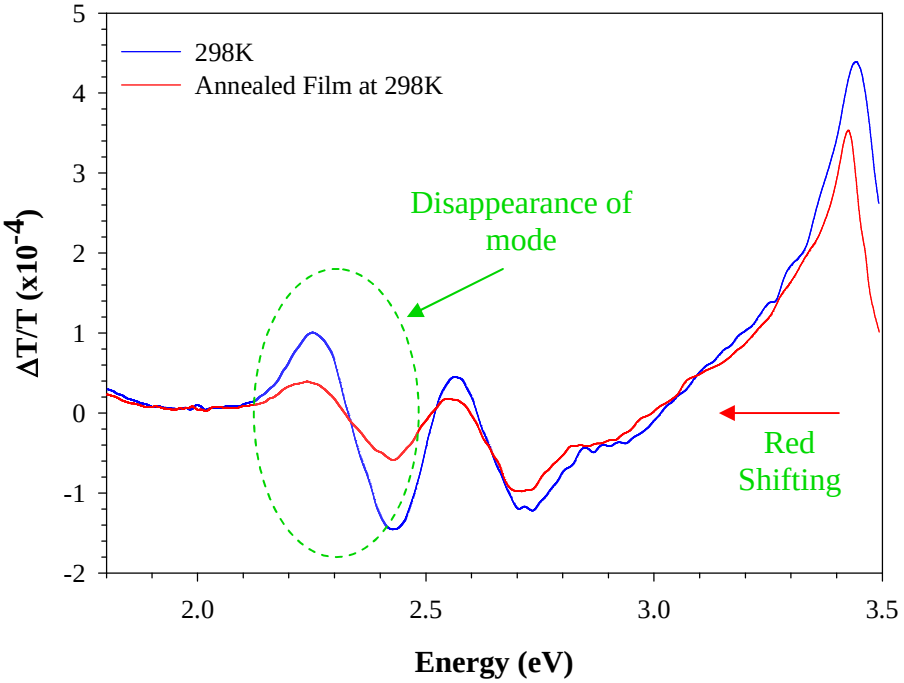

Figure 7.3 The comparison of the EA spectral of a pristine fullerene C_{60} film before heating and the EA signal of the same film after annealing. Of particular interest is the relatively large decrease in the EA signal of the feature at 2.43eV compared to the feature at 2.7eV, indicating that the two features arise from separate CT states.

Figure 7.3 shows the EA spectra recorded for a C_{60} film before and after an annealing cycle to 423K. Inspection of the data reveals an apparent overall loss in intensity of all

the spectral features. Also of interest is the apparent red shift of all the features which is a manifestation of the annealing effects observed in the absorption data. Inspection of the EA signal of the annealed sample shows large differences to the EA signal of the pristine sample. While there are losses in the oscillator strength of both features at 2.43eV and 2.70eV, the greatest reductions in signal intensity are observed for the feature at 2.43eV. Calculating the change in dipole moment via band analysis of the data allows for a correlation to be drawn between the annealing temperature and the degree of intermolecular communication between adjacent molecules in the lattice. As mentioned in Chapter 6, the dipole moment of the 2.43eV feature before the annealing process was calculated to be 16.8D. As can be seen in figure 7.4 there is a gradual decrease in the dipole moment of the 2.43eV CT state with increasing temperature.

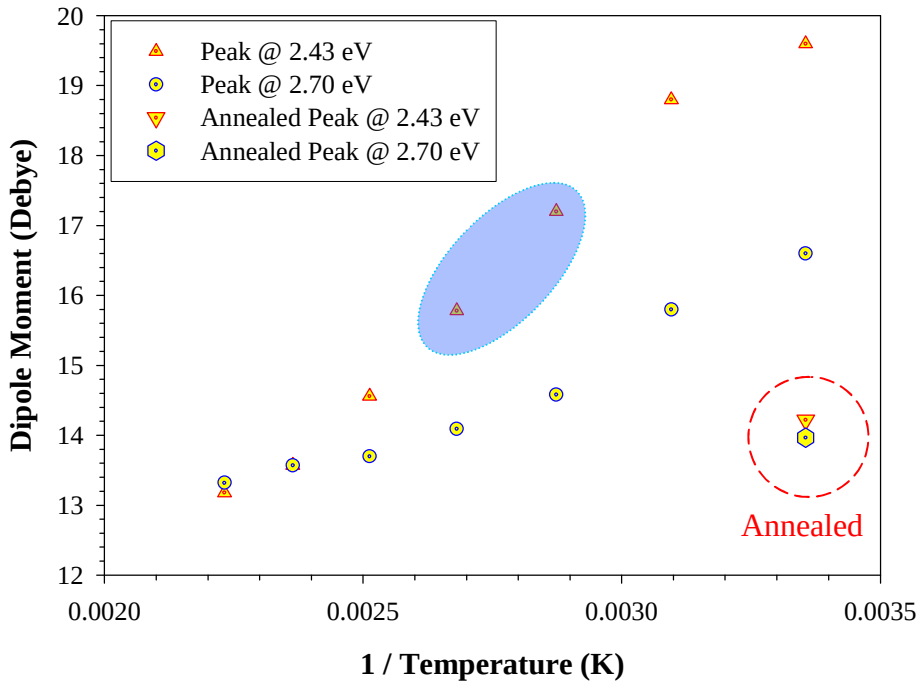

Figure 7.4 The effect of temperature on the change in dipole moment for the peaks at 2.43eV and 2.70eV. The blue shaded region indicates the annealing phase temperature. The broken red circle indicates the calculated dipole moments of the two features after annealing.

In contrast, while the feature at 2.70eV also experiences a gradual decrease, the change in dipole moment of the 2.43eV is far more drastic, indicating a greater susceptibility of this state to changes in the local environment. Indeed fitting the EA signal of the annealed film upon cooling to room temperature reveals an associated dipole moment of 14.2D, which corresponds to an electron-hole separation of 5.9Å. This represents a reduction of 1.1 Å in the electron hole separation as a result of the annealing process. Since the state at 2.43eV is derived from the transfer of an electron from the unit cell origin to the molecule located at (½½0) site, this reduction would be consistent with the idea that there is a change in the crystalline phases present in the material.

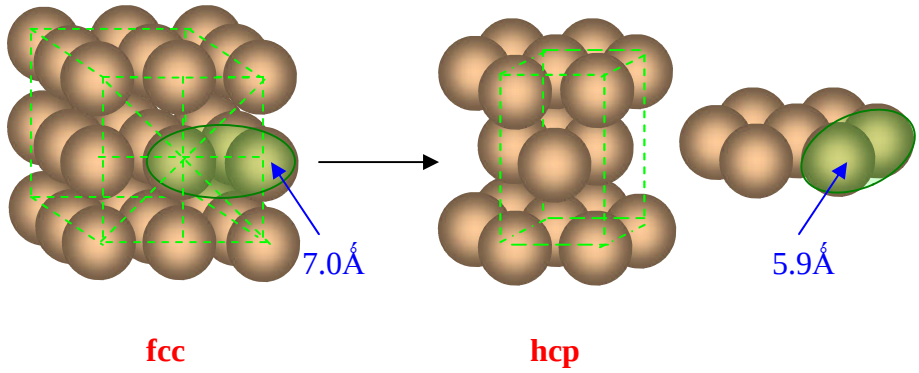

Figure 7.5 Shows the proposed structural change due to annealing. The broken green lines indicate the relevant unit cell for each lattice

The EA feature at 2.70eV also experiences a decrease of approximately 3D which approximates to a decrease in the CT state electron–hole separation of ~1Å after annealing which is similar to that decrease observed for the 2.43eV feature.. The above data would indicate that selective use of thermal treatments can alter the crystalline environment of the films and thus the degree of intermolecular communication between fullerene C_{60} in a solid state lattice can be controlled and by implication the electronic properties can be tuned to meet desired requirements.

7.3 Electronic evidence of annealing in C_{70}

Given the known susceptibility of C_{60} to changes in the local environment, and given the similarities between the two molecules it would seem reasonable to assume that a similar process might also govern the electronic properties of C_{70}. In order to elucidate whether or not this is the case the study is extended to investigate the effects of thermal modification on C_{70} lattice. Similar to the case of C_{60} the changes observed in the optical absorption spectrum of C_{70}, reflect the structural reordering of the bulk crystalline structure as a result of the thermal treatment. However, upon cooling and in contrast to the properties of C_{60}, certain modes in the annealed absorption spectrum of C_{70} exhibit larger oscillator strengths when compared to the pristine sample, as shown in figure 7.6.

.

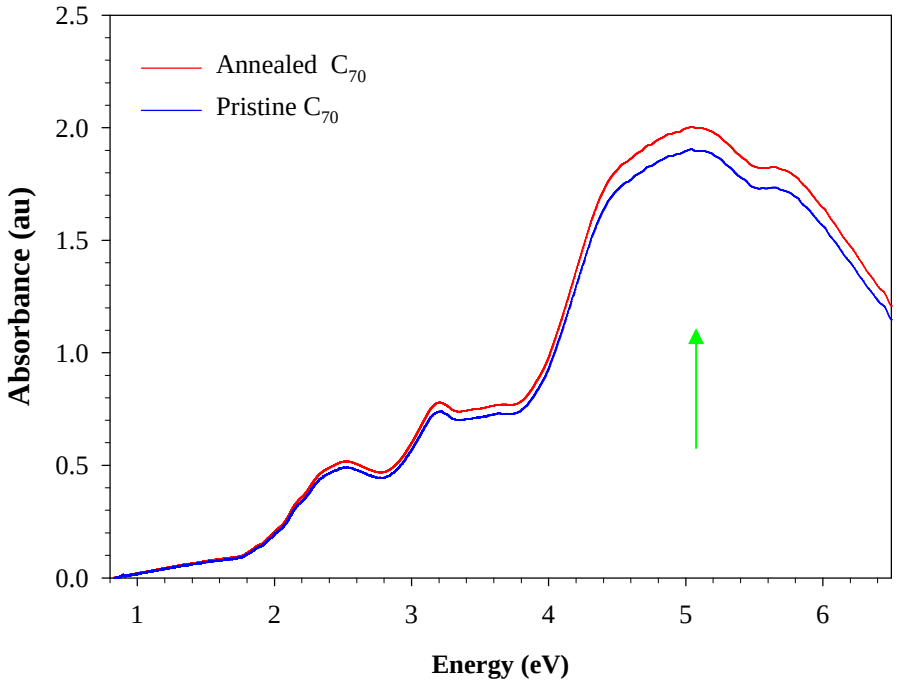

Figure 7.6 The comparison between the absorbance spectra of pristine C_{70} and a heat treated sample after been cooled to room temperature. The green arrow indicates the increase in oscillator strength.

In particular the region from 2.5eV to 6.0eV exhibits the largest increases. It is possible that these increases may be due to the conversion of the remaining hcp domains to fcc type phases in a fashion similar to that described by Almairac et al [94]. Such a reorientation would result in relaxed packing in the (110) directions and a contraction along the (111) axis and consequently result in an increase in oscillation strengths. A similar increase in oscillator strength was observed by Capozzi et al in C_{70} films deposited at incrementally higher temperatures [95]. They ascribed the increase in the optical absorption as resulting from a higher thermal mobility of the molecules, thus allowing them to reach the correct position within the lattice [95]. However inspection of the data shows only a minor increase in the oscillator strength of the CT peak at 2.26eV.

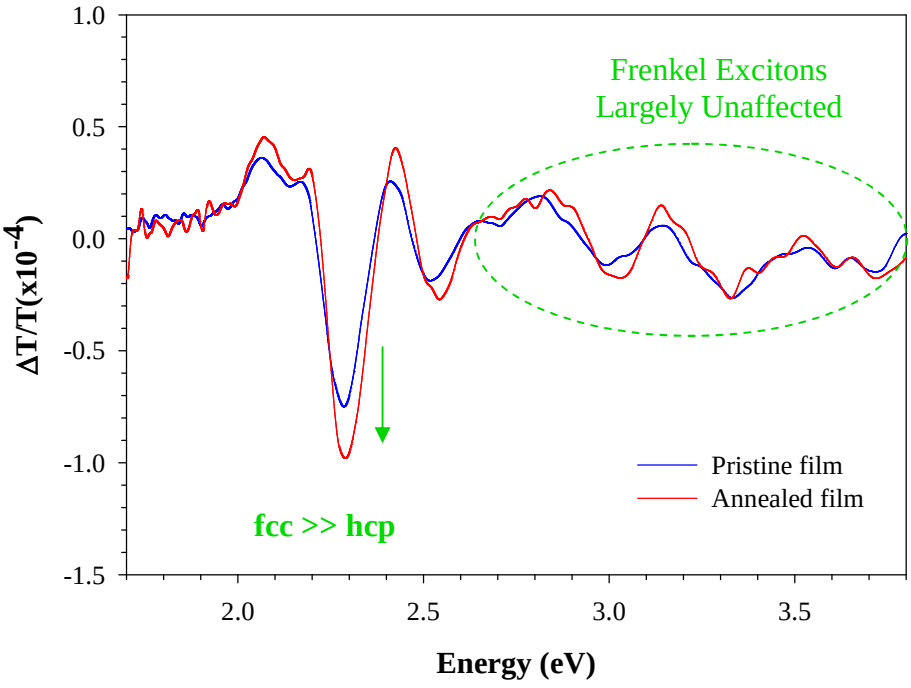

Figure 7.7 The compared EA signals for a pristine film of C_{70} and subsequent affect of annealing the film. The increase in the CT state at 2.26eV is clearly visible while the Frenkel excitonic states remain unaffected. This increase may be due to a higher portion of the lattice adopting a fcc structure than a hcp structure.

This is to be expected given the masking effect of the Frenkel type intramolecular excitions. Thus in order to probe the annealing effect on the intermolecular excitation which should exhibit a more pronounced sensitivity to changes in the crystalline environment it is necessary to compare the EA spectra of the pristine and annealed film, figure 7.7. Upon cooling the film to room temperature and rerecording the EA spectrum a number of the features in the EA spectrum experience an increase in intensity as shown in figure 7.10. Deconvolution of the EA into weighted sums of the derivative absorption bands reveals that the CT state at 2.26eV experiences a large increase in dipole moment from 24.6D to 28.0D. As shown in figure 7.8, cooling the film to room temperature after a thermal treatment results in an increase of 3.4D which represents an increase in the charge size distribution of 1.4Å.

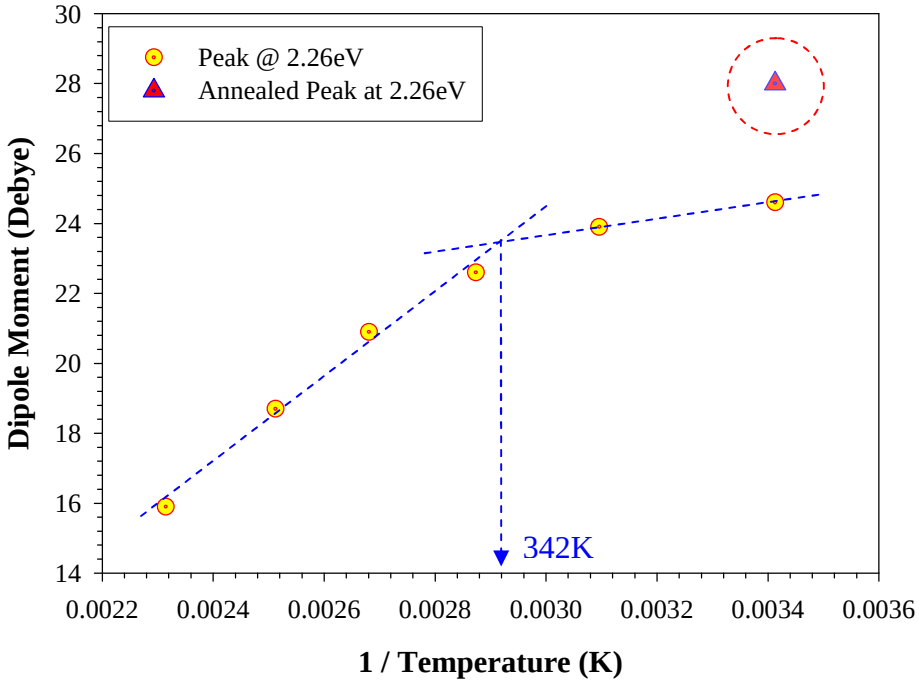

Figure 7.8 The change in dipole moment as a function of temperature. Of particular note is the calculated dipole moment of the 2.26eV feature in the annealed film. Also indicated on the graph is the position of a possible phase transition at 342K

Overall this represents an electron hole separation of approximately 12Å. This increase in size would indicate that there has been a reduction in the ABA… stacking of the C_{70} film and an increased in the ABC type stacking sequence. Almairac et al reported a similar reconstruction process occurring in C_{70} films after being stored for an extended period of time at room temperature [94]. Similar to the process observed for the CT state at 2.26eV the forbidden Frenkel exciton at 2.45eV also experiences an increase in intensity, while most notably the allowed Frenkel excitons at higher energies do not. The implication is that a reorientation of the equivalent molecules within the lattice has occurred and as a result of this decreased disorder within the lattice the excitonic states sensitive to such alterations experience changes in intensity. This would be consistent with the idea that annealing the film provides sufficient energy to overcome any local minima associated the rotational hindrance of the molecules within a mixed lattice and allows for the formation of a greater number of fcc phases or other phases within the lattice.

7.5 Vibrational analysis of thermally modified films

An obvious explanation to account for observed changes in the absorption spectrum would be the possible formation of oxidative products due to the intercalation of oxygen into the lattice and/or the formation of photopolymer. While every attempt was taken to reduce this possibility of oxygen contamination, the possibility still existed and as such it was necessary to confirm that the observed changes were structural rather than chemical in nature. In order to elucidate the origins of these spectral differences, infra red(IR) spectra were recorded on the sample before and after a heat treatment cycle. For a vibration to be IR active there must be a change in the dipole moment of the molecule.

Consequently in fullerene C_{60} IR selection rules only allow for four active modes i.e. $4F_{1u}$, while the remaining modes are silent in IR [96]. Inspection of the pristine film of C_{60} reveals the presence of the four typical strong bands which result from allowed F_{1u} vibrational modes.

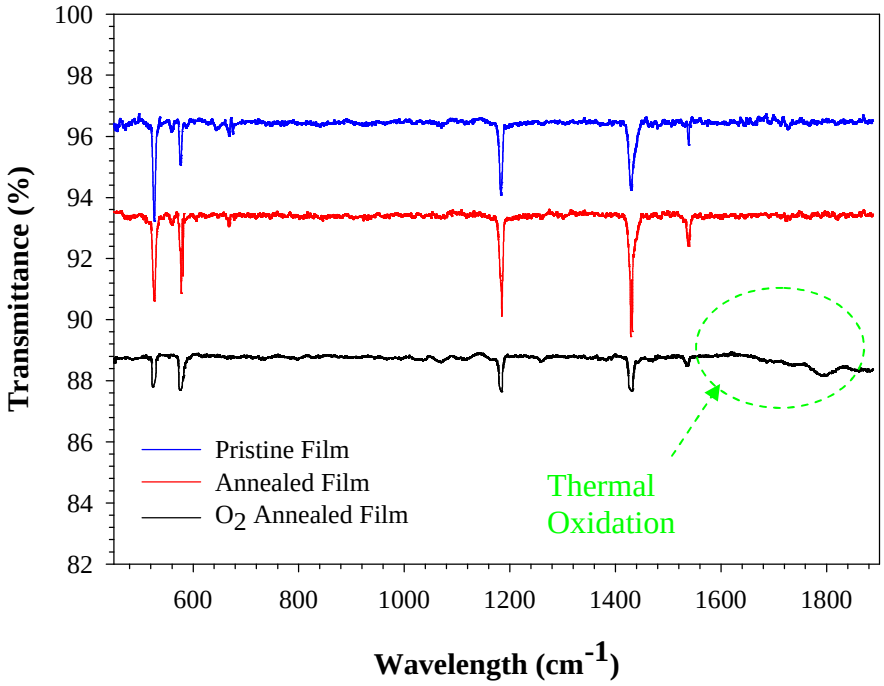

Figure 7.9 The FTIR spectra for a pristine, annealed and oxygen intercalated annealed film. The green circle indicates the effect of oxidative products which are absent in the other two spectra.

Comparing the vibrational spectrum of C_{60} to the heat treated film shows no discernable differences between the two spectra providing evidence that no chemical change has occurred due to the treatment process. As an indication of the effect of oxygen intercalation into the lattice, the spectrum of an oxygen intercalated heat treated film is also presented. In order to fabricate such a film a pristine film was heated to 473K for 48 hours in air. Inspection of the data reveals the presence of broad feature centred at 1750cm^{-1}. This mode is associated with the presence of a C=O bond within the sample and is indicative of oxidation of the lattice. Given that the un-oxygenated annealed film

shows no corresponding feature, it can be concluded that the films have not undergone a chemical change as a result of the annealing process. Extending the study to C_{70} yields the same conclusion. Since a C_{70} molecule is basically a C_{60} molecule with a belt of 10 extra carbon atoms, there exists a structural relationship between the two molecules. The addition of these extra structural elements in a C_{70} molecule results in new vibrational species the net result of which is a far richer vibrational spectrum [97].

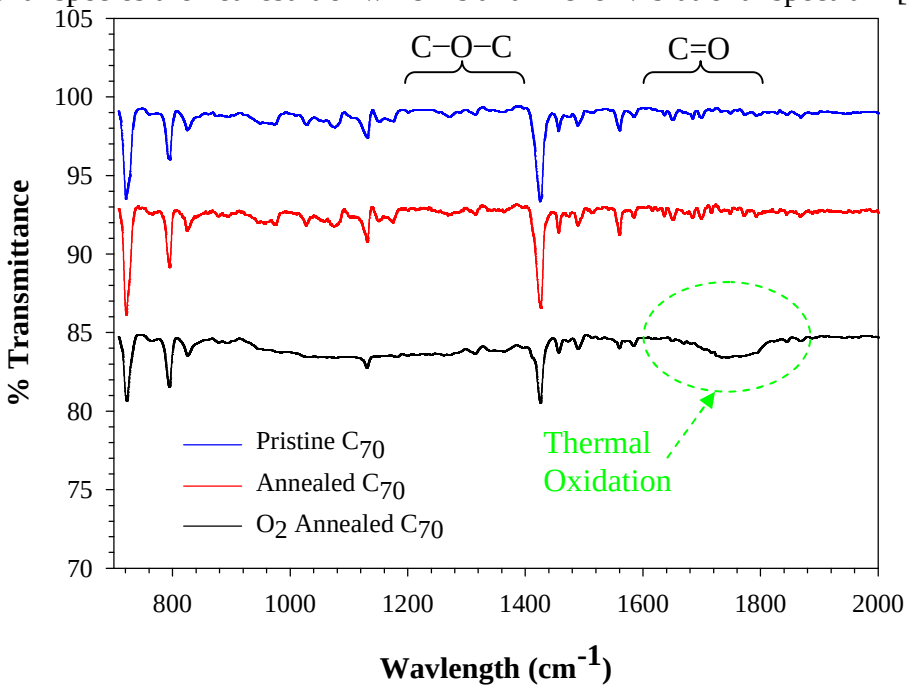

Figure 7.10 The FTIR spectra for Fullerene before and after a thermal treatment. Also shown is the oxygen intercalated annealed film which exhibits the effect of oxidation of the films.

In fact as a result of the reduced symmetry of C_{70} the $4F1_u$ modes in C_{60} are correspondingly split into $4A_2$" and $4E_1$' modes in C_{70}. Inspection of the vibrational spectrum of the pristine sample of C_{70} shown in Figure 7.10 reveals numerous modes, the frequencies of which are in excellent agreement with the literature values [97]. Comparing the IR spectrum of annealed C_{70}, there is no evidence of oxidative products or photopolymer formation. For comparison, a film was deliberately exposed to oxygen

for 24 hours and then subsequently heated to 423K for 24 hours in an oxygen atmosphere. Inspection of the oxygen intercalated films reveals the presence of a broad new feature at ~1750cm^{-1}, which again is similar to that observed in C_{60} and reminiscent of the photo-assisted oxygen intercalation of films described by Eklund et al [44]. This feature corresponds to the C=O stretching mode which is associated with the oxidation of the crystal lattice. In addition there is a reduction in the strength of the $F1_u$ modes. Since none of these trends are observed in the un-oxygenated annealed films it can be concluded that the films have not undergone a chemical change and consequently the observed changes must be structural in nature.

7.5 Morphological analysis of fullerene films

The morphological effect of thermally annealing the films was also investigated. in the absence of chemical alteration of the film itself implies a structural change has occurred.

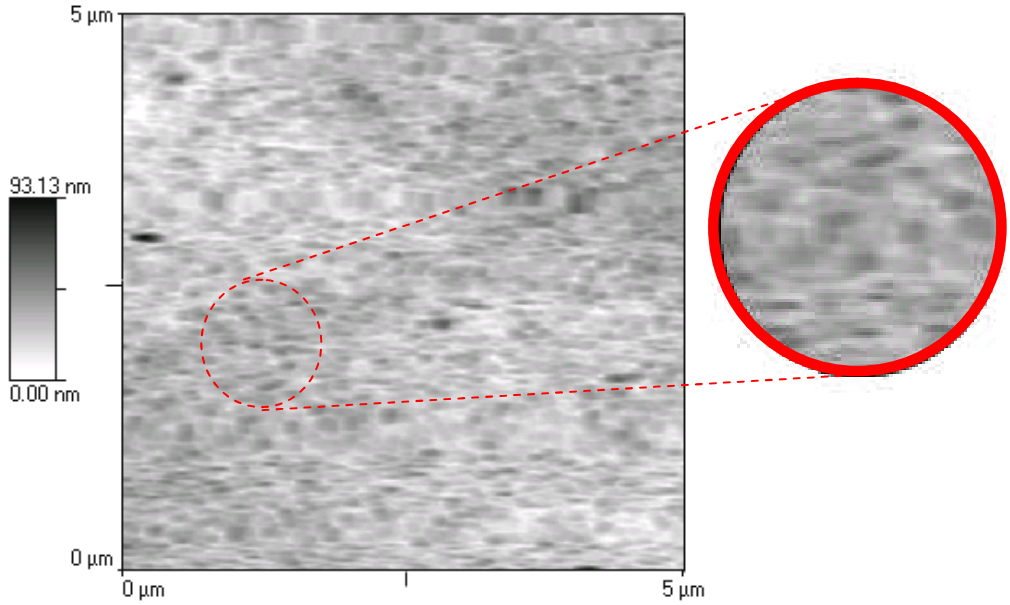

Figure 7.11 The AFM image shows the surface of a pristine C_{60} film. As indicated the surface is composed of irregular shaped grains approximately 45nm in diameter.

To monitor the effects on the films integrity, the films were examined using a TopoMetrix Explorer Atomic Force Microscope (AFM) before and after a thermal treatment. Initial inspection of the AFM images of C_{60} shows the film surface to be relatively free of defects, figure 7.11.

The pristine film shows small closed packed grains approximately 45nm in diameter. This is in close agreement with the reported grain boundaries by previous works [98]. As can be seen the granules are uniform in nature and the films themselves are typical for rapid sublimation conditions onto cold substrates [99]. However upon heating significant differences can be seen between the pristine and annealed samples. As the temperature is increased the grain size increases to approximately 350nm in diameter and the granules form triangular crystallites, as shown in figure 7.12. The evolution of triangle shaped grains can clearly be seen in the annealed sample, which again is in agreement with previous reports [98].

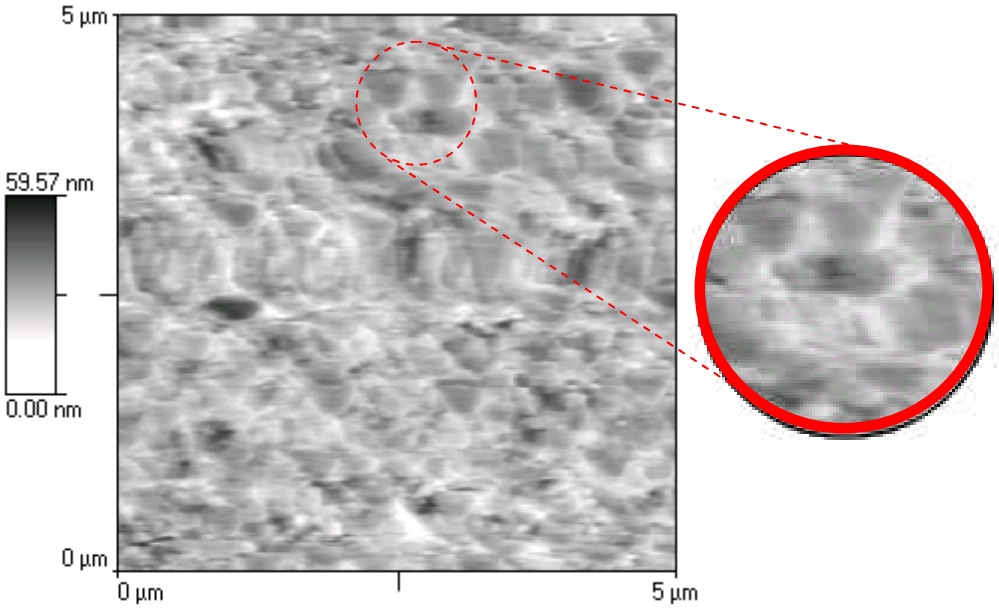

Figure 7.12 The effect of thermal annealing a fullerene C_{60} surface at 423K for 2 hours. The net result of the thermal treatment is the coalescence and reorientation of the grains.

In addition the surface roughness of the film reduces which indicates that some morphological changes have taken place. Similar findings were reported by Jayatissa et al and the hypothesis put forward was that the microcrystalline structure of C_{60} films can be modified by relatively low temperature thermal treatments [100]. It is interesting to note that both of these authors report structural changes occurring between 363K to 373K. These findings agree well with the current data obtained from the electronic spectroscopic measurements.

Once again extending the study to incorporate C_{70} evidence is found of structural change in the crystalline domains. The AFM images of C_{70} also confirm that the annealing process results in structural change of the microcrystalline environment. In the pristine film the grain size was between 80nm to 160 nm. The grains appear to be slightly elongated in comparison to C_{60} grains, but nonetheless are indicative of fast deposition onto a cold substrate, figure 7.13.

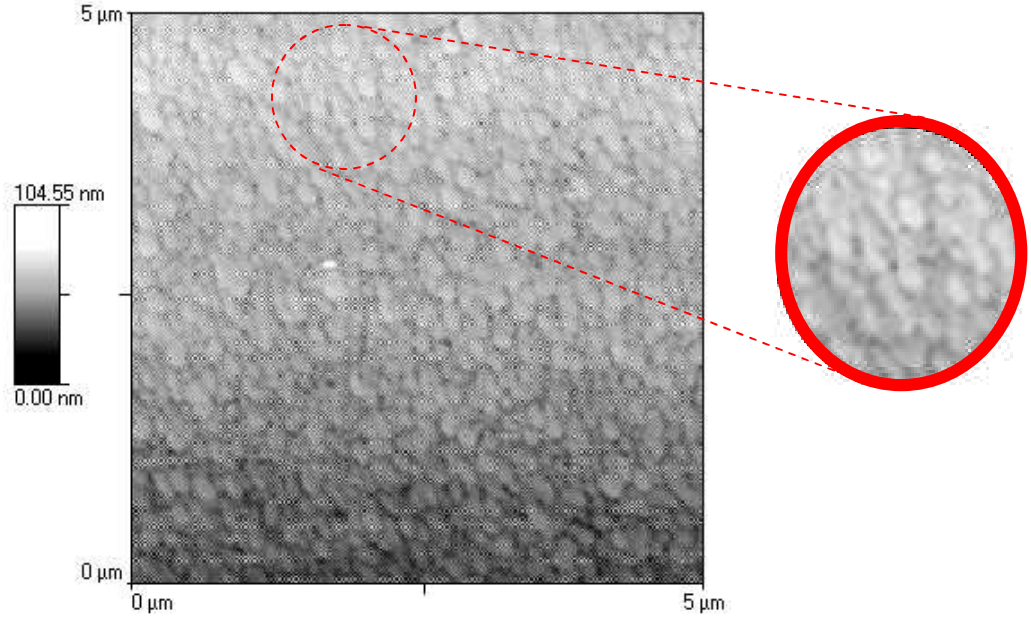

Figure 7.13 The AFM image shows the surface of a pristine C_{70} film. As can be seen the film is polycrystalline and composed of many small grains.

Analysis of the annealed film shows that the grain size has increased to approximately 400nm in diameter, figure 7.14. The surface roughness of the films also decreased after a thermal treatment as indicated by the decrease in step height. Iwata suggested that during a heating cycle C_{60} molecules may migrate to comfortable positions in the lattice by overcoming the barrier caused by van-der Waals forces [98]. Given the similar properties of C_{60} and C_{70} it is not unreasonable to assume that a similar process occurs in C_{70}.

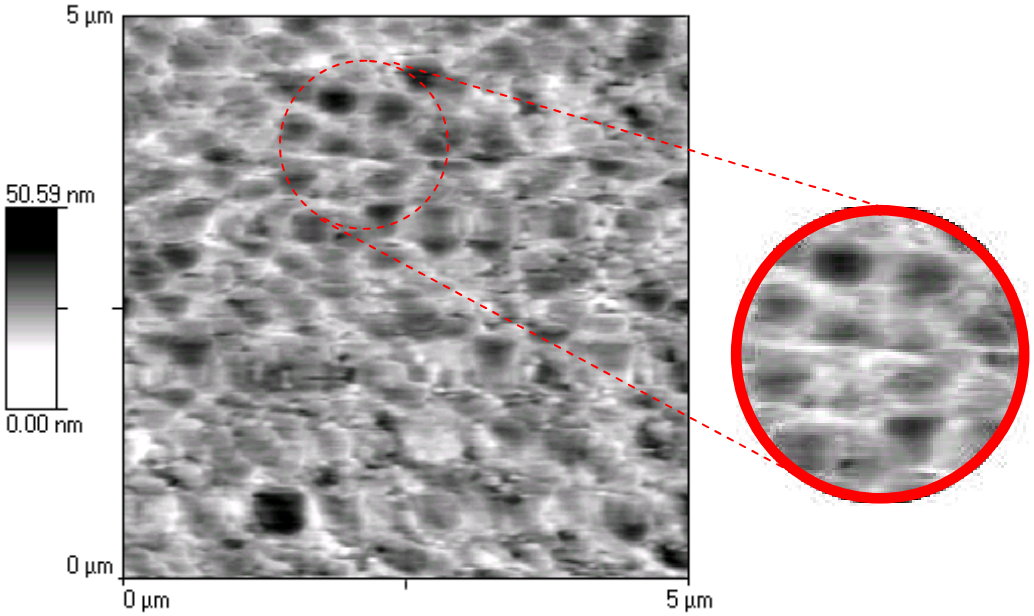

Figure 7.14 The AFM shows the affect of annealing to 423K for 24 hours. As can be clearly seen there is a coalescence of the grains

Overall the morphological data suggests that heat treatments do induce changes in the bulk crystalline structure. Both C_{60} and C_{70} exhibit larger grains in their annealed form than are present in the pristine material which would suggest a bulk structural reordering of each material's lattice. These findings are consistent with the data obtained from the electronic measurement that changes in the films have occurred.

7.6 Crystallographic measurements

The information yielded by absorption and EA spectroscopy prompted further investigation of the changes in the structural packaging of the lattice. In order to achieve this, samples were prepared for examination using X-ray diffraction (XRD). While the majority of the present work has focused on the investigation of thin films of fullerenes, recording X-ray diffraction patterns of thin fullerene films is difficult. These difficulties stem from the fact that the films are very thin, carbon is a weak X-ray scatterer and also that these films are not orientated through all possible rotations. To overcome these problems, the as purchased fullerene material was sublimed inside an Edwards Auto 306 evaporator at a base pressure of 10^{-6} mbar. Following deposition, the sublimed fullerene material was collected from the inside of the dome using a foil backed razor blade. Annealed films were prepared by heating in-situ inside the vacuum chamber following deposition so as to ensure minimal oxygen contamination.

7.7 X-ray measurements on C_{60}

To confirm the theory that the changes observed in the absorption and electroabsorption measurements on C_{60} are structural in nature it is necessary to examine the crystalline packing arrangements of the pristine and heat treated sample using XRD. Figure 7.15 shows the recorded X-ray diffraction pattern of a pristine C_{60} polycrystalline powder sample. Inspection of the data reveals that are a number of reflections from various planes of the cubic lattice. Also shown in figure 7.15 is the calculated diffraction pattern for an fcc crystallite with a lattice constant of a=14.2Å [101]. As can be seen the agreement between experiment and calculated data is reasonably accurate.

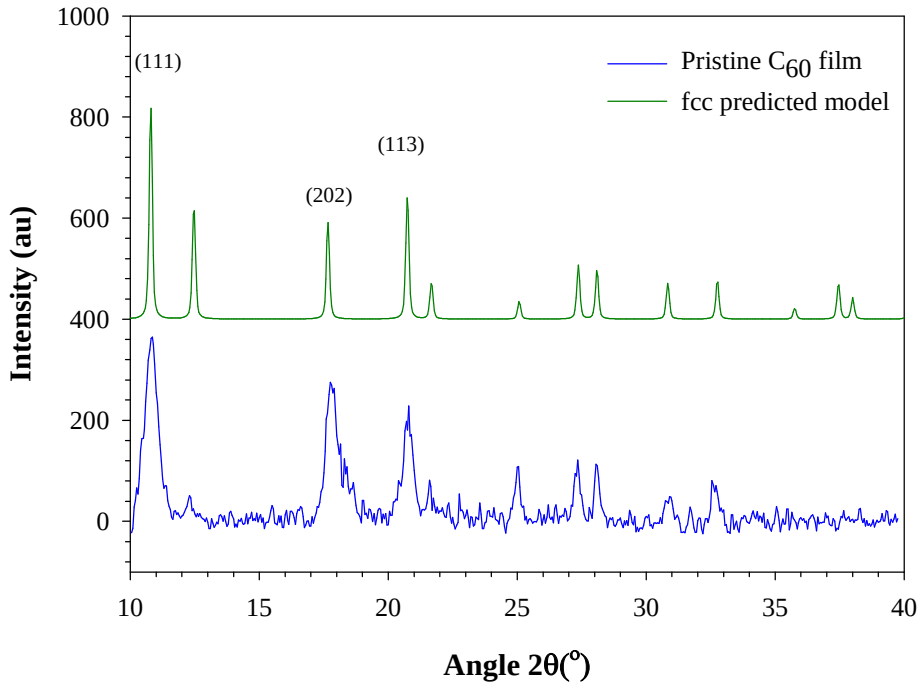

Figure 7.15 The XRD pattern for a typical fcc pristine C_{60} powder. Also shown for comparative purposes is the calculated XRD pattern for a fcc lattice with indexed reflection planes.

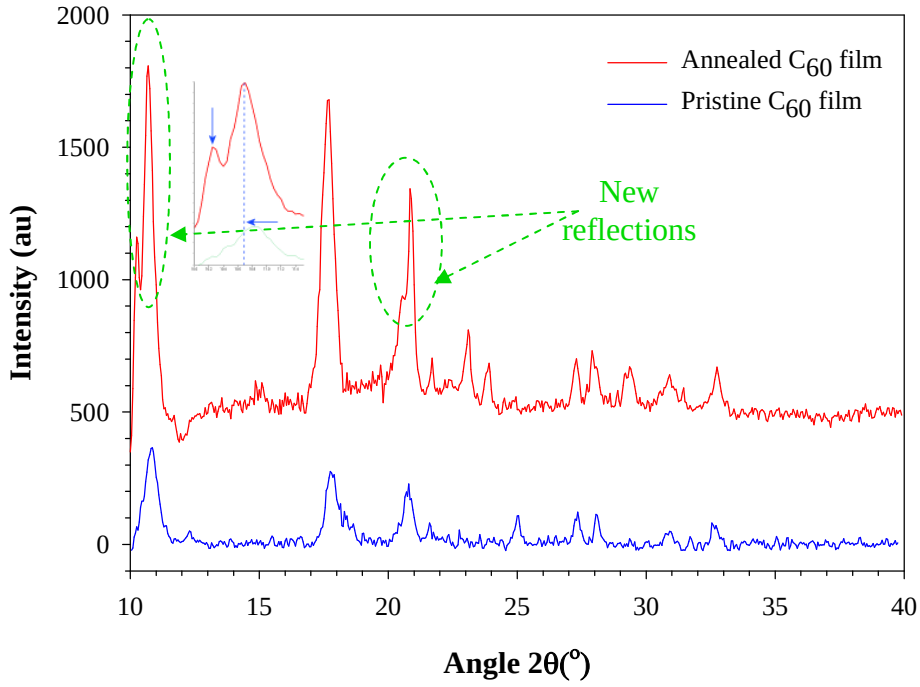

Figure 7.16 The comparative XRD for a C_{60} film before and after a thermal treatment process. The green circles indicate new reflections.

In general room temperature polycrystalline films of C_{60} are dominated by fcc phases with some distortions resulting from mis-packing. These distortions generally occur as a combination of a three layer cubic and two layer hexagonal patterns, (see figure 7.18). However the recorded data in figure 7.15 would seem to indicate that the pristine film (powder) is predominantly composed of fcc phases within the lattice.

In order to reproduce the effects seen in the absorption and the electroabsorption measurement the sample was heated to 473K for 24 hours and cooled to room temperature before its X-ray diffraction spectrum was taken as shown in figure 7.16.

Comparing the X-ray diffraction patterns of the annealed film to the original pristine film, figure 7.13 reveals numerous features which are present in both sets of data. The annealed film also exhibits a sharpening of the peaks which is associated with an increased crystallinity of the material.

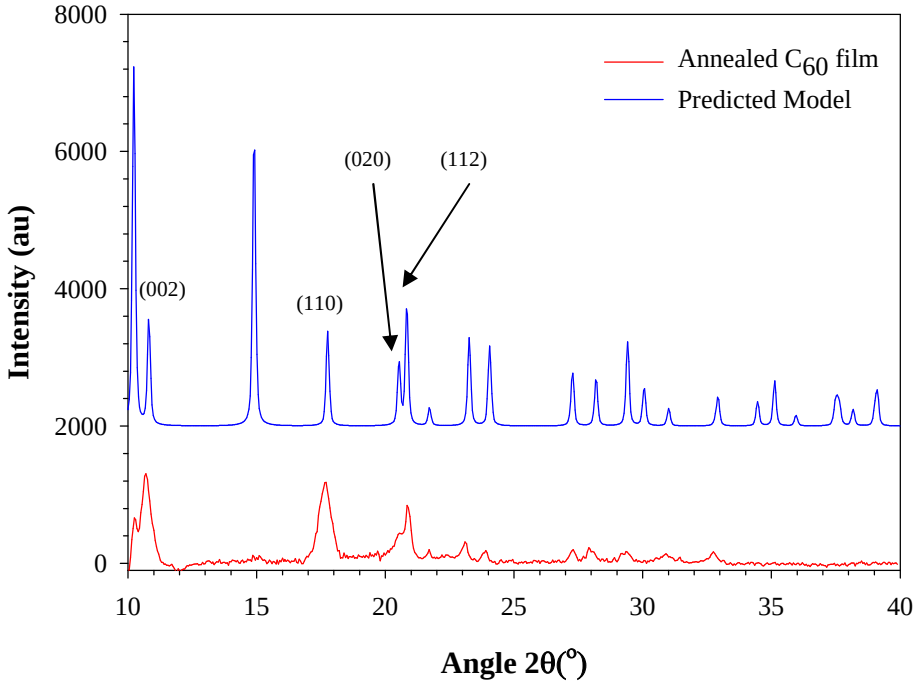

Figure 7.17 XRD pattern for a annealed C_{60} film after being subjected to a temperature of 473K for 24 hours. Also shown for comparative purposes is the calculated XRD pattern for a hcp lattice.

Also apparent is the presence of split peaks which is indicative of mixed phases and similar to those reported by Akselrod et al [90]. The implication of the above findings is that there is a possible formation of a new phase or a mixture of phases. Asklerod proposed that heat treated films of C_{60} actually contained a number of hexagonal phases inidicative of a hcp/fcc crystalline mixed lattice. Based on a simple hexagonal unit cell, $P6_3/mmc$ the predicted reflections were calculated using Poudrix software [102], using cell constants of a=10.02Å and b=16.36 Å. Calculating the lattice constant using $a\sqrt{2}$ reveals a nearest neighbour molecular distance of 7.0Å which is comparable to the electron hole separation of 5.9Å as calculated by the electroabsorption measurements. Again similar to the data obtained for the pristine film, there is good agreement between the calculated reflections and the measured reflections.

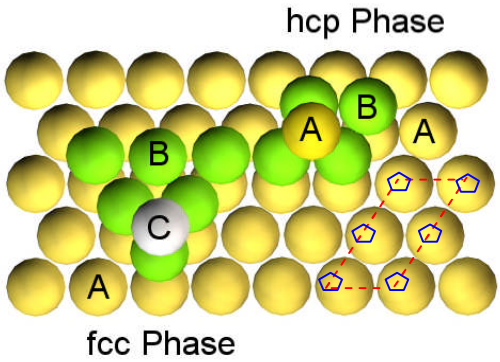

Figure 7.18 The molecular mixed phase stacking sequences for a hcp lattice (ABA) and a fcc lattice (ABC). Here AB and C correspond to different stacking layers

It should be noted that it is the position of the spheres taken up in the third layer which actually determines the closed packed structure, with the stacking arrangement in a fcc body being ABCABC… and in a hexagonal closed packed structure being ABABA… as shown in figure 7.18. These variations in this stacking sequence will result in a broadening of reflections of X-rays from the certain planes, while others will remain

sharp [20]. It should be noted that it is the equivalence of individual molecules within the lattice that changes. Annealing the films results in the partial formation of a hcp phase whereby equivalent molecules are separated by a larger distance than that experienced by the molecules in a fcc lattice. Since the lattice equivalency is determined by the rotational alignment of the molecules, a possible explanation of the observed effect in the annealed films may be the interlocking of the molecules within individual layers, similar to the theoretical model proposed by Dyskin et al, whereby the molecules may be situated at the nodes of a deformed hexagonal lattice [103]. The existence of a hexagonal phase in single crystals of C_{60} has also been reported by Ceolin et al where the authors suggested that the C_{60} molecules may undergo a reorientational motion around their 3-fold axis which lies parallel to the crystallographic 6-fold z axis instead of the spherical motion associated with the fcc phase [104].

7.8 X-ray measurement on C_{70}

As many as five different crystallographic phases have been reported for C_{70} in the solid state, primarily depending on the temperature [45]. The relatively high temperature phases include hcp, rhombohedral, and fcc. At high temperatures, i.e. those above 300K, solid C_{70} is found to adopt a fcc crystal structure. However the difference in cohesive energy between the hcp and fcc phases is only 0.35kcal/mol and this small difference may result in a localised equilibrium between the two phases in the bulk material at room temperature [105]. At 280K the rhombohedral distortion results in the molecules aligning themselves with their long axis pointing towards the unit cell diagonal. The effect of this reorientation is the sudden contraction of the close packing along the (110) direction and an expansion along the (111) axis.

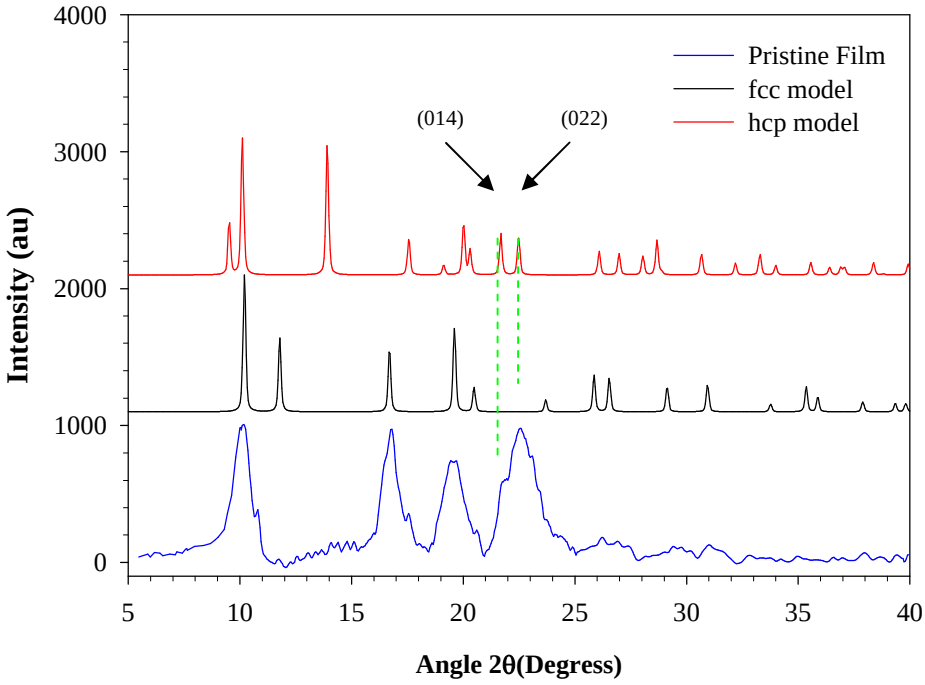

Figure 7.16 The X-ray diffraction pattern for a pristine C_{70} film compared to the predicted models for an ideal fcc cubic lattice and a hcp lattice [reference].

While the fcc and rhombohedral phases coexist over a wide range of temperatures the monoclinic phase is only observed below 180K [41]. It is known that the high temperature fcc structure contains a large number of defects which leads to an extensive under cooling of the high temperature phase as well as over heating of the low temperature phase. By heating the overheated rhombohedral lattice to 350K sufficient energy is provided to overcome the hindrance potential barrier associated with micro strains and defects and results in the formation of a fcc phase [41]. As such it is expected that the room temperature X-ray diffraction pattern of C_{70} would contain facets of both phases, intermixed. Additionally many of the reflections associated with the fcc phase also exist in the hcp phase, thus making identification of the origins of these reflections difficult to ascribe to one particular phase.

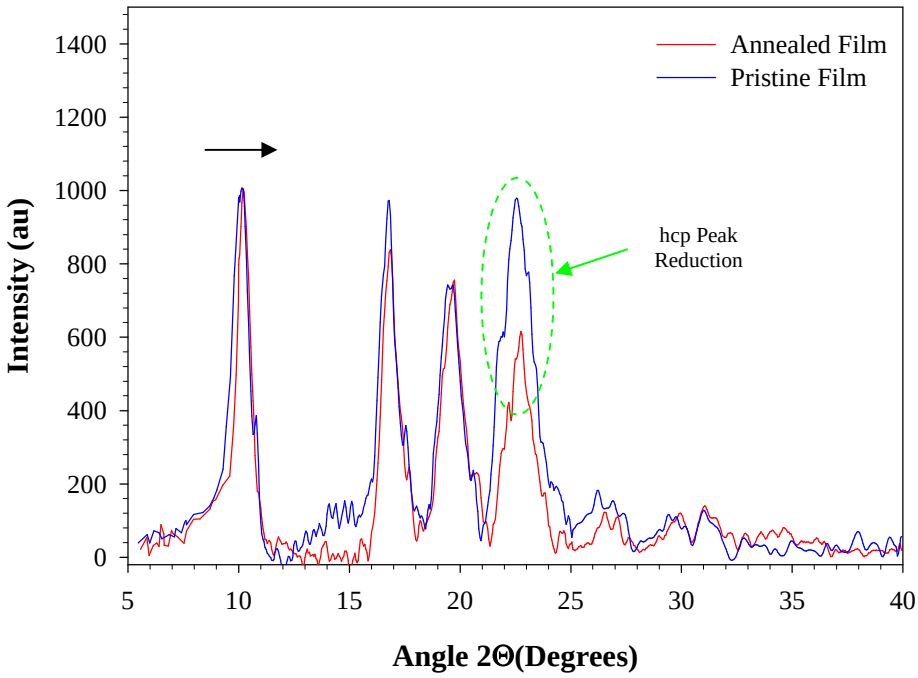

Figure 7.17 The comparison between the X-ray diffraction pattern for a pristine C_{70} film and the effect of a thermal treatment. The green circle indicates a large decrease in reflections associated with a hcp lattice.

Inspection of the X-ray data for pristine C_{70} in figure 7.16 reveals the presence of numerous reflections some of which are a result of a fcc type lattice and others which can arise from a hcp unit cell. The obtained data agrees well with diffraction patterns reported in literature [106]. Of particular interest are the two hcp reflections at 10.8 degrees and 11.2 degrees, which have no counter-part in the fcc lattice. Additionally, these reflections are suitably isolated from other observed peaks, thus reducing the possibility of any interference occurring. Although the resolution is not sufficient to completely resolve both of the peaks, the presence of a shoulder on the peak at 11.2 degrees does indicate the peak is actually composed of two individual hcp reflections.

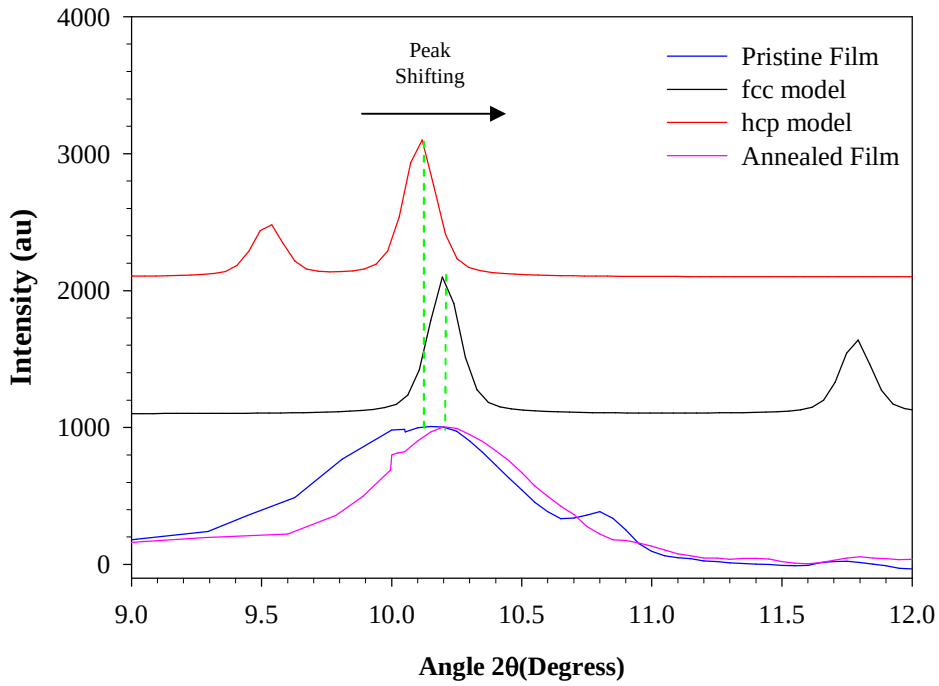

Figure 7.18 The change in the angle of reflection of the pristine C_{70} feature at 10.1 degrees. The pristine films exhibits a broad peak at 10.1 degrees due to the presence of mixed phases, of both fcc and hcp origins. Thermally cycling increases the proportional of fcc crystalline phases in the lattice.

As such these reflections provide a valuable means of observing the structural changes in the lattice due to the annealing treatment. Figure 7.18 shows the comparison between a pristine film and one which has undergone a subsequent thermal treatment. Immediately obvious is the large decrease in the reflections associated with the hcp lattice. Although reduced in amplitude, the fact that these reflections are still observed indicates that the films are actually composed of multiple phases with the fcc type being more dominant the an the hcp phase. Another indication that the lattice has undergone a structural change is the apparent narrowing and shifting of the (010) reflection at 10.1 degrees to 10.2 degrees which has been predicted as resulting from a (111) reflection in an fcc lattice, see figure 7.18. The lattice constant was calculated to be 14.51Å which is

0.5Å smaller that that reported in literature for the fcc lattice of C_{70}. The electroabsorption measurements on the annealed film indicated an electron hole separation of 12Å and while there is a discrepancy between the two set of values it does indicate the interpretation of the electroabsorption data is least internally consistent.

7.9 Conclusions

With regard to fullerene C_{60}, the data presented shows that there are irreversible changes in the electronic spectrum following exposure to high temperatures. This process results in the dramatic loss in oscillator strength of the high energy Frenkel type excitons and also of the low lying charge transfer excitons. A plot of peak area against temperature shows that the reductions in oscillator strength are reversibly thermochromic in nature until 362K. However above this temperature an irreversible annealing process occurs which is time dependent. The selective decrease in the relative magnitude of the 2.43eV CT state indicates that there is a reduction in the electron-hole separation within the lattice. The Vibrational analysis shows that the films remain pristine throughout the thermal treatment and exhibit no indications of oxidation of the lattice supporting the assumption that the changes in the electronic spectrum are structural in origin. AFM images confirm the existence of structural changes in the C_{60} films as a result of the annealing process. The presence of new reflections in the crystallographic measurements indicates that the films have undergone a structural ordering as a result of the thermal processing. The existence of these new hexagonal reflections and the information yielded by the electroabsorption measurements help support the theory that the thermal processing result in the formation a new hexagonally dominant crystalline structure.

Extension of the study to C_{70} reveals marked differences to that of C_{60}. The absorption spectrum of C_{70} displays a far less pronounced reduction in the oscillator strength as a function of temperature. However decomposition of the spectrum into overlapping Gaussian bands does reveal a non thermochromic affect at 340K. This corresponds to one of the known phase transition temperatures in C_{70}. Comparison of the annealed optical absorption spectrum with that of the pristine film reveals that there is an overall increase in the oscillator strengths. This increase is most likely due to the reordering of the rhombohedral hcp phase to a more stable fcc phase. A similar trend is also observed in the electroabsorption analysis, where by the CT state at 2.26eV experiences an increase in intensity after a thermal treatment. Analysis of FTIR data shows that the films did not oxidise during the thermal treatment as confirmed by the absence of any C=O vibrational modes in the annealed spectrum. AFM images reveal a similar trend to that observed for C_{60} with the coalescence of grains at high temperatures resulting in the formation of large crystallites. From the analysis of the X-ray diffraction of C_{70}, the decrease in the hexagonal reflections and the accompanying shifting of the (010) reflection, indicate the formation of a fcc dominant phase. Thus based on the collected data it can be concluded that exposing fullerene films to selective thermal treatments results in a reorder of the material's crystalline structure, with a more hexagonal phase being favoured in C_{60} and a greater fcc phase being adopted in C_{70}

CHAPTER 8

Summary Discussion and Conclusion

8.1 Introduction

The field of fullerene science has expanded considerably since the early 1990's particularly as a result of the ability to produce large quantities of material. The purpose of this study has been to examine the unique electronic and optical properties of the fullerene molecule in the solid state. These properties have been the subject of intensive research over the past two decades [107]. In spite of this, there are still a number of unanswered questions regarding the bulk electronic properties of these materials. The primary focus throughout this work has been to further understand and investigate the possible control of these electronic properties of the bulk crystalline structure through thermal manipulation of the films.

8.2 Summary of chapters

Chapter 1 introduced the potential importance of fullerenes since their discovery in 1985. In their molecular form they are electron rich and yet any real applications will rely on their solid state form. In electronics applications, the electronic communication between the molecules is of paramount importance. Since the communication mechanisms are ill understood to date, there are still numerous questions surrounding the degree and nature of the interactions, the influence of structure and the potential for manipulation of these interactions through structural control. Thus the motivation of the study is established.

Chapter 2 demonstrated that the electronic structure of C_{60} and C_{70} and the role of their symmetry are well understood, but that slight distortions to the symmetry can significantly enhance for example the optical absorption. It was highlighted that the fullerenes largely retain their molecular characteristics in the solid, but that there are noticeable features in the optical absorption which occur only in the solid state, indicating intermolecular communication in the excited state.

Chapter 3 describes the underlying experimental methodology used throughout the study. It furnishes detailed information on the fabrication of the fullerene the thin films, and goes on further to describe the more traditional spectroscopic techniques and instruments used in characterisation of the pristine and modified materials.

The focus of Chapter 4 is concerned with the design and construction of the electroabsorption spectrometer. The chapter also provides information on the performance characteristics of the electroabsorption spectrometer and its components as characterised using a standard fullerene C_{60} film. This chapter also details the two types

of sample geometries available as substrates and following on from this it details the need for development of a high temperature EA spectrometer.

In Chapter 5 some background theory on electronic spectroscopy and its importance in detailing the excitonic processes in fullerenes is explained. The role of excitons in determining the optical properties of the bulk material is also described while also highlighting the sensitivity of these excitons to electric fields thus allowing techniques like electroabsorption spectroscopy to probe their properties. The relationship between the degree of charge transfer and lattice constant of the bulk material is also drawn and consequently provides a means of relating changes in the materials electronic properties to alterations in the lattice structure.

In Chapter 6 the reversible effects of temperature on the absorption and electroabsorption spectra of both C_{60} and C_{70} are examined. Subsequently the large irreversible effects of high temperature treatments on the absorption spectra and electroabsorption spectra of C_{60} are detailed. Particular emphasis is placed on the exhibited irreversibility associated with the temperature dependence spectra, which is indicative of structural changes or possible annealing of the lattice. The chapter also examines the irreversible effects of above ambient temperatures on C_{70} which exhibit a far less pronounced effects than those associated thermally treated C_{60} films.

Chapter 7 examines the data collected from the changes in the absorption electroabsorption, XRD and AFM as a result of the annealing process. Initially the effect of the annealing process on the material's absorption and electroabsorption spectra are examined. Particular attention is paid to the changes in CT excitonic contributions as the fullerene films are annealed, which are indicative of a structural change. The noticeable difference between C_{60} and C_{70} in this regard, is also explored

and the possible causes of such differences are examined. Interpretation of XRD data reveals that the films have undergone structural changes during the annealing process.

8.3 Discussion

Of all the elements in the periodic table carbon is arguably the most important since it forms the basis of all life on this planet. Indeed such importance is placed on carbon, that the field of organic chemistry is devoted to the study of the molecules originating from the covalent bonding of carbon atoms together. However in spite of the historical attention paid to this branch of science, the third allotropic form of carbon was only discovered by accident in 1985. This new allotrope exhibited different physical and chemical properties from those associated with the only two previously known allotropes of carbon, diamond and graphite. As a result an entirely new field of science has developed, which has influenced fields of study as diverse as astrochemistry to fresh water biological science. However, initial research into the field was hindered by the limited amount of material available for study. The advent of the arc discharge production method as developed by Krätschmer, allowed for the large scale production of fullerenes, thus fuelling the research into the area. The fact that C_{60} was only the archetype molecule for a whole family of molecules has meant that over the last two decades the chemical and physical properties of fullerenes have been the subject of intense research and development, a trend which is likely to continue for some time to come. It was quickly realised that the unique properties these materials were dependent on their molecular and structural symmetry. The fact that different members of the fullerene family possessed varying degrees of molecular symmetries meant that the molecules all possessed unique physical and electronic properties. Indeed it is these

electronic properties which hold the interest of the semiconductor industry. While the electronic processes in the isolated molecule are well defined, any potential fullerene based semiconductor device will ultimately utilise the material's solid state electronic properties. In such devices it is the electronic communication between the molecules is of vital importance. Thus understanding the process which controls the flow of electrons within these materials is essential, if any future electronic based applications are to be realised. In solid state C_{60} the fullerene molecules are held together by weak van der Waals forces with the existence of numerous empty spaces between the molecules. Indeed it is the existence of these void spaces within the molecular lattice and their subsequent filling with various ions, molecules and alkali metals which fuelled much of the initial research into the electronic properties of these solids. The molecules are stable in the solid state and possess a rich vibrational and electronic band structure, which results from the overlapping of the individual π molecular orbitals. The next most abundant stable fullerene higher than C_{60} is C_{70}, which can be imagined as a C_{60} molecule with an extra belt of hexagons around its equator. Its lower symmetry means that it has a much more ordered electronic band energy structure than that associated with C_{60}. As a result of its elongated shape the solid state structure of C_{70} exhibits a number of different phases which depend on the molecular packing and orientational ordering of the lattice.

The data obtained during the course of this study on both C_{60} and C_{70} shows that fullerenes in the solid state are finely balanced between noninteracting in the ground state and interacting in the excited state. This interaction in the solid state material is strongly influenced by temperature and the lattice structure. In the low temperature regime, the CT states associated with both molecules are strongly influenced by their

local thermal environment, when compared to the Frenkel type excitons. In C_{60} at temperatures below the phase transition, (260K), the molecules adopt a simple cubic crystalline structure with four C_{60} molecules per unit cell. Increasing the temperature of the system and passing through the phase transition results in the C_{60} molecules adopting a predominantly fcc crystalline structure. Since the degree of intermolecular communication between the molecules is dependant on the relative orientations of the molecules within the in the lattice, the intermolecular transitions, in particular the CT states at 2.43eV and 2.70eV exhibit a reversible susceptibility to changes in the lattice crystalline structure. Continued heating of the lattice to temperatures below 362K results in a similar process whereby no loss in oscillator strength is observed upon cooling the films back to room temperature. However, exposing films to temperatures in excess of this results in an irreversible loss of oscillator strength of all the low and high energy electronic transitions. Infra red analysis confirms that the observed changes in the absorption spectra are not as a result of polymerisation of the bulk structure or as a result of oxidation of the material. The electroabsorption analysis reveals a continuing decrease in dipole moment as the temperature of the material is increased. Calculating the changes in dipole moment as a function of temperature reveals that the charge separation between nearest neighbour molecules experiences a decrease as a result of the annealing the film. The results would indicate that the lattice crystallinity has changed somewhat compared to the pristine material. These findings are supported by the XRD analysis which shows the formation of a new hexagonally closed packed phase intermixed with fcc phases. From the results it would seem that the extent of this lattice conversion is both temperature and time dependant, whereby no hcp formation occurs below 362K irrespective of the annealing time. However at temperatures above 362K,

longer annealing times result in the formation of a greater number of hcp phases within the lattice. The micro crystalline morphology of the films is also affected by the thermal treatments with the formation of larger grains with reduced surface roughness of the films.

In extending the study to C_{70}, a similar effect to that observed in C_{60} would have been expected. However analysis of the data for C_{70} reveals marked differences to that of C_{60}. The crystalline lattice structure of C_{70} is more complex than that observed in C_{60} with numerous phases co existing over a wide range of temperatures. At temperatures below 180K the C_{70} molecules adopt a monoclinic structure. This monoclinic structure is converted to a rhombohedral phase as the temperature of the system is increased above 280K whereby the molecules align themselves along their long axis. The relatively high temperature phases include hcp, rhombohedral, and fcc. In the high temperature regimes, ie those above 300K, solid C_{70} is found to adopt an inter-dispersed fcc crystalline and hcp structure. This localised equilibrium of phases results from the small difference in cohesive energy between phases in the bulk material at room temperature. There is an extensive under cooling the high temperature fcc crystalline structure due to the large number of defects intrinsic within the lattice. Heating the overheated rhombohedral lattice to 350K provides sufficient energy to overcome the potential barrier associated with micro strains and defects and results in the formation of a fcc phase. As with C_{60} the CT state in C_{70} should also be very sensitive to changes in the crystalline environment. However unlike C_{60}, the high temperature absorption spectrum of C_{70} displays a far less pronounced reduction in its oscillator strength as a function of temperature. However since the CT state of C_{70} at 2.26eV is masked somewhat by Frenkel excitons, changes in this CT state's oscillator strength are difficult

to observe in the absorption spectrum, thus prompting the use of a more sensitive technique such as electroabsorption spectroscopy. Even so, decomposition of the absorption spectrum does reveal a non thermochromic affect occurring at temperatures above at 340K corresponding to the formation of an fcc phase. The analysis of the electroabsorption data, which is not hindered by masking effects of Frenkel excitons also reveals a strong thermal dependence of this state which is reversible below 340K. The process is temperature dependant, with complete recovery of spectral features possible at treatment temperatures below 340K while irreversibility sets in at temperatures above 340K. Comparison of the annealed spectrum with that of the pristine film reveals a substantial increase in the oscillator strengths, which is most likely due to a reordering of the lattice from a mixed rhombohedral and fcc phase into a more predominant and stable fcc phase. Similar to data gathered for C_{60} the FTIR analysis of the annealed C_{70} films reveals that the thermal treatment did not result in the formation of any oxidised material as confirmed by the absence of any C=O vibrational modes in the annealed spectrum. This would indicate that the changes observed in the absorption and electroabsorption data are structural rather than chemical in nature. This hypothesis is confirmed by X-ray analysis of the films which indicate that the annealed films are composed of a greater ratio of fcc to hcp phases than the pristine material. The AFM images on both the pristine and annealed film confirm that a structural change has taken place as a result of the annealing process. Thus the results indicate that the crystalline structure of the material and consequently its electronic properties can be altered by subjecting the film to an annealing process.

In comparing the ease with which the electronic properties of both molecules can be altered as a result of structural modification of the lattice, it would seem that of the two,

C_{70} is more resistant to alterations. The molecules oblong structure may offer a possible explanation for this behaviour, since it may induce a restrained orientation around the lattice positions. By comparison the near spherical structure of C_{60} should allow for a greater degree of oriental freedom thus allowing for a greater reacceptance to structural reordering.

From the data analysis it would seem that there are significant differences in the response of these materials to changes in the external temperature. With the structural changes in mind the associated affects on the materials electronic properties are of paramount importance particularly with regard to the development of any future electronic devices. In organic conductors it is movement of an electron between the molecules within the lattice which determine its conductive properties. In fullerenes a key issue with regard to understanding the electronic properties of the materials is the nature of the duality between intramolecular and intermolecular electronic processes. The most significant CT states in both materials have been identified as occurring at 2.43eV and 3.5eV for C_{60} and 2.26eV and 3.6eV for C_{70}. In C_{60} the CT state at 2.43eV has been ascribed to as from a series of CT states created by the transfer of an electron from the HOMO of one molecule at the (000) lattice coordinate to the LUMO of its nearest neighbour located at (½½0) lattice site. The forbidden intramolecular excitation at 2.7eV is believed to be activated as a result of coupling of all the nearest neighbouring molecules to the Frenkel manifold. The state at 3.5eV, although originally thought to derive from an intramolecular excitation [80] has also more recently been described as resulting from an electron transfer from the HOMO-1 of one molecule to the LUMO of another [43]. In C_{70} the 2.26eV feature, with its distinctly second derivative shape has been firmly ascribed to as result form the CT from the HOMO of

one molecule to the LUMO of its nearest neighbour. A second CT state has also been identified at 3.6eV. The lowering of energy of the of the nearest neighbour HOMO to LUMO CT state in C_{70} when compared to C_{60} is as a consequence of the molecules lower ionisation potential and greater electron affinity.

The distinct differences in the photocurrent generation thresholds between C_{60} and C_{70} highlights the different origins of the conductive mechanisms in these materials [43]. The photocurrent generation processes in fullerenes are governed by their low energy states which have a sufficient intensity. In the low energy spectral region of C_{60} the Frenkel excitonic transitions are electric dipole forbidden and consequently the only contributors to the initial generation of a photocurrent is the (½½0) CT transition at 2.43eV. In C_{70} the photocurrent efficiency increases sharply in the range from 1.80eV to 1.85eV, and rises again at 2.26eV which is associated with the CT exciton indicating that in C_{70} the Frenkel excitons have a greater role to play in the conduction mechanisms than compared to C_{60}. Thus in solid state fullerenes, the origins of the conduction mechanisms are different, with those in C_{60} being dominated by CT states and those in C_{70} being governed by an admixture of Frenkel and CT states.

8.4 Conclusion

Throughout the course of this study it has been shown that Fullerenes are uniquely balanced between noninteracting isolated molecules and strongly interacting solids. Their high sensitivity to their crystalline environment and external influences, complex molecular dynamics, sensitivity to impurities, temperature and oxygen intercalation means that an apparently simple system is rather difficult to understand. Nevertheless they represent a fascinating molecular system in which to study molecular versus solid

properties of a material and the role that charge transfer mechanisms have to play in determining the properties. It has been shown that the electronic properties of both fullerene C_{60} and C_{70} are sensitive to changes in their lattice structure can be altered by the selective use of heat treatments. The extent and final outcome of the thermal treatment on the material's properties is dependent on the fullerene being investigated but that aside the use of these annealing processes does represent a potential means of manipulating the material's electronic properties. The net affect of these thermal treatments is a material which exhibits an increased communication between molecules and therefore opens up possible role in future electronic applications. If nothing else, they represent a model system in which to study and understand the role excitons play in determining the bulk electronic properties of organic conductors.

REFERENCES

1. H.W Kroto, J.R Heath, S.C O'Brien., R.F. Curl, and R.E. Smalley, *Nature* 318, 162, (1985).
2. D.E.H. Jones, New Sci., 32, 245, (1966).
3. E. Osawa, Chem. Abstr., 75698, 74, (1971).
4. W. Krätschmer, K, Fostiropoulos and D.R. Huffman Chem. Phys. Lett. 170, 167, (1990).
5. H. Ajie, M. A. Marcos, J.A. Samir, B.D. Rainer, and W. Krätschmer, J. Phys. Chem., 94, 8630, (1990).
6. R.C. Haddon, L.E. Brus and K. Raghavachari, Chem. Phys. Lett., 125, 459, (1986).

7. D.E. Manolopoulos, J.C May and S.E. Down, Chem. Phys. Lett., 181, 105, (1991).

8. S.H. Freidman, D.L. DeCamp, R.P. Sijbesma, G.Srdanov. F. Wudl, and G. L. Kenyon, J. Am. Chem. Soc., 115, 6506, (1993).

9. R.C. Haddon, A.F. Hebard, M.J. Rosseinsky, D.W. Murphy, S.J. Duclos, et al, Nature, 350, 320, (1991).

10. A.F. Hebard, M.J. Rosseinsky, R.C. Haddon, D.W. Murphy, S.H. Glarum, T.T.M. Palstra, A.P. Ramirez and A.R.Kortan, Nature, 350, 600, (1991).

11. M.J. Rosseinsky, A.P. Ramirez S.H. Glarum,. D.W. Murphy, R.C. Haddon, A.F Hebard, T.T.M. Palstra, A.R.Kortan, Am. Phys. Soc., 66, 2830, (1991).

12. S. Yasufuku, Electrical Insulation Magazine, 21(1), 54, (2005).

13. J.C.Withers, R. O. Loufty, T.P.Lowe. Fullerene Science and Technology, 5(1), 1, (1997).

14. R.M. Fleming, A.P.Ramirez, M.J. Rosseinsky, D.W. Murphy, R.C. Haddon, Nature, 352, 787, (1991).

15. H. Weber App.Phys Lett. 81, 3749, (1998).

16. M.J. Rosseinsky, A.P. Ramirez S.H. Glarum,. D.W. Murphy, R.C. Haddon, A.F Hebard, T.T.M. Palstra, A.R.Kortan, Am. Phys. Soc., 66, 2830, (1991).

17. A.T. Werner, H.J. Byrne, D. O'Brien and S. Roth, J. Mol. Crys. Liq. Crys., 256, 795, (1994).

18. M. Muccini, Synth. Met., 213-219, (1996).

19. P.C. Eklund, A.M.Rao, P. Zhou, Y. Wang, K. Wang, J.M. Holden, Thin solid films, 257, 185-203, (1995).

20. W. Krätschmer, L. D. Lamb, K, Fostiropoulos and D.R. Huffman, Nature, 347,

354, (1990).

21. H.J.Byrne, "Physics and Chemistry of Fullerenes", H. Kuzmany, J. Fink,M. Mehring, S. Roth, ed., World Scientific, (1995).
22. J. Daintith, R.D. Nelson, “Dictonary of Mathematics”, Penguin, (1989).
23. M.S. Dresselhaus, G Dresselhaus, NanoStructured Materials, 9,33-42, (1997).
24. M. Cases, “Single and Multiple addition to C_{60}, A Computational Chemistry Study, University of Girona, (2003).
25. M.S. Dresselhaus, G Dresselhaus, P.C. Eklund, “Science of fullerenes and carbon nanotubes”, Academic press inc. (1995).
26. C.C Chancey, M.C.M. O’Brien, The Jahn-Teller Effect in C_{60} and Other Icosahedral Complexes, Princeton University Press, (1997).
27. K. Hedberg, L. Hedberg, D.S. Bethune, C.A. Brown, H.C. Dorn, R.D. Johnson, M. de Vries, Science, 254, 410, (1991).
28. C.S.Sundar, Y. Hariharan, A. Bharathi, M. Premila, V.S. Sastry, G.V. N. Roam J. Janaki, D.V. Devadhasan, T.S. Radhahrishnan, N. Subramanian, P.Ch. Sahu, M. Yousuf, S. Raju, V.S. Raghunathan, M.C. Valsakumar, Prog. Crystal Growth and Charact., 34, 11-23, (1997).
29. J.Shunway, S. Satpathy, Chem. Phys. Lett., 211, 597, (1993).
30. J. Baker, P.W. Fowler, P. LAzzeretti, M.Malagoli, R. Zanasi, Chem. Phys. Lett., 184, 182-186, (1991).
31. S.V. Smaalen, V. Petricek, J.L de Boer, M. Dusek, M. A. Verheijen, G. Maijer, Chem. Phys. Lett., 223, 323-328, (1994).
32. S. Leach, M. Vervloet, A. Desprès, E. Bréheret, J.P. Hare, T. J. Dennis, H.W.

Kroto, R. Taylor, D.R.M. Walton, Chem. Phys., 160, 451, (1992).

33. M.S. Dresslhaus, G. Dresselhaus, A.M. Rao, P.C. Eklund, Synth Met., 313-325, (1996).
34. W.Z. Wang, C.L. Wang, A.R. Bishop, L. Lu, Z. B. Su, "Physics and Chemistry of Fullerenes", H. Kuzmany, J. Fink,M. Mehring, S. Roth, ed., World Scientific, (1995).
35. P.W. Fowler, P. Lazzeretti, M. Malagoli, R. Zanasi, Chem. Phys. Lett., 179, 174-180, (1991).
36. G. E.Scuseria, Chem. Phys. Lett., 180, 451-456, (1991).
37. M.Ichida, M. Sakai, T. Yajima, A. Nakamura, H. Shinohara, Chem. Phys. Lett., 271, 28, (1997).
38. S. Kazaoui, N. Minami, Synth. Met., 86, 2345-2346, (1997).
39. I.V. Arkhangel'skii, E.V. Skokan, Yu.A. Velikodnyi, V.V. Chernyshev, L.N. Sidorov, Doklady Akademii Nauk, 363, 494-496, (1998).
40. J.E. Fisher, P.A. Heiney, D.E. Luzzi, and D.E. Cox, Fullerenes: Synthesis, Properties, and Chemistry of Large Carbon Clusters, from the American Chemical Society Symposium Series, 481, 55, (1992).
41. K. Prassides, Electronic Properties of Fullerenes, H. Kuzmany, J. Fink, M. Mehring, S. Roth, Ed, 117, 139-145, (1993).
42. H. Kuzmany , M. Matus, B. Burger, J. Winter Adv Mater 10, 731, (1994).
43. S. Kazaoui, N. Minami, Y. Tanabe, H.J. Byrne A. Elimes, P. Petelenz, Phys. Rev. B., 58, 7689, (1998).
44. A.M. Rao, M. Menon, K.Wang, P.C Eklund, K.R. Subbaswamy, D.S Cornett,

M.A. Duncan, I.J. Amster, Chem. Phys. Lett., 224, 106-112, (1994).

45. G.Van Tendeloo, S. Amelinckx, Electronic Properties of Fullerenes, H. Kuzmany, J. Fink, M. Mehring, S. Roth, Ed, 117, 182-188, (1993).
46. G. Chambers, H.J. Byrne, Chem. Phys. Lett., 302, 307-311,(1999).
47. G. U. Bublitz and S.G Boxer, Annu. Rev. Phys. Chem., 48, 213, (1997).
48. S. A. Locknar, L. Peteanu, J. Phys. Chem. B, 102, 4240-4246, (1998).
49. W. D. R. Joseph, N.R. Pradhan, S. Singh, D. N. Rao, Current Science, 86, 1283-1287, (2004).
50. W. Guo, Ph.D. Dissertation, University of Dresden, (2003).
51. Hamamatsu Photonics, L2194-02/C6979 Lamp/Power supply Manual.
52. E.S. Park, S. Boxer, J. Phys. Chem. B., 106, 5800-5806, (2002).
53. M. Leiss, Z. V. Vardeny, P.A. Lane, Phys. Rev. B., 59, 11053-11061, (1999).
54. Digikrom CVI CM110 Technical Manual.
55. Perkin Elmer Technical Note, “What is a Lock-in Amplifier”, TN1000.
56. I. H. Campbell, P.S. Davids, J.P. Ferraris, T.W. Hagler, C.M. Heller, A. Saxena, D.L Smith, Synth. Met., 80, 105-110, (1996).
57. Oxford Instruments, CCC1204 Technical Manual.
58. B. Bowe, Dublin Institute of Technology, “Introduction to LabVIEW”, (1999).
59. CM110 vi subroutine downloaded from National Instruments Homepage: http://www.ni.com/cvi110.
60. H.H. Perkampus, Encylopedia of Spectroscopy, VCH publishers Inc, (1995).
61. D.A. Skoog, F.J. Holler, T. A. Nieman, “Principles of Instrumental Analysis”, (1998).

62. J. Mc Hale, “Molecular Spectroscopy”, Prentice Hall, (1999).

63. H.H. Perkampus, UV-VIS Spectroscopy and its Application, Springer-Verlag, (1992).

64. J. M. Hollas, “Modern Spectroscopy”, Wiley, 33 (2005).

65. J.Wilson, J.F.B. Hawkes, “Optoelectronics: An introduction”, Prentice Hall, (1983).

66. P.J. Bound, W. SieBrand, I. Eisentein, R.W, Munn, P. Petelenz, Chemical Physics, 95, 197-212, (1985).

67. L. Sebastian, G. Weiser, Chemical Physics, 62, 447-457, (1981).

68. L. Akselrod, H.J. Byrne, J. Callaghan, A. Mittelbach and S. Roth, in "Electronic Properties Fullerenes", H. Kuzmany, J. Fink, M. Mehring and S. Roth eds., Springer Series in Solid state Sciences, Springer Verlag Heidelberg, 117, 219, (1993).

69. S, Leach in "Physics and Chemistry of Fullerenes",K.Prassides (ed.) NATO ASI Series, Kuluwer Academic Publishers, 443, 117, (1994).

70. M. Kaiser, J. Reichenbach, H.J. Byrne, J. Anders, W. Maser, S. Roth, A. Zahab and P. Bernier, Solid State Commun., 81, 261, (1992).

71. P.C. Eklund, A.M. Rao, Y. Wang, P. Zhou, M.J. Holden, M.S. Dresselhaus, G. Dresselhuas, Thin solid Films, 257, 211-232, (1995).

72. M.Ichida, M. Sakai, T. Yajima, A. Nakamura, H. Shinohara, Chem. Phys. Lett., 271, 30, (1997).

73. W. Liptay, Exited States, ed EC, New York Academic, 1, 129-229, (1974).

74. D.H. Oh, M. Sano, SG. Boxer, J.Am. Chem. Soc., 113, 6880-6890, (1991).

75. L. Sebastin, G. Wieser, Chem Phys, 61, 125, (1981).

76. S. Moller, G. Weiser, F. Garnier, Synth. Met., 116, 305-309, (2001).

77. K. Pichler, SGraham, O. M. Gelsen, R. H. Friend, W. J Romanow, P. McCauley, N. Coustel, J. F. Fisher, A.B. Smith, J. Phys.:Condens. Matter, 3, 9259-9270, (1991).

78. S. Jeglinski, Z.V. Vardeny, D. Moses, V.I. Srdanov, F. Wudl, Synth. Met., 49-50. 557-563, (1992).

79. P. Petelenz, M. Slawik, B. Pac, Synth. Met., 64, 335-339, (1994).

80. B.C. Hess, D.V. Bowersox, S. H. Mardirsian, L. D. Unterberger, Chem. Phys. Lett., 248, 141-146, (1996).

81. B. Pac, P. Petelenz, M. Slawik, R.W. Munn, Journal of Chemical Physics, 109(18), 7932-7939, (1998).

82. B. Pac, Chem. Phys. Lett., 357, 259-262, (2002).

83. P. Petelenz, Organic Electronics, 5, 115-127, (2004).

84. PeakFit™ v4 Users Guide, SeaSolve Software, (2003).

85. N. Minami, S. Kazaoui, and R. Ross. Synthetic Metals, 70, 1397, (1995).

86. P. Petelenz, J. Jlumin., 110, 325-331,(2004).

87. S. Kazaoui, R. Ross, N. Minami, Phys. Rev. B., 52(16), 11665-11668, (1995).

88. P. Petelenz, M. Andrzejak, S. Kazaoui, N. Minami, Chem. Phys., 243, 149-157, (1999).

89. L. Forro, L. Mihaly, Rep. Proh. Phys., 64, 649-699, (2001).

90. L. Akselrod, H.J. Byrne, T.E. Sutto, S. Roth, Chem. Phys. Lett., 233, 436-443, (1995).

91. K. Ohno, J.Z. Yu, Y. Maruyama, Y. Kawazoe, T. Takahashi, Chem. Phys. Lett., 255, 367-372, (1996).

92. G. Chambers, Ph.D. Dissertation, Dublin Institute of Technology, (2001)

93. X. Wu and S.E. Ulloa, Phys. Rev., B 49, 7825, (1994).

94. R. Almairac, J. Moret, J.L. Sauvajol, M. Descamps, Synth. Metal, 103, 2358-2359, (1999).

95. V. Capozzi, G. Perna, Thin Solid Films, 515, 7247-7252, (2007).

96. D.S. Bethane, G. Meijer, W.C. Treacy, and H.J. Rosen, Chem. Phys. Lett., 174, 219, (1990).

97. W. Brockner, F. Menzel, Journal of Molecular Structure, 378, 147-163, (1996).

98. N. Iwata, K. Mukaimoto, H. Imai, H. Yamamoto, Surface and coatings Technology, 169-170, 646-649, (2003).

99. A. Hassanien, I. Musevic, D. Mihailovic, A. Omerzu, S. Tomic, "Physics and Chemistry of Fullerenes", H. Kuzmany, J. Fink,M. Mehring, S. Roth, ed., World Scientific, (1995).

100. A. H. Jayatissa, T. Gaupta, A. D. Pandya, Carbon, doi:10.1016/ J.carbon.2003.12.058, (2004).

101. S. Gao, P. M. Nagel, A.L Deeringt, S.M Van Lue, S. A Kandel, Surf. Sci. doi:10.1016/j.susc.2006.11.042, (2006).

102. Poudrix Software, Ken Sakai, University of Kyushu, (2004)

103. A. V. Dyskin, Y. Estrin, A. J. Kanel-Brlov, E. Pasternak, Phsics Letters A., 319, 373-378, (2003).

104. R. Ceolin, J. L. Tamarit, D.O. Lopez, M. Barrio, V. Agafonov, H. Allouchi, F.

Moussa, H. Szwarc, Chem. Phys. Lett., 314, 21-26, (1999).

105. L. Jiang, T. Iyoda, N. Kino, K. Kitazawa, K. Hashimoto, A. Fujishima, Surf. Sci., 349, L101-L106, (1996).

106. T. S. Radhakrishnan, V. Sridharan, G. Gosh, Journal of Physics and Chemistry of Solids, 61, 1127-1136, (2000).

107. H. Kroto, International Journal of Mass Spectroscopy, 200, 253-260, (2000).